Improving Efficiency of 1D Thermopower Wave Devices and Studying 2D Reaction Waves

by

Sayalee G. Mahajan

M.S.CEP., Massachusetts Institute of Technology (2013)

B. Chem. Eng., Institute of Chemical Technology (2010)

Submitted to the Department of Chemical Engineering

In Partial Fulfillment of the Requirement for the Degree of

DOCTOR OF PHILOSOPHY IN CHEMICAL ENGINEERING

at the

MASSACHUSETTS INSTITUTE OF TECHNOLOGY

September 2015

Signature of Author: Signature redacted

Department of Chemical Engineering
July 2015

Certified by: Signature redacted

Michael S. Strano
Professor of Chemical Engineering
Thesis Advisor

Accepted by: Signature redacted

Richard D. Braatz
Professor of Chemical Engineering
Chairman, Committee for Graduate Students

Improving Efficiency of 1D Thermopower Wave Devices and Studying 2D Reaction Waves

by

Sayalee G. Mahajan

Submitted to the Department of Chemical Engineering on July 27, 2015

in Partial Fulfillment of the Requirements for the Degree of

Doctor of Philosophy in Chemical Engineering

Abstract

With growing energy consumption, current research in the field is focused on improving and developing alternatives for energy storage and conversion. Factors such as efficiency of energy conversion, usability of this converted form of energy, power density, energy density etc. help us in determining the right energy source or conversion technology for any specific application. The main aim of this thesis was to study self-propagating reaction waves as a means of converting chemical energy into electrical energy.

We carried out numerical simulations to study these self-propagating reaction wave systems and their heat transfer properties. Our analysis shows that for certain specific system heat transfer properties, self-propagating reaction waves can sometimes lead to superadiabatic temperatures, which are temperatures higher than the predicted adiabatic reaction temperature. Having energy available at higher temperature has advantages in heat harvesting applications such as thermoelectricity and thermophotovoltaics. We calculated the improvement in efficiency of a modified thermophotovoltaics setup, when the input is a reaction wave, operating under superadiabatic conditions.

Experimentally, we studied these self-propagating reaction waves by launching 1D thermopower waves. We demonstrated improved chemical-to-electrical conversion efficiency of these devices (from about 10^{-4} % to 10^{-2} %) by operating with newer fuels such as sodium azide and sucrose with potassium nitrate on single-walled carbon nanotube-based thermal conduits. The net efficiency of operation of the device was also improved to up to 1% by using external thermoelectric harvesters to capture the heat energy lost via convection and radiation.

We proposed a model combining the 1D reaction heat and mass balance equations with the theory of excess thermopower to predict the output voltage profiles of thermopower wave devices and extract useful data from the voltage plots obtained experimentally. This model allows us to quantify the impact of the device-to-device variation of the fuel and thermal conduit properties, and can guide us to a better choice of fuel-thermal conduit pairs to improve the efficiency of operation.

Finally, we experimentally studied 2D reaction waves. These waves were launched with a nitrocellulose fuel layer atop an aluminum foil thermal conduit. A wave front characteristic, the shape of these wave fronts, was studied as a function of heat loss. Energy released by these reactions was again harvested using external thermoelectrics to convert heat energy into electricity. We demonstrated that such a setup of 2D reaction waves can be used to illuminate a light-emitting diode (LED).

Thesis supervisor: Michael S. Strano

Title: Professor of Chemical Engineering

Acknowledgments

I would like to take this opportunity to thank a few of the many people who have made this thesis possible and have been instrumental in making graduate school an enjoyable yet learning experience and an unforgettable part of my life.

First and foremost, I would like to thank my thesis advisor, Prof. Michael Strano. Prof. Strano has been an exceptional guide, teacher and mentor. His passion for research is impossible to miss and has often been a source of motivation for me during times when things haven't always worked out in the first attempt. Apart from teaching me a lot about research methods and approaches to solving scientific problems; generic science and industry related discussions with Prof. Strano always helped keep things in perspective. I will always be thankful to him for giving me the opportunity to work not only in his lab but also on the project of my choice, with ample freedom to pursue research directions that interested me.

I would like to thank my thesis committee members, Prof. Martin Bazant and Prof. Gang Chen. Throughout the course of my PhD, their feedback and questions ensured that my thesis stayed on track, in terms of technical content, motivations and timeline.

These past 5 years in graduate school would definitely have not been possible without the fun times shared with my lab-mates. I would like to specifically mention Anton Cottrill and Tianxiang (Albert) Liu who have been exceptional collaborators and were immensely helpful in all the project related (or even otherwise) discussions, experiments and analysis. Joel Abrahamson, Qing Hua Wang, Zachary Ulissi and Steven Shimizu also deserve a mention for always being there as friends.

Finally, I would like to thank all my friends and family members who have been a beam of constant support and motivation for when things got rough, and companions for the fun times as well.

I would like to conclude by thanking my parents, Medha and Girish, who have always been there for me, and have whole-heartedly supported me through all of the important decisions of my life.

I am indeed thankful for the opportunity to have interacted and learnt from everyone, all those mentioned here or not. I hope I am blessed with your continued support and wishes in the future too and I wish all the best of opportunities and successes.

Table of Contents

Chapter 1 Introduction to Thermopower Waves

Parts of this chapter have been reproduced with permission from John Wiley and Sons.

Mahajan, S. G.; Wang, Q. H.; Strano, M. S.; Abrahamson, J. T., Energy generation using thermopower waves: Experimental and analytical progress. AIChE Journal ***2013,*** *59 (9), 3333-3341.*

1.1 Introduction

With growing demand for energy consumption, a lot of current research is focused on improving current sources and developing alternatives for energy storage and conversion. When considering any of the forms of energy conversion such as chemical energy to heat energy or heat energy to electricity, factors such as efficiency of conversion and usability of this converted form of energy are of importance. Other important factors include size of the energy source, ability to store energy over long periods of time or long shelf life, electrical power density, energy density, economic and environmental impact etc.[1] These factors combined with the need for any specific application helps us determine the right energy source or energy conversion technology.

Thermopower waves is one such novel concept for converting chemical energy into electrical energy.[2] By exploiting the phenomenon of thermoelectricity and excess thermopower, we can convert the chemical energy stored in the bonds of various chemical fuels to electrical energy by launching a self-propagating fuel reaction wave along a conduit with appropriate electrical and thermal properties.[3] Thermopower reaction waves have been launched using various fuels such as 2, 4, 6-Trinitroaniline (TNA),[2] picramide (with sodium azide),[4,5] nitrocellulose (with sodium azide)[6,7,8,9], nanothermites consisting of aluminum (Al) and iron oxide (γ-Fe_2O_3)[10] etc. Different conduits that have been successfully used include multi-walled carbon nanotubes (MWNTs),[2]

single-walled carbon nanotubes (SWNTs),[4] SWNT yarns i.e. SWNTs twisted or intertwined together to form macroscopic thread or yarn like structure, ZnO,[8,11] Bi_2Te_3 coated on alumina and terracotta,[6,7] Sb_2Te_3 coated on alumina and terracotta and MWNT,[7,12] MnO_2 coated alumina[9], surface-oxidized copper sub-microparticles films[13] etc. Analytical work in the field of thermopower waves included finding an expression for the temperature for a steady state self-propagating reaction wave, governed by coupled heat and mass balance equations. A logistic wave function was found to be a good fit to explain the time and space dependent temperature profile for such a one dimensional (1D) self-propagating reaction wave system.[14] Analytical analysis of the system of governing equations studied the relationship between β, the non-dimensional inverse adiabatic reaction temperature rise with the oscillations in the output voltage from thermopower wave devices.[15] Also, work on the topic of solitons derived conditions for oscillations in self-propagating thermal waves exchanging heat with the surrounding while propagating.[16]

Comparing the electrical output from these thermopower wave devices with that of other energy sources shows us of the possibility of using thermopower wave devices for niche nano and micro-scale applications such as power sources for Micro-Electro-Mechanical-System (MEMS) devices[17] or 'smart dust' applications[18] or wireless sensor networks[19]. Thermopower reaction waves allow us to utilize high energy density of chemical fuels. Previous thermopower wave experiments have shown devices to give specific power output as high as 7 kW/kg and power density as high as 80,000 $\mu W/mm^3$.[20] Figure 1-1 shows a comparison of the volume and power density of thermopower wave devices as compared to other common electrical energy sources.

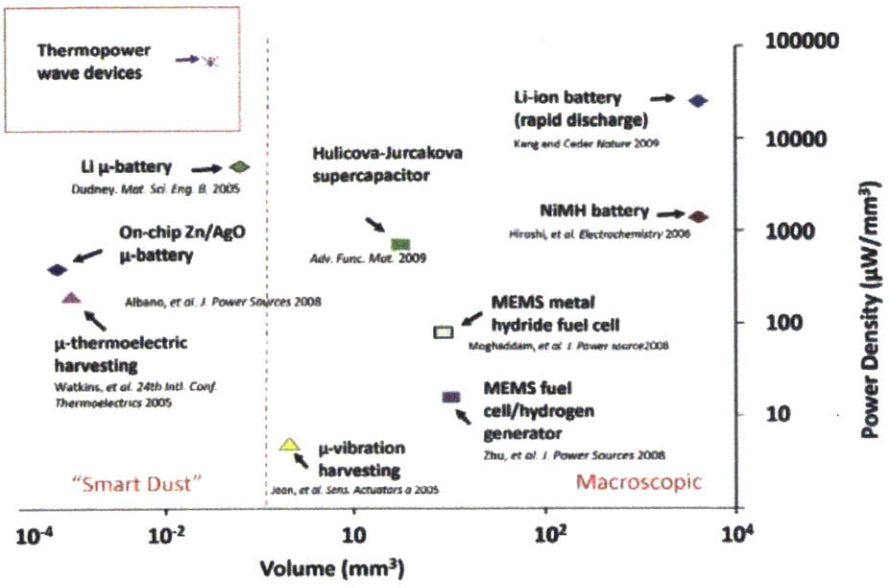

Figure 1-1 Comparison of volume and power density of multiple electrical energy sources. Power sources less than 1 mm^3 are usually desirable for 'smart dust' applications.[20] Reproduced from Ref 20, with permission from Elsevier Ltd.

Thus even with short duration of the voltage output (over the range of milliseconds to seconds), thermopower wave devices' performance parameters such as specific power output, power density and device stability over long durations of time of definitely make them an attractive candidate for further research.

1.2 Basics of Thermoelectricity

Thermopower waves involve coupling the exothermic nature of chemical reaction with advantageous electrical and thermal properties of the conduit on which the reaction is carried out. It is a novel means of obtaining electrical output using a thermal gradient, beyond what is possible via conventional thermoelectric effect.

The conventional Seebeck effect or thermoelectric effect describes the phenomenon of electric output generated by a temperature difference across the ends of a thermoelectric material. The output voltage ΔV_{TE} as a function of the temperature gradient is given by the relation

$$\Delta V_{TE} = \int_{T_{left}}^{T_{right}} S \nabla T \tag{1}$$

In equation (1), S is the Seebeck coefficient. According to the nomenclature used traditionally, ΔV_{TE} is defined for the cold side with respect to the hot side. Exploiting the traditional Seebeck effect requires thermoelectric materials having high electrical conductivity σ to enhance electron transport, but low thermal conductivity k to maintain the temperature difference across the ends of the device. The suitability of a material for thermoelectric applications is measured by means of 'the figure of merit' ZT, defined as[20]

$$ZT = \frac{S^2 \sigma T}{k} \tag{2}$$

The higher the value of ZT, the better suited is the material for thermoelectric applications.

1.3 Basics of Thermopower Waves

Thermopower waves rely on exploiting the effect of carrying out an exothermic chemical reaction on a conduit with improved electrical and thermal properties. They were first demonstrated using carbon nanotubes as the conduit material. Carbon nanotubes are one-dimensional molecular structures having high thermal conductivity of the order of 3000 W m^{-1} K^{-1} and possessing electrical conductivity of around 10^6 S m^{-1}.[20] The high thermal conductivity of carbon nanotubes along with Seebeck coefficient lower than traditional thermoelectric

materials renders them less effective for traditional Seebeck applications. However, the phenomenon of thermopower waves effectively exploits this property of high thermal conductivity to drive the heat from the exothermic fuel reaction along the length of the nanotubes to sustain a chemical reaction wave.

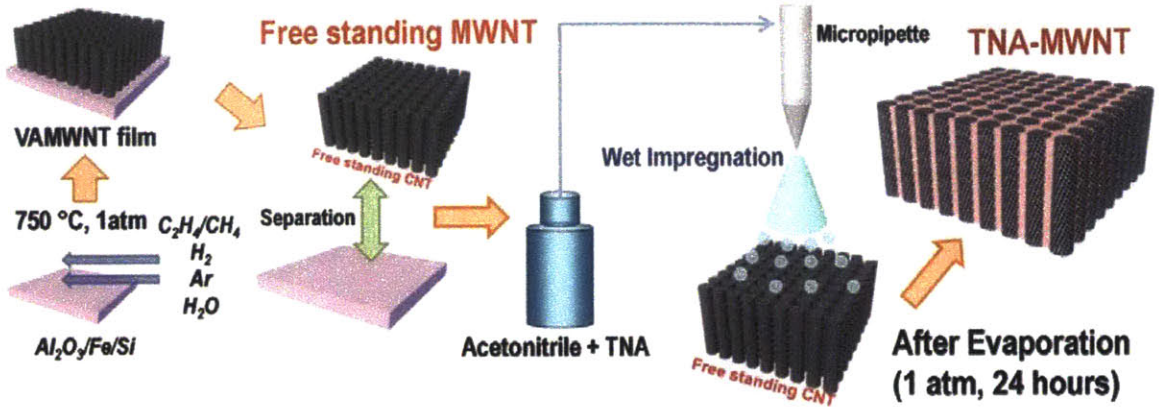

Figure 1-2 Schematic of the production of CNT-based thermopower wave generators using TNA solution in acetonitrile.[20] Reproduced and adapted from Ref 20 with permission from Elsevier Ltd.

The preparation of a thermopower generator (TWG) device involves coating a layer of fuel (cyclotrimethylene-trinitramine (TNA) in the example of Figure 1-2) onto a conduit. The schematic depicts multi-walled carbon nanotubes (MWCNTs) as the conduit, although as mentioned before, single-walled nanotubes (SWNTs) also support thermopower waves.[2,4] The fuel, TNA, is dissolved in acetonitrile, impregnated into the MWCNT array, and allowed to dry.[20] A small amount of an initiator, in this case sodium azide (NaN_3), is also added because it reacts exothermically with a lower energy of activation, thus requiring less input energy. The chemical structures of fuels, NaN_3, and acetonitrile used in TWGs are shown in Figure 1-3.

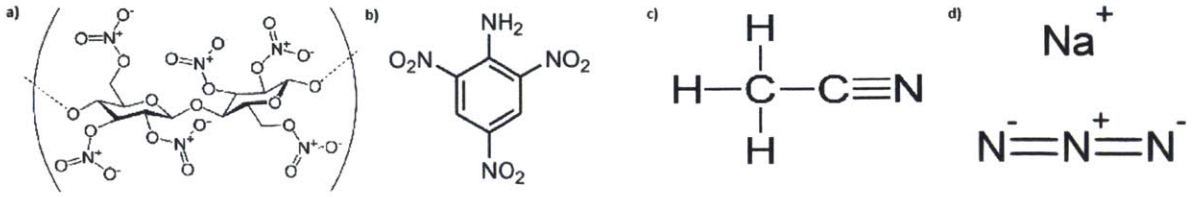

Figure 1-3. Chemical structures of compounds used for thermopower waves experiments a. Nitrocellulose b. 2, 4, 6-Trinitroaniline or picramide c. Acetonitrile d. Sodium Azide

As shown in Figure 1-4, in a TWG, the fuel-coated conduits are connected to copper tape electrodes with silver paste.

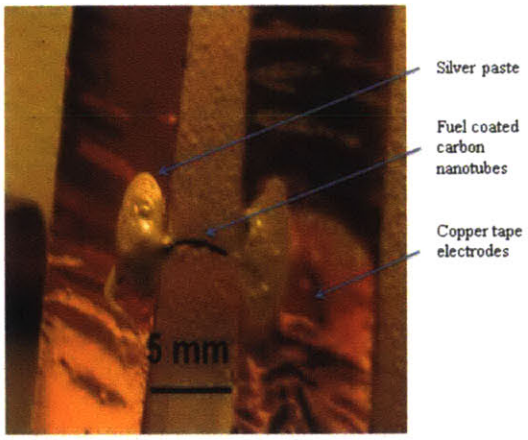

Figure 1-4. A typical TWG consisting of fuel-coated carbon nanotubes.[4] Silver paste is used to connect CNTs to copper tape electrodes, through which an oscilloscope can measure voltage output. Reproduced and adapted from Ref 4, with permission from American Chemical Society.

A thermopower wave is initiated with an external ignition source such as a butane torch, joule heater, or laser, helping the sodium azide overcome its reaction barrier.[20] Exothermic reaction of sodium azide provides initiation for the fuel reaction. The fuel reacts and releases heat, which is then accelerated forward because of the high thermal conductivity of the CNTs. This heat now

ignites the fuel that lies in its path, and thus a continuous reaction wave is sustained. Figure 1-5 shows a schematic of how heat propagates in a CNT–TNA system once a self-propagating TNA reaction wave is launched.

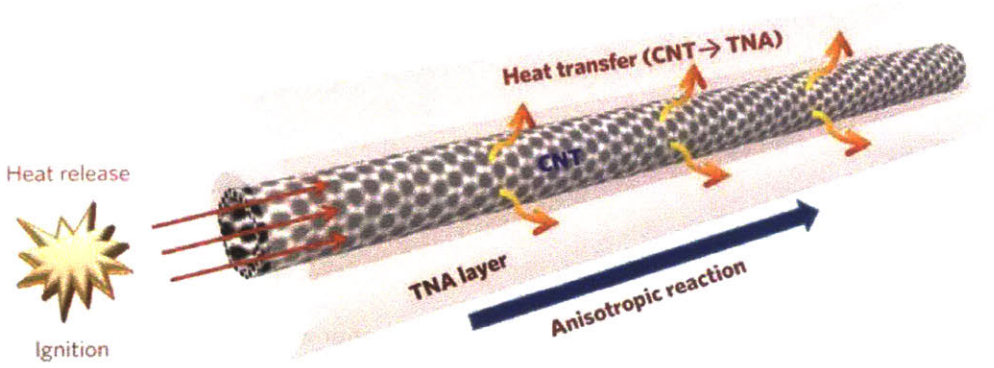

Figure 1-5. Schematic of the principle of thermopower waves. A self-propagating reaction wave is initiated by means of a heat source and is sustained because of high thermal conductivity of CNTs.[2] Reproduced and adapted from Ref 2, with permission from Nature Publishing Group.

Because of electron-phonon coupling exhibited by carbon nanotubes, we also obtain an electrical output.[2] Examples of experimentally obtained voltage outputs are shown in Figure 1-6. Depending on the direction of the wave propagation, the polarity of the voltage can be positive or negative.[2]

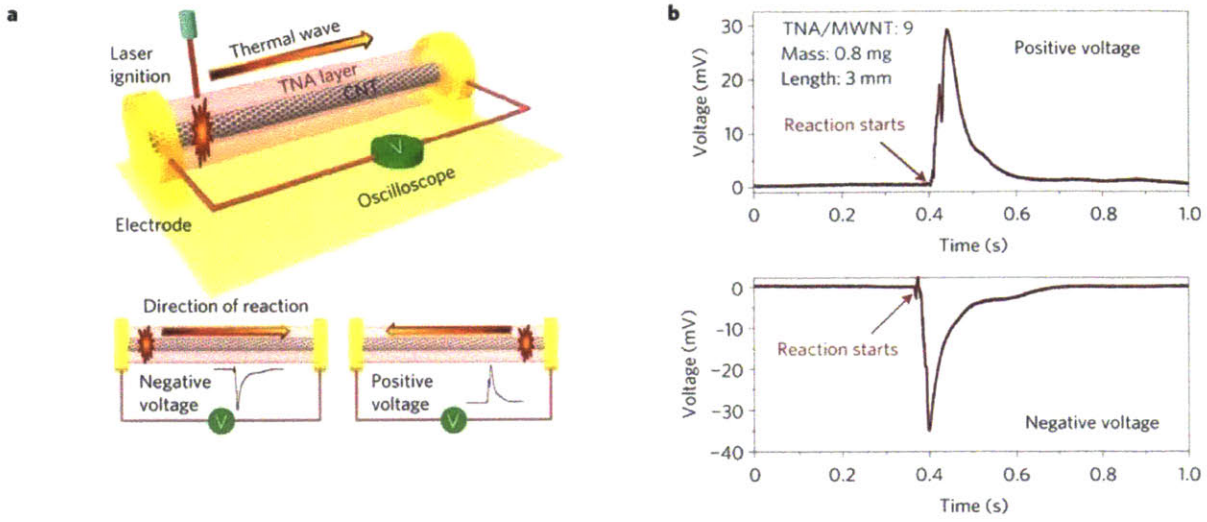

Figure 1-6. Electrical output obtained by operation of a thermopower wave device. a) Schematic of a thermopower waves device and dependence of the voltage output polarity on the reaction wave direction. b) Actual voltages obtained during thermopower waves experiments.[2] Reproduced and adapted from Ref 2, with permission from Nature Publishing Group.

1.4 Covalently functionalized carbon nanotubes as thermopower conduits

Diazonium chemistry was used to synthesize single-walled carbon nanotubes decorated with mono-, di-, and trinitrobenzenes, with the purpose of increasing the energy density of the carbon nanotubes.[4] Differential scanning calorimetry revealed the effect of covalent functionalization of nanotubes on the reaction activation energy, which was lower at lower values of conversion. Covalent bonds to the nanotube lattice can create defects that tend to scatter electrons and phonons and thus reduce electrical and thermal conductivity, both of which are essential for thermopower wave propagation. Figure 1-7 shows the increase in the disorder (D) mode in Raman spectroscopy due to covalent functionalization of nanotubes. Fourier Transform - Infrared (FT-IR) spectra confirmed attachment of nitro groups on these carbon nanotubes.[4]

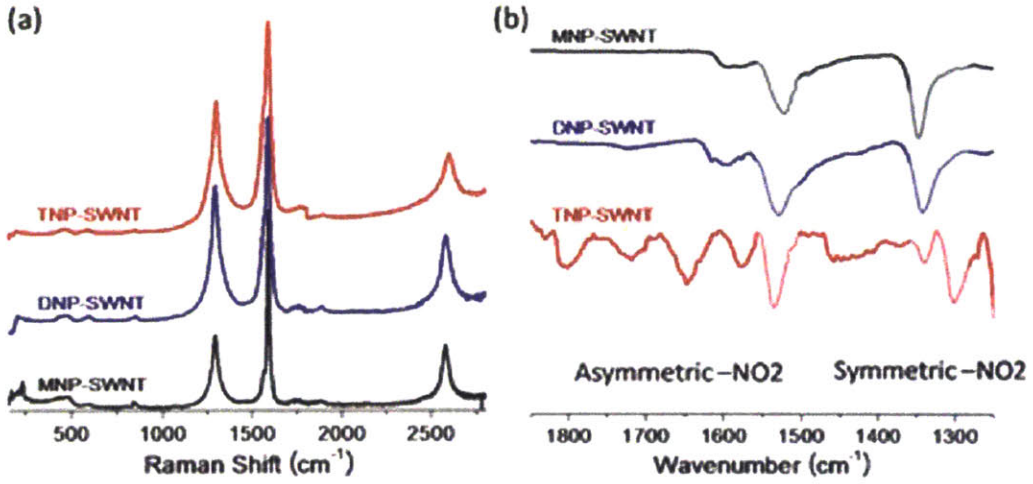

Figure 1-7. Raman and FT-IR analysis of energetically decorated SWNTs (a) Raman spectra show an increase in disorder modes after covalent functionalization with any of three nitrophenyl species. (b) FT-IR spectra using ATR (attenuated total reflectance) confirmed presence of nitro groups in thin films. MNP-, DNP-, and TNP-SWNTs stand for mono-, di-, and trinitrophenyl-functionalized SWNTs, respectively.[4] Reproduced from Ref 4, with permission from American Chemical Society.

Work by Chakraborty et al. shows that electrical resistivity of single-walled CNTs increases almost three-fold post functionalization by mono-nitrophenyl (MNP).[21] Heating the samples to 500^{O}C under ultra-high vacuum showed the electronic changes caused by functionalization to be reversible.[21] Thermopower experiments however showed that it was possible to launch thermopower waves and produce electrical power from such nitrobenzene functionalized conduits. The electrical power generated was affected little by functionalization. Also, both the reaction wave velocity and the specific power did not show a drastic decrease after functionalization. Thus, though the electrical[21] and thermal conductivities of functionalized CNTs might be lower than that of bare CNTs, the values are still high enough to allow propagation of a thermopower wave. Raman spectroscopy on functionalized conduit samples before and after thermopower wave reaction shows a reduction in the ratio of intensity of D peak

to G peak i.e. D/G ratio after the reaction wave has passed over the conduit. D/G ratio is indicative of the number of defects present in the sample being analyzed. Through this Raman analysis, we can infer that reaction wave breaks the covalent bonds attaching the functional groups to the carbon nanotubes, thus leading to fewer defects after reaction.

1.5 The effect of thermal conductivity of thermopower conduits

The effect of thermal conduits of different values of thermal conductivity has been studied. Terracotta (k = 1 W m^{-1} K^{-1}, low thermal conductivity) and alumina, Al_2O_3 (k = 20 W m^{-1} K^{-1}, comparatively higher thermal conductivity) were chosen for the comparison.[6] Additionally, a layer of Bi_2Te_3 (bismuth telluride), a thermoelectric material, was deposited on top of the thermal conduit to generate voltage from its high Seebeck coefficient (287 μV K^{-1}) and high electrical conductivity on the order of 10^5 S m^{-1}.[6,7] The Bi_2Te_3 layer must be thin for the heat transfer to be dominated by the thicker conduit layer beneath it. Bi_2Te_3 films were sputtered onto both the conduits. The fuel layer is deposited on top of the Bi_2Te_3 for direct heating and maximal voltage generation. Nitrocellulose was used as fuel and NaN_3 was used as initiator for the reaction.[6] These devices are shown schematically in Figure 1-8.

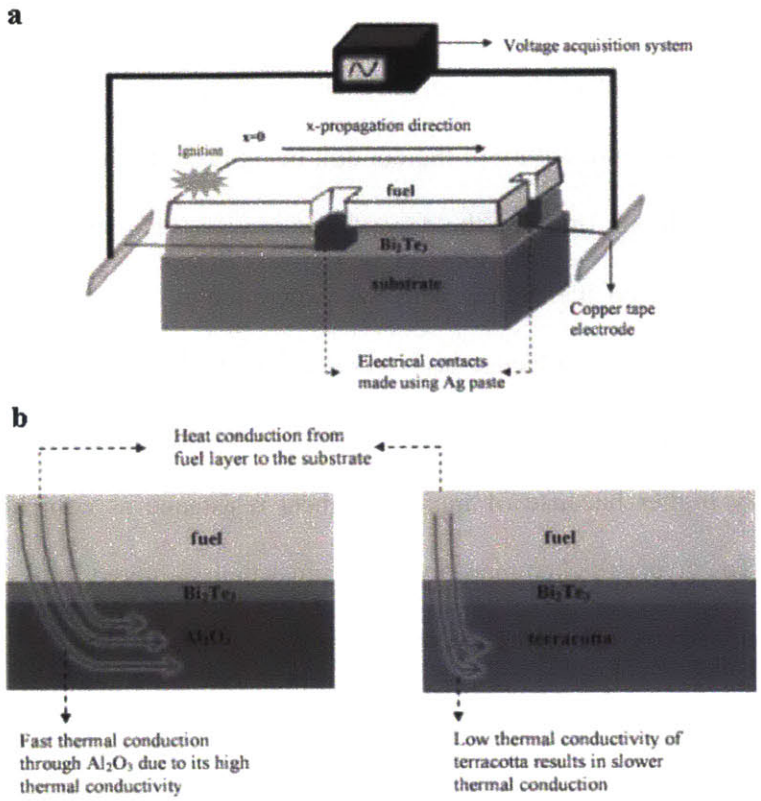

Figure 1-8. Nitrocellulose / Bi_2Te_3 / Thermal conduit configuration for thermopower waves studies. a) Schematic of experimental setup. b) Schematic of heat conduction from the fuel to the conduit layer and the effects of conduit thermal conductivity.[6] Reproduced from Ref 6, with permission from John Wiley and Sons.

Thermopower wave experiments using both the conduits were carried out and the voltage output and wave velocity studied. Experiments using the Al_2O_3 conduit showed oscillations in velocity and voltage. The average velocity of these waves was around 0.01 to 0.9 m s^{-1}, with the median value being around 0.4 m s^{-1}.[6] These large velocity devices generated voltages in the range of 40 to 150 mV, with power output up to 10 mW. Experiments with varying mass of fuel showed 24-27 mg of fuel to be the optimum range to obtain maximum voltage and power.[6] Study of systems using terracotta as conduit showed no oscillations in wave velocity, with average value of

velocity around 0.01 m s^{-1}.[6] Thus, wave velocity of the self-propagating reaction wave and presence or absence of oscillations in velocity and voltage output was found to be highly dependent on the thermal conductivity of the conduit being used. In the forthcoming section, we discuss the analytical solution studying the dependence of wave velocity on thermal conductivity of the conduit and how well it matches with the experimental observations. Also, a study of effect of thickness of the thermoelectric layer showed that both 10 μm and 5 μm thick Bi_2Te_3 films showed similar trends in the voltage generated. Voltage output from the 10 μm Bi_2Te_3 device was slightly higher because of increased sheet resistance as compared to the thinner Bi_2Te_3 layer.[6] Bi_2Te_3 layers thicker than about 30 μm when sputtered onto Al_2O_3 reduced the overall thermal conductivity leading to no oscillations in the voltage output.

1.6 Effects of P-type and N-type thermoelectric materials in thermopower conduits

To exploit thermoelectric materials with higher Seebeck coefficients than that of CNTs, TWGs were made with bismuth telluride (Bi_2Te_3), an n-type thermoelectric (Seebeck coefficient = 287 μV K^{-1}), and antimony telluride (Sb_2Te_3), a p-type thermoelectric (Seebeck coefficient = 243 μV K^{-1}), referring to their majority carriers of electrons and holes, respectively.[6] Here again, experiments were repeated with two base thermal conduits, alumina and terracotta. The experimental setup is similar to that shown in Figure 1-8 a. Changing the type of thermoelectric reverses the polarity of the voltage output. As observed before, using nitrocellulose with sodium azide as the fuel and alumina as the conduit generated oscillating voltage for the duration of wave propagation.[6] Figure 1-9 shows typical voltage outputs from both thermoelectric materials. Reaction waves on Sb_2Te_3 are faster, with mean reaction propagation velocities of about 660 mm

s^{-1} compared to about 210 mm s^{-1} for Bi_2Te_3 devices.[7] This was attributed to Sb_2Te_3 having a thermal conductivity that is almost 2.5 times that of Bi_2Te_3.

Both Sb_2Te_3 and Bi_2Te_3 systems produced high-power pulses, 0.6 kW kg^{-1} and 1.0 kW kg^{-1}, respectively.[7] This work shows that certain conduit properties can lead to oscillating voltage.[6,7] It also opens avenues for generating alternating voltage output from thermopower wave devices by using p-type and n-type semiconductors simultaneously as conduits.

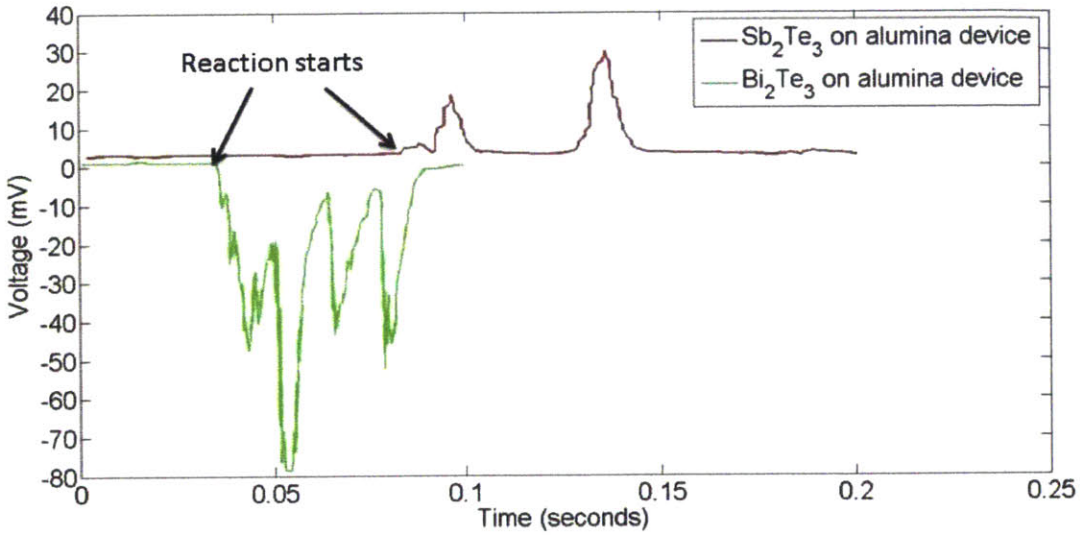

Figure 1-9. Oscillatory voltage output from thermopower waves devices using Sb_2Te_3 on alumina and using Bi_2Te_3 on alumina. Adapted from Ref 7.

1.7 ZnO thermal conduits

Recent work incorporated zinc oxide in a TWG device. ZnO has a high Seebeck coefficient of about -360 μV K^{-1} at 85 °C, high thermal conductivity of about 15 W m^{-1} K^{-1} at 300°C, and high electrical conductivity at elevated temperatures.[8] A ZnO film was deposited on an alumina conduit, followed by a fuel layer of nitrocellulose and sodium azide. The reaction was initiated

using a fine-tip butane torch, and produced voltage pulses as large as 500 mV.[8] Here again, wave propagation gave rise to oscillating voltage output. Power output from some devices was as high as 1 mW with device efficiencies around 0.2%.[8]

The efficiency of a TWG device is the ratio of the electrical power output to the heat energy released from the exothermic chemical reaction.

$$\% \text{ Efficiency} = \frac{\text{Electrical power output}}{\text{Energy released due to the fuel chemical reaction}} \times 100$$

$$\therefore \% \text{ Efficiency} = \frac{\int \left(\frac{V^2}{R_C} \right) dt}{m(-\Delta H)} \times 100 \tag{3}$$

Here, V is the voltage output, R_c is the electrical circuit load, m is the mass of the fuel reacting and $(-\Delta H)$ is the exothermic heat of reaction. Although the overall energy conversion efficiency of TWG devices is <1%, they are able to provide large voltage pulses for applications requiring energy to be released over short durations, unlike batteries or fuel cells.

Recent work has also been carried out using the solid fuel of collodion (5% nitrocellulose) with ZnO nanostructure based thermal conduits consisting of ZnO nanorods- and cube-like nanoparticles-based hybrid composites and has shown thermopower wave output voltage as high as 3V.[11]

1.8 Analytical solution of equations governing one dimensional thermopower waves

The governing analytical equations of thermopower waves have been further studied. For solid fuels, the mass diffusion is negligible, and hence that term can be neglected. Using a reaction

term with a 1st order Arrhenius form for the fuel reaction and using Fourier's law for heat diffusion, coupled heat and mass balance equations can be set up as below:

$$\rho C_p \frac{\partial T}{\partial t} = k \frac{\partial^2 T}{\partial x^2} - (\Delta H\, k_o Y)\, e^{-\frac{E_a}{RT}} \tag{4}$$

$$\frac{\partial Y}{\partial t} = -(\, k_o Y)\, e^{-\frac{E_a}{RT}} \tag{5}$$

Here, ρ is the fuel density, T is the temperature, C_p is the specific heat of the fuel, k is fuel thermal conductivity, x is the distance or space coordinate, $(-\Delta H)$ is the exothermic heat of reaction, k_0 is Arrhenius pre-factor, E_a is the activation energy of the fuel reaction, R is the universal gas constant and Y is mass concentration of the fuel.[14] Coupled heat and mass balance equations are widely applicable to many other fields, such as high temperature self-propagating synthesis reactions. Non-dimensionalizing the above set of equations simplifies them:

$$\frac{\partial u}{\partial \tau} = \frac{\partial^2 u}{\partial \xi^2} + y e^{-\frac{1}{u}} \tag{6}$$

$$\frac{\partial y}{\partial \tau} = -\beta y e^{-\frac{1}{u}} \tag{7}$$

Here, $u = (R/E_a)T$ is the non-dimensional temperature and $y = Y/\rho$ is the non-dimensional fuel concentration. Similarly, $\xi = x[\left(\frac{\rho C_p}{k}\right)\left(\frac{(-\Delta H)k_o R}{C_p E_a}\right)]^{1/2}$ is the non-dimensional space coordinate and $\tau = \left(\frac{(-\Delta H)k_o R}{C_p E_a}\right) t$ is the non-dimensional time. The new parameter that arises due to this non-dimensionalization is $\beta = \frac{C_p E_a}{(-\Delta H)R}$. β corresponds to the (dimensionless) inverse adiabatic reaction temperature rise, the temperature behind the wave front during steady state adiabatic reaction wave propagation. Thus, ideally, the (non-dimensional) temperature difference that leads to the traditional Seebeck voltage output from thermopower wave generators is $1/\beta$.

Solving the above non-dimensional equations (6) and (7) using numerical methods and assuming ideal adiabatic boundary conditions showed the temperature profiles $u(\xi)$ to be unchanging in shape with respect to time.[14,22,23] Examples of the numerically calculated temperature profile as a function of time and space are shown in Figure 1-10.

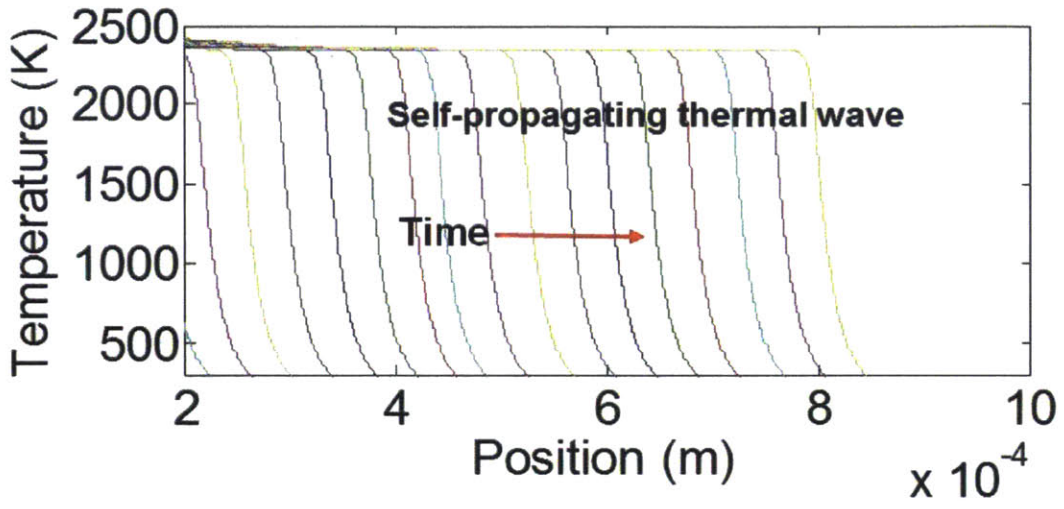

Figure 1-10. Examples of numerically simulated temperature waves. The different color curves in the diagram represent the temperature at different time points.

The waves propagate with constant velocity for certain values of β. In order to solve this equation, a new variable η was introduced to combine the time and distance of propagation.

$$\eta = \xi - ct \tag{8}$$

Here c is the constant wave velocity.

A logistic wave function can describe the wave form observed during numerical simulations. Thus, we set

$$u(\eta) = \frac{u_{max}}{(1 + Qe^{s\eta})^{1/Q}} \tag{9}$$

Here, u_{max} is the maximum temperature behind the reaction wave front, and s is a parameter that affects the slope of the u growth. Q is a symmetry parameter and affects the curvature of the function near asymptotes. As mentioned before, $u_{max} = {}^{1}/_{\beta}$, which corresponds to the maximum possible temperature behind the wave front in event of adiabatic boundary conditions. On substituting this in the above set of non-dimensional equations, an equation for wave velocity was obtained:

$$c = e^{-(\frac{\beta}{2})(1+Q)^{1/Q}} \sqrt{\left(\frac{\beta}{2}\right)\left(-1 + (1+Q)^{\frac{1+Q}{Q}}\right)} \tag{10}$$

This equation holds for 1st order fuel reactions. One can then back-solve for $Q(\beta)$. An expression was obtained by empirical fitting.[14]

$$Q = 0.0061\beta^3 - 0.077\beta^2 + 1.2531\beta - 0.208 \tag{11}$$

The temperature profiles obtained from numerical solution and from the logistic form analytical solution are compared in Figure 1-11. A coupled system of heat and mass transfer equations under adiabatic boundary conditions is well described by the logistic functional form, especially for smaller β values. Above $\beta = 6$, the logistic form becomes less accurate as the wave velocity is no longer constant.

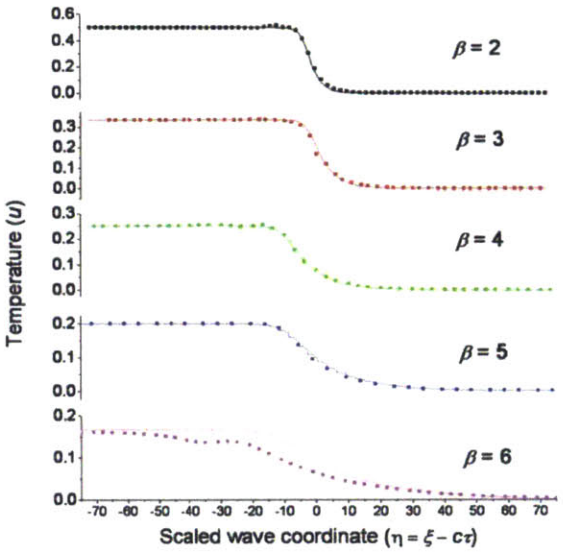

Figure 1-11. Analytical and numerical solutions using a logistic temperature profile. Analytical solutions are represented by lines, numerical solutions by points. The profiles match closely for several different values of β.[14] Reproduced from Ref 14, with permission from American Chemical Society.

1.9 Velocity oscillations in thermopower waves

The system of coupled mass and heat transfer equations shown above is a simplified set of equations considering the balances for only the fuel. A more rigorous approach incorporates the heat balance for the conduit as well. The non-dimensional equations used here are:

$$\frac{\partial u}{\partial \tau} = \frac{\partial^2 u}{\partial \xi^2} + (1-\omega)e^{-\frac{1}{u}} - \gamma_1(u-u_2) \tag{12}$$

$$\frac{\partial u_2}{\partial \tau} = \alpha_0 \frac{\partial^2 u_2}{\partial \xi^2} + \gamma_2(u-u_2) \tag{13}$$

$$\frac{\partial \omega}{\partial \tau} = \beta(1-\omega)e^{-\frac{1}{u}} \tag{14}$$

Here, u is the fuel temperature, u_2 is the conduit temperature and ω is the fuel amount that has been consumed i.e. $\omega = 1 - y$. τ, ξ and β have same meaning as before. γ_1, γ_2 and α_0 depend

on system properties like fuel and conduit thermal conductivities, interfacial conductance between the fuel and the conduit, conduit diameter, diameter of the fuel-conduit system, β, their densities and their molecular weights.[15]

Terms for heat transfer between the fuel layer and the carbon nanotubes must be included with a term for interfacial energy exchange.[15] With added complexity, the analytical solution above does not hold and the equations must be solved numerically to evaluate the wave velocity. This analysis shed light on the interesting phenomenon of oscillating wave velocity. Increasing β leads to increased amplitude of velocity oscillations but decreased fundamental frequency.[15] Wave front velocity simulations were carried out on a system of CNT wrapped by a TNA layer. Figure 1-12 shows results from this study where wave front velocity is studied as a function of β. As can be seen from the figure, the average velocity decreased with increase in β from 4 to 9. The nature of the velocity profile also undergoes drastic change as β changes. Starting with low amplitude velocity oscillations, the velocity becomes almost constant at about $\beta = 6$. Beyond $\beta = 7$, the wave velocity starts showing oscillations with varying regions of velocity having different frequencies of oscillations.

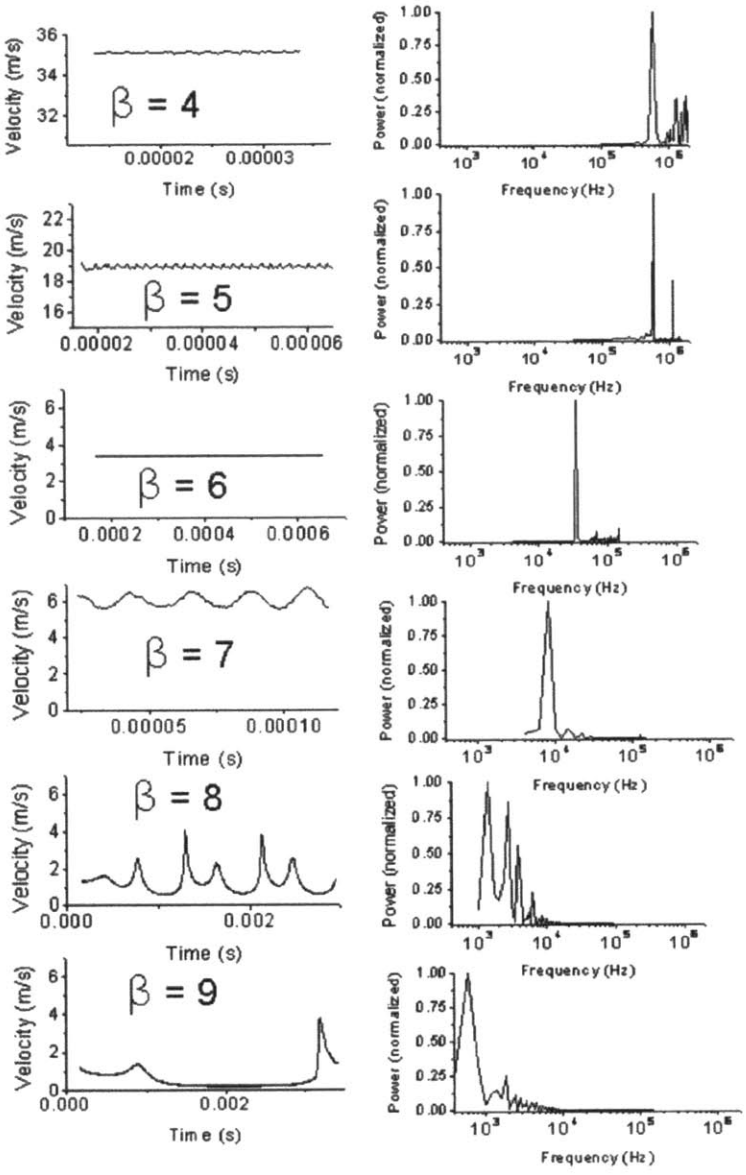

Figure 1-12. Variation of wave velocity over time and frequency spectra from different β values.[15] Reproduced from Ref 15, with permission from American Chemical Society.

Experimentally, β can be adjusted by changing the fuel. Experiments with TNA on MWNTs confirmed the theory of velocity oscillations,[15] followed by nitrocellulose with NaN_3 on Bi_2Te_3/alumina.[6] The output voltage and wave velocity were correlated, with voltage oscillating

during wave propagation, followed by a smooth return to baseline during conduit cooling. These results provide scope for developing nanoscale power sources with oscillating single polarity voltage by using appropriate combinations of fuel and conduit.

To explore the effects of the thermal conduit on the magnitude of voltage oscillations, the earlier work using Bi_2Te_3/alumina and Bi_2Te_3/terracotta conduits was also studied analytically with a system of non-dimensional heat and mass balance equations, similar to equations (6) and (7).[6] However, this analysis also included a parameter accounting for heat transfer from fuel to the conduit and the surroundings, so the system was not adiabatic. The modified non-dimensional equations are:

$$\frac{\partial u}{\partial \tau} = \frac{\partial^2 u}{\partial \xi^2} + y e^{-\frac{1}{u}} - l(u - u_a) \tag{15}$$

$$\frac{\partial y}{\partial t} = -\beta y e^{-\frac{1}{u}} \tag{16}$$

Here, l is a parameter for non-dimensional heat transfer and u_a is the ambient non-dimensional temperature.

$$l = \frac{hAE_a}{VR\rho(-\Delta H)k_0} \tag{17}$$

In equation (17), h is the heat transfer coefficient from the fuel to the surrounding and A/V is the surface area to volume ratio for the fuel.[6] Theoretical calculations yielded the combination of β and l values that lead to oscillations. Simulations showed that the conduit with higher thermal conductivity (alumina) showed oscillations in velocity, unlike the lower-thermal-conductivity conduit (terracotta). Also, an analytical expression obtained from literature was used to predict the wave velocity for terracotta conduit systems.[6]

$$c - \frac{l}{c} = \frac{1}{c} e^{-\beta} (e^{2l\beta/c^2} - e^{-\beta}) \tag{18}$$

Here, c is the wave velocity in m s^{-1}. Predicted and experimental wave velocities matched to an order of magnitude. Using equation (18), average wave velocity was estimated to be around 0.007 m s^{-1} for Bi_2Te_3 / terracotta system used with nitrocellulose and sodium azide fuel. As predicted by theory, experiments showed low and non-oscillating reaction wave velocities for fuel / Bi_2Te_3 / terracotta systems, with wave velocity of the order of magnitude of 0.01 m s^{-1}.[6] Thermopower waves propagate at 0.4 m s^{-1} in the Bi_2Te_3 / alumina system, with oscillations observed for samples with lower thickness of Bi_2Te_3 layers.[6]

1.10 Theory of excess thermopower: advantages of thermopower waves over traditional thermoelectric materials

In most TWG devices, despite using conduits such as CNTs with a relatively low Seebeck coefficient, the Seebeck effect still contributes somewhat to the output voltage during the exothermic fuel reactions. For $T_{rxn} \sim 1100$ K, which is representative of theoretical temperatures attained during thermopower experiments using nitrocellulose fuel, a traditional Seebeck effect alone would produce about 11 mV using CNTs.[3] This is much lower than typical voltage outputs of thermopower waves devices, which can generate voltage up to 220 mV using CNT conduits.[3] Mathematically, the Seebeck effect expression is derived from Boltzmann transport equation for carriers:

$$J = \sigma_h \left(E + \frac{\Delta\mu}{e} \right) + L_{12} \nabla T \tag{19}$$

where J is current density, σ_h is electrical conductivity, E is electric field, μ is chemical potential, e is the elementary charge, L_{12} is an Onsager coupling coefficient, and T is temperature. In the conventional thermoelectric treatment, in the limit of zero current density, we obtain

$$V = \int_{x_L}^{x_R} \left(\frac{\Delta\mu}{e} - \frac{L_{12}}{\sigma_h} \nabla T \right) dx \tag{20}$$

Here, V is the voltage difference and x_L and x_R represent the positions for electrical measurements at the two ends of the device. Most of the experiments in thermoelectricity do not involve changing chemical potential and thus lead us to a simplified equation for voltage generated as

$$V_{TE} = \int_{x_L}^{x_R} \left(\frac{L_{12}}{\sigma_h} \nabla T \right) dx \sim \Gamma_s (\Delta T) \tag{21}$$

The 'excess power' observed during thermopower waves' experiments was found to be correlated to doping in the CNTs. CNTs coated in fuels showed shifts in the G^- peak position of Raman spectra, correlated to changes in carrier concentration, which in turn affect the chemical potential. Excess power observed during thermopower waves can be described as

$$P_{xs} = P_{out-} P_{TE} = \frac{V_{out}^2}{R_c} - \frac{V_{TE}^2}{R_c} \tag{22}$$

Here, V_{out} is the actual voltage output, V_{TE} is the thermoelectric prediction and R_c is the circuit load. The G^- peak position shifted by as much as 5 cm^{-1} when comparing fueled and bare CNTs, which translates to about 25 holes/μm doping and up to 100 mV additional voltage difference.[3] Figure 1-13 shows the shift in position of the G^- peak during the process of making thermopower devices. As can be seen, addition of the fuel picramide (PA) and the initiator (NaN_3) leads to a

shift in the position of G^- peak. Also, from Figure 1-13, experiments studying the ratio of the mass of the adsorbed fuel to the mass of carbon nanotubes show a rough increasing trend for improved maximum voltage with increasing adsorption ratio.

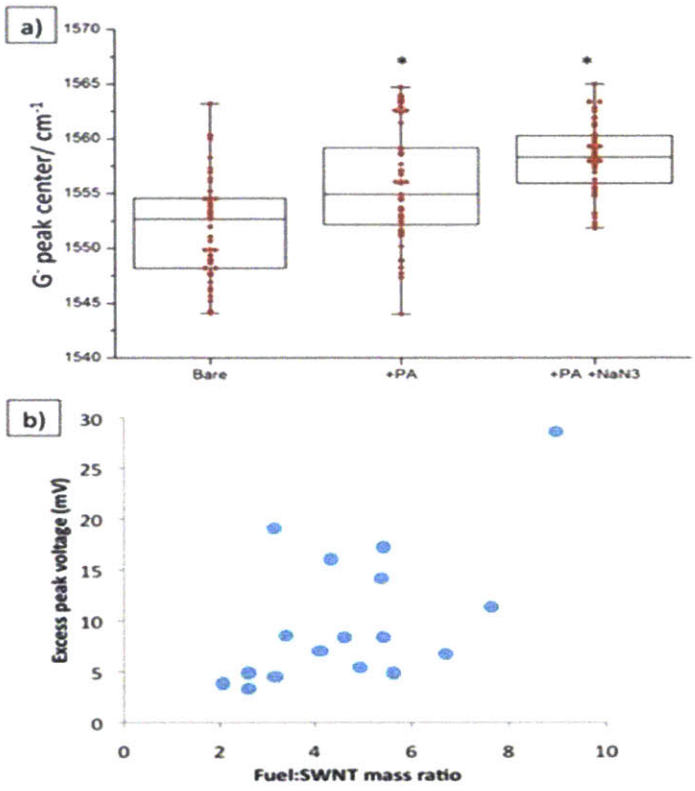

Figure 1-13. Excess thermopower from fuel doping. a) A shift of about 5 cm^{-1} in G peak position is observed on fuelling the CNTs (left to right). Boxes show the middle quartiles of the Raman measurements, and the arms show the maxima and minima. b) Excess peak voltage generally increases with increased fuel loading (defined as ratio of fuel mass to SWNT mass), which could stem from increased doping from the fuel.[3]

Thus a possible explanation for excess thermopower is that the change in chemical potential because of adsorption of the fuel followed by desorption during the chemical reaction leads to changing chemical potential across the electrical measurement terminals. A TWG exploits non-zero $\Delta\mu$ to lead to additional voltage output.[3]

The theory of excess thermopower tries to explain how the voltage generation of thermopower wave devices exceeds that of a comparable thermoelectric device and suggests methods for improving efficiency by suitably doping the conduits.

1.11 Conclusion

We have reviewed thermopower waves, a new approach to using chemical reactions to produce electricity. Current experiments have been predominantly carried out using highly exothermic fuels like TNA and nitrocellulose and conduits with high thermal and electrical conductivities. Experiments have been conducted exploring different fuels and conduits with varying thermal and electrical properties, which influence the voltage output's magnitude and oscillatory behavior. The logistic function was found to be a good analytical solution describing these self-propagating thermal waves. Thermopower waves look to be a promising technology for nanoscale power sources providing high power in short periods of time.

Chapter 2 Superadiabaticity in Reaction Waves as a Mechanism for Energy Concentration

Mahajan, S. G.; Abrahamson, J. T.; Birkhimer, S.; Friedman, E.; Wang, Q. H.; Beck, M.; Strano, M. S., Superadiabaticity in reaction waves as a mechanism for energy concentration. Energy & Environmental Science ***2014,*** *7 (10), 3391-3402.*

Reproduced by the permission of the Royal Society of Chemistry

2.1 Introduction

In an exothermic reaction, the maximum temperature that can be attained is bounded by the adiabatic reaction limit.[24,25,26] The adiabatic temperature rise, similar to the adiabatic flame temperature[26] or adiabatic combustion temperature of a system,[27] corresponds to the condition at complete chemical conversion whereby the enthalpy of reaction is translated into sensible heat of the product mixture without phase change. This limiting temperature is an inherent reactant property and determined exclusively by thermodynamics. Reaction temperature, in turn, is central to energy conversion mechanisms for a variety of reasons. It sets the high temperature reservoir for Carnot efficiency via the 2nd law of thermodynamics.[28,29,30] It also determines the relative weighting of thermal energy transport mechanisms with poor efficiency such as conduction against those of high efficiency such as radiation.[31,32,33] For many energy conversion technologies, such as thermoelectrics,[29,30] thermophotovoltaics,[34,35,36] and combustion synthesis,[27] performance metrics such as efficiency, power density or final product properties are governed by temperature. In these processes, their overall efficiency increases with increased temperature. Hence, mechanisms that concentrate thermal energy and elevate temperature have utility in such conversion technologies.

Reaction waves feature prominently in the analysis of combustion synthesis or solid phase materials synthesis,[27,37] and more recently as an electrical energy generation mechanism in thermopower waves.[2] Reaction waves exhibiting self-propagation have been previously studied by Zeldovich and Frank-Kamentskii who investigated flame propagation for gaseous mixtures.[23,38] Abrahamson *et al.* studied 1D reaction waves for solid fuels and found an analytical expression for the system temperature.[14] Ji-Huan He performed an analysis to obtain an expression for the condition to obtain oscillatory thermal waves in a non-adiabatic system.[16] Weber *et al.* obtained expressions for temperature profiles of the reaction wave front for both gaseous and solid fuels.[22] Numerical analysis of the governing heat and mass balance equations was also carried out by Weber *et al.*,[22] Mercer *et al.*[39,40,41] and Gray *et al.*[38]

In this work, we identify for the first time the property of superadiabaticity that occurs when a reaction wave in either one dimension (1D) or two dimensions (2D) impinges upon an adiabatic boundary under specific but broadly applicable conditions, leading to a temperature rise above the adiabatic limit. Superadiabaticity is shown to enable the concentration of thermal energy, increasing the reaction temperature to up to 1.8 times the adiabatic limit. For example, for an energetic material like nitrocellulose which shows an adiabatic temperature rise of about 1100 K, superadiabatic temperatures up to 2000 K are possible. This superadiabaticity can form the basis of new energy conversion schemes. Thermal radiation is a transfer mechanism more easily captured and efficiently converted than conduction. Increasing the temperature will allow us to effectively harvest an increased amount of energy transported via radiation by using high efficiency energy conversion technologies such as photovoltaics. In this work, we propose how a thermophotovoltaic wave system can be used to convert chemical energy to electrical energy with efficiency and power density predicted to increase for superadiabatic conditions.

We begin by reviewing past work in the field of numerical analysis of reaction waves. Then, we demonstrate our new finding of superadiabaticity by numerical analysis of different types of reaction systems. Finally, we demonstrate the operation of a thermophotovoltaic wave system for energy conversion from chemical to electrical energy.

2.2 Introduction to reaction waves for energy conversion

In this section, we review previous work on reaction waves, specifically their temperature and velocity when propagating at steady state. We discuss results for numerical analysis of 1D reaction waves and 2D reaction wave systems simplified to 1D systems. The equations presented in this section act as a precursor for our analysis of superadiabaticity.

Consider a reaction wave propagating in a 1D incompressible, immobilized medium according to 1st order reaction kinetics without phase change. The corresponding version of Fourier's law that applies is shown in equation (1):

$$\rho C_p \frac{dT}{dt} = k\frac{\partial^2 T}{\partial x^2} + (-\Delta H)k_0 W e^{-\frac{E_a}{RT}} \tag{1}$$

$$\frac{dW}{dt} = -k_0 W e^{-\frac{E_a}{RT}} \tag{2}$$

In the heat transfer equation (1),ρ is the density of fuel, C_p is the specific heat of the fuel, T is the temperature, x is the distance coordinate, k is the thermal conductivity of the fuel, $(-\Delta H)$ is the exothermic heat of reaction, k_o is the first order reaction constant and E_a is the activation energy of the fuel reaction. In the mass transfer equation (2), W is the mass concentration of the fuel. The Arrhenius form of rate constant is used for the assumed 1st order reaction mechanism for fuel reaction. For solid fuels, the diffusion term in the mass balance equation is ignored. Both of

these equations are non-dimensionalized to give the following non-dimensional variables: temperature u, time τ, mass w, and distance ξ.

$$u = \frac{R}{E_a}T,\ \tau = \frac{t(-\Delta H)Rk_0}{C_pE_a} = \frac{tk_0}{\beta},\ w = \frac{W}{\rho},\ \xi = x\left[\left(\frac{\rho C_p}{k}\right)\left(\frac{(-\Delta H)k_0R}{C_pE_a}\right)\right]^{\frac{1}{2}} \tag{3}$$

The non-dimensional governing equations for heat and mass transfer are equations (4) and (5):

$$\frac{\partial u}{\partial \tau} = \frac{\partial^2 u}{\partial \xi^2} + we^{-\frac{1}{u}} \tag{4}$$

$$\frac{dw}{d\tau} = -\beta we^{-\frac{1}{u}} \tag{5}$$

While the adiabatic temperature rise for a reaction accounts for the specific heat capacity of the reaction mixture, traditional numerical analysis of self-propagating reaction waves analyzing systems based on solid fuel define the adiabatic temperature rise as 1/β which depends only on the reacting solid fuel's properties.[14,41,15]

Hence, the inverse non-dimensional adiabatic temperature rise in the system after the fuel has completely reacted is represented by β where $(-\Delta H)/C_p$ is the dimensional adiabatic temperature rise.[14]

$$\beta = \frac{C_pE_a}{(-\Delta H)R} \tag{6}$$

We exclude the case of a phase change as the reaction proceeds from reactants to products. The adiabatic temperature rise can be either found experimentally by using a calorimeter or calculated analytically by assuming an exothermic reaction and its products. Values of the adiabatic temperature rise for various fuels have been calculated by Hada *et al.*[25]

Abrahamson *et al.* performed a numerical analysis of this system of equations for 1D self-propagating waves for solid fuels by using COMSOL, a finite element method software for partial differential equations.[15] An analytical expression for the reaction wave temperature profile, u_{ana}, was found using a logistic function.[14,15] We make use of this expression when studying superadiabaticity in an adiabatic batch reactor system.

$$u_{ana} = \frac{1/\beta}{(1 + Qe^{cQ(\xi - c\tau)})^{1/Q}} \tag{7}$$

In equation (7), c is the constant reaction wave front velocity. Here, $Q=f(\beta)$ is a system property and is related to the curvature of the temperature profile near the asymptotes and informs the wave symmetry at the reaction front. This analytical expression for the steady wave, u_{ana}, was used with the non-dimensional form of the equations along with Dirichlet boundary conditions to obtain an expression for the wave velocity c:

$$c = e^{-(\frac{\beta}{2})(1+Q)^{1/Q}} \sqrt{\frac{\beta}{Q}\left[-1 + (1+Q)^{\frac{(1+Q)}{Q}}\right]} \tag{8}$$

Also, an expression for $Q(\beta)$ was obtained by empirical analysis.

$$Q = 0.0061\beta^3 - 0.077\beta^2 + 1.2531\beta - 0.208 \tag{9}$$

Choi *et al.* introduced the experimental realization of the concept of thermopower waves to convert chemical energy to electrical energy using self-propagating chemical reaction waves.[2] While that work mainly focused on multi-walled carbon nanotubes as thermal conduits, there have been other advances in the field of thermopower waves. As described in a recent review paper on thermopower waves,[42] apart from multi-walled carbon nanotubes, other conduits such as single-walled carbon nanotubes,[4,3] ZnO,[8] Bi_2Te_3 on alumina and terracotta,[6] Sb_2Te_3 on alumina and terracotta,[7] MnO_2 on alumina[9] and Sb_2Te_3 on carbon nanotubes[12] have also been

tested for launching thermopower waves. All these systems have a common feature of self-propagating reaction waves launched on thermal conduits with specific thermal and electrical properties, and all such waves can be theoretically described by simplified system of equations given by equations (4) and (5).

Recently, Ji-Huan He performed analysis on various systems of equations that model soliton waves,[16] which are the solution to non-linear partial differential equations that give rise to non-diffusive waves.[16] The analysis carried out by Abrahamson *et al.* is one example of a soliton wave. The non-diffusive nature of such reaction waves is the cause of adiabatic temperature rise being maintained in the region behind the reaction wave front. Ji-Huan He performed an analysis of modified system of equations by accounting for heat loss from the thermal wave as it moves ahead and found the condition that gives rise to oscillatory waves.[16]

Weber *et al.* performed an asymptotic analysis of a system of equations for a 1D system accounting for heat loss in systems containing gaseous and solid fuels. They derived expressions for temperature in the region far away ahead of and behind the wave front as a function of position and time.[22] Similarly, expressions predicting wave velocity were found to be dependent only on the value of β for both gaseous and solid fuels.

Numerical and asymptotic analyses have also been performed for 2D reaction waves. Work by Mercer *et al.* studied a generalized system of equations representative of a 1st order reaction occurring in a 2D system.[39] To study these dependent partial differential equations, a numerical analysis was carried out by a conventional finite difference scheme for the spatial coordinates and an Euler scheme for the time variable. Numerical analysis was also carried out by reducing the 2D model to a 1D model by using 'center-manifold analysis'. Results obtained from both

methods of analyses support the existence of self-propagating reaction waves in 2D. The wave velocity analyzed using both these approaches i.e. numerical analysis and center-manifold analysis showed good agreement.[39] Mercer *et al.*[40,41] and Gray *et al.*[38] have also performed numerical analysis on a system of self-propagating exothermic reaction waves.

In this paper, we study such reaction waves when impeded by an adiabatic boundary. Under certain system conditions, our numerical results show the system temperature rising beyond the adiabatic temperature for both 1D and 2D reaction waves. We have formulated an analytical expression that shows superadiabaticity to be a function of the thermochemical properties of the fuel and wave heat transfer properties. We conclude by performing calculations to show how superadiabaticity can be used to establish a new thermophotovoltaic wave system which can operate at higher energy conversion efficiency because of the improved focusing of heat energy by superadiabaticity.

2.3 Numerical analysis of superadiabatic temperatures shown by various fuel configurations with an adiabatic boundary

A self-propagating reaction wave system can be visualized and studied in a variety of fuel and system configurations. We began our study of superadiabaticity in reaction waves by considering a simple system of a single batch reactor being initiated by a 1D reaction wave.[14] This was followed by studying increasingly complex reaction wave systems such as multiple batch reactors in series, a 1D layer of fuel and a 2D fuel layer, each with a simple Gaussian heat input and an adiabatic boundary.

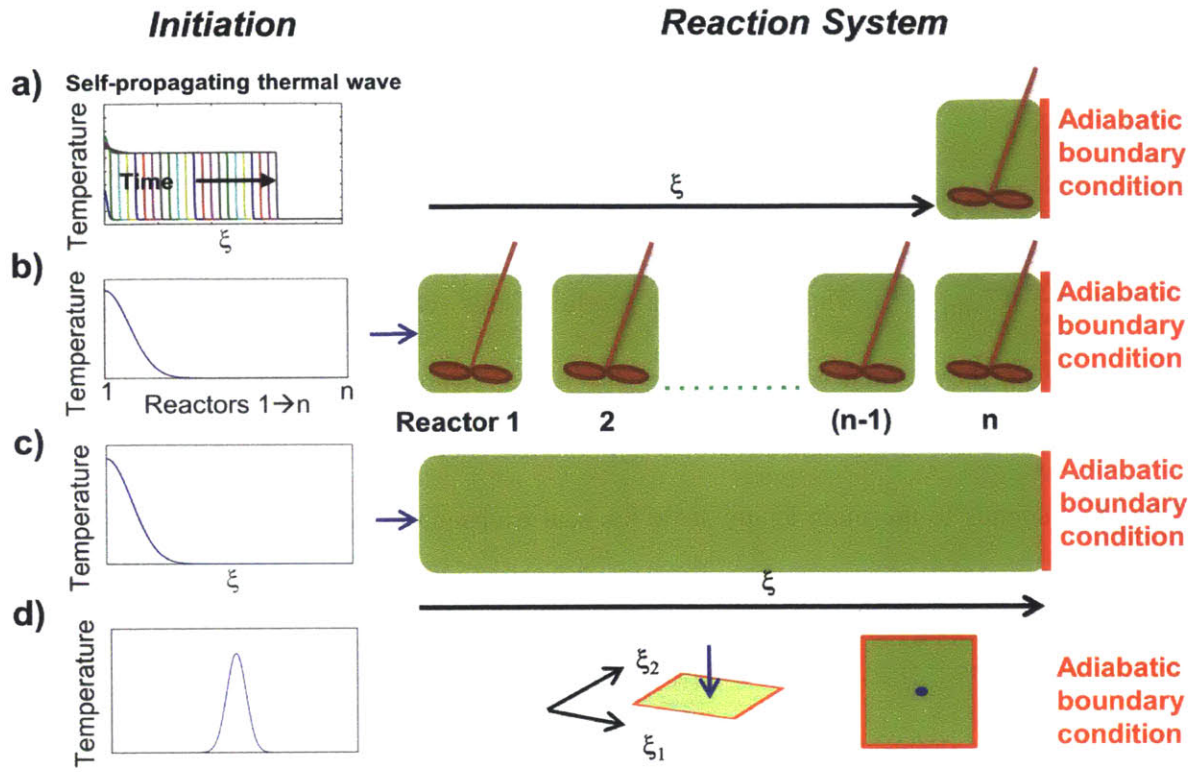

Figure 2-1 Schematic of various reactor configurations used to illustrate superadiabaticity. a) A batch reactor with adiabatic boundary, receiving heat input from a 1D self-propagating reaction wave. b) Multiple batch reactors in series used to simulate a self-propagating reaction wave. Only the first batch reactor receives heat input. The last reactor has an adiabatic boundary and cannot exchange heat with the surroundings. c) A 1D fuel layer with a Gaussian temperature input. d) A 2D fuel layer, also with a Gaussian temperature input.

2.3.1 Superadiabaticity in a batch reactor with an adiabatic boundary and an incoming 1D reaction wave initiation

Consider a region of fuel in a layer, equivalent to a single batch reactor being surrounded by an adiabatic boundary. Figure 2-1 a) shows a schematic of such a system. On one side of the reactor, it is exposed to a self-propagating reaction wave that acts as a source of ignition. The other side of the reactor is an adiabatic boundary. The reactor can only exchange heat with the incoming wave and not with any region of its surrounding atmosphere.

The temperature of this fuel is governed by the energy balance equation (10).

$$mC_p\frac{dT}{dt} = (-\Delta H)\left(-\frac{dW}{dt}\right) + (\frac{kA}{\delta})(T_{ana} - T) \tag{10}$$

The heat transfer between the fuel layer and the incoming 1D reaction wave is accounted for by the term $(\frac{kA}{\delta})(T_{ana} - T)$. The temperature profile of this self-propagating 1D reaction wave is given by T_{ana}, the thermal conductivity of the fuel is denoted by k, the surface area of heat exchange is A and δ is the thickness of a hypothetical membrane that limits the transfer. Thus (A/δ) corresponds to the main length scale for heat exchange. A simple first order reaction rate equation with Arrhenius rate constant is used in the fuel mass balance.

$$\frac{dW}{dt} = -k_0 W e^{-\frac{E_a}{RT}} \tag{11}$$

The corresponding non-dimensional forms of the equations are shown in equations (12) and (13), using the non-dimensional variables defined in equation (3).

$$\frac{du}{d\tau} = \left(\frac{1}{\beta}\right)\left(-\frac{dw}{d\tau}\right) + (\gamma\beta)(u_{ana} - u) \tag{12}$$

$$\frac{dw}{d\tau} = -\beta w e^{-\frac{1}{u}} \tag{13}$$

where

$$u_{ana} = \frac{1/\beta}{(1 + Qe^{cQ(\xi - c\tau)})^{1/Q}}$$

Here, the analytical temperature profile u_{ana} starts at a distance $\xi = \xi_0$ from the reactor and it affects the time it takes for the wave to reach the batch reactor. The value of ξ_0 is chosen to generate a defined region of zero reaction, $(\xi = \xi_0) > c\tau$. As time progresses, the self-propagating wave approaches the batch reactor and the (non-dimensional) temperature rises to (1/β) i.e. (uβ) ~ 1. The dimensionless heat transfer coefficient for the batch reactor is $\gamma = \frac{kA}{C_p\rho}\frac{1}{k_0}$.

Both β and γ are dependent on the fuel and system properties respectively and are hence tunable. Changing the geometry of the reactor or fuel layer alters γ while the source of the fuel modifies β.

In our work, the set of coupled differential equations (12) and (13) was numerically solved using MATLAB ordinary differential equation solver *ode15s*. We studied the value of the normalized variable (uβ), which equals 1 for the adiabatic temperature. For a chosen value of β and τ, refer to the maximum temperature reached in the system as u_{max} and the time at which it occurs as τ_{max}. In Figure 2-2, we plot color maps of ($u_{max}\beta$) for various values of β and γ.

As seen from Figure 2-2, the numerical results show that superadiabatic temperatures up to values of (uβ) ~ 1.8 exist for certain values of β and γ. Figure 2-2 b) shows an output for ($u_{max}\beta$) reached by the fuel in the reactor zone for the values ($1 \leq \beta \leq 25$) and ($0 \leq \gamma \leq 10^{-4}$) and ξ_0=5000. We chose values of β that are comparable to previously studied systems,[14,15] and we chose γ values to account for a wide range of system heat transfer properties. Superadiabaticity is observed to be dependent on both β and γ with β having a greater influence on existence of temperatures beyond the predicted (uβ) = 1. Interaction between factors such as the energy of activation, heat of reaction, specific heat of fuel and the heat loss coefficient determines whether the fuel layer demonstrates superadiabaticity under these conditions. As seen from Figure 2-2, fuels with β between values of 5 to 15 have the potential to exhibit superadiabatic temperatures. As the value of γ increases, the rate at which the fuel loses heat increases and accordingly for high enough values of γ, no value of β can show superadiabatic temperature rise. If we extend the analysis for a less fine step size in γ but for values of γ up to 1, superadiabaticity ceases to exist for any value of β.

We note that the problem addressed in this work is one of closed reactant mass. The reactant mass and heat transfer rate cannot be adjusted independently. This closed mass condition is the case considered by Zeldovich and Frank-Kamenetskii and Mercer et al.,[23,41] and corresponds to the physical systems of solid phase inorganic synthesis, thermopower wave generation, and combustion synthesis. A trivial superadiabatic result arises if one allows reactant injection at regular intervals along the length of a propagating wave, but the result is a temperature that increases linearly and without bound along the length, leading to an unphysical system.

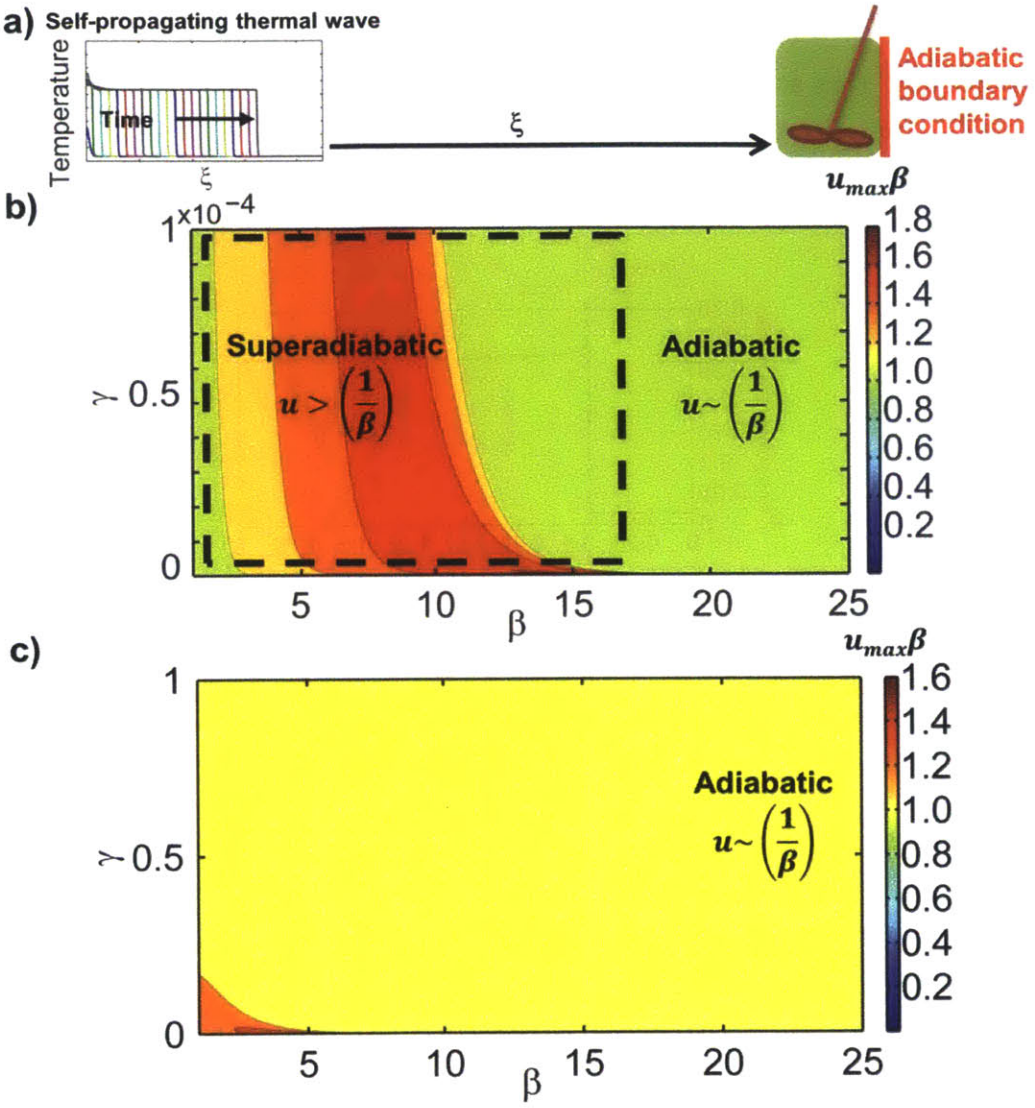

Figure 2-2 a) Schematic showing a batch reactor subjected to a 1D self-propagating reaction wave input. b) For a single batch reactor, contour plot for $(u_{max})\beta$ as a function of $1 \leq \beta \leq 25$ with a step size of 0.1 and $0 \leq \gamma \leq 10^{-4}$ with a step size of 10^{-7}. The area included in the dashed box shows region predicted to show superadiabaticity. c) Contour plot for $(u_{max})\beta$ for extended values of $0 \leq \gamma \leq 1$ with a step size of 10^{-4}.

An order of magnitude analysis was performed on the governing heat balance equation in order to obtain an estimate of the bounds on the value of superadiabaticity. Assuming a continuous

temperature profile, the temperature profile undergoes a maximum at the point of superadiabaticity. Thus at temperature u_{max}, as shown in Figure 2-3, the first order derivative of temperature u with respect to time τ should be equal to zero.

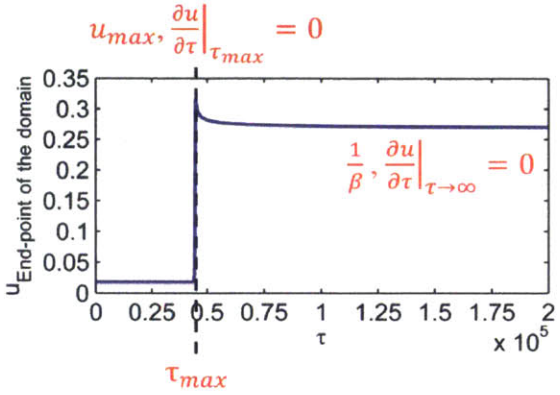

Figure 2-3 Calculated temperature profile at the end-point of the reaction domain as a function of time, showing superadiabatic temperature u_{max}. According to the principles of derivatives, at the point of maxima, the first order derivative of temperature with respect to time will be zero.

$$\frac{du}{d\tau} = \left(\frac{1}{\beta}\right)\left(-\frac{dw}{d\tau}\right) + (\gamma\beta)(u_{ana} - u)$$

$$0 = \left(\frac{1}{\beta}\right)\left(-\frac{dw}{d\tau}\right) + (\gamma\beta)(u_{ana} - u) \tag{14}$$

$$\therefore \left(\frac{1}{\beta}\right)\left(\frac{dw}{d\tau}\right) = (\gamma\beta)(u_{ana} - u_{max})$$

Using substitution from equation (13), we get:

$$\therefore -we^{-\frac{1}{u_{max}}} = (\gamma\beta)(u_{ana} - u_{max})$$

If $we^{-\frac{1}{u_{max}}} = 0$, there is no superadiabaticity. Thus, theoretically, the superadiabatic temperature is only attained at a non-zero fuel concentration.

$$u_{max} = u_{ana} + \frac{we^{-\frac{1}{u_{max}}}}{\gamma\beta} \tag{15}$$

Equation (15) is an implicit equation for u_{max}. The 2nd term in equation (15) accounts for heat generation within the reactor zone, and constants γ and β are critical to determine u_{max}. Equation (15) allows one to evaluate the maximum possible value of superadiabaticity that can be theoretically obtained for a chosen system.

To validate our results from Figure 2-2, we solved equation (15) for w by choosing $\gamma = 10^{-5}$ and using corresponding numerical values for $u_{max}\beta$ from Figure 2-2. In order to obtain bounds on the maximum value possible for u_{max}, we used maximum possible value of $u_{ana} = 1/\beta$. As can be seen from Figure 2-4, systems showing superadiabatic temperatures showed such temperatures for low values of w. Thus, by calculation using equation (15), we showed physically possible values of fuel concentrations at which systems might show superadiabatic temperature.

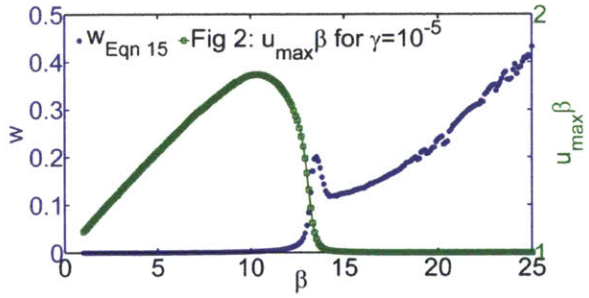

Figure 2-4 w as a function of $1 \leq \beta \leq 25$ with a step size of 0.1 calculated using equation (15) with $\gamma = 10^{-5}$, $u_{ana} = 1/\beta$ and corresponding numerical values of ($u_{max}\beta$) from Figure 2-2. On the right hand side y-axis is the numerical data extracted from Figure 2-2 for ($u_{max}\beta$) values corresponding to $\gamma = 10^{-5}$. This is for the case of a batch reactor subjected to a 1D self-propagating reaction wave input. We see that reactors which show superadiabatic temperature do so for w ~ 0. For systems showing maximum temperature of adiabatic temperature rise, they do so before complete conversion.

2.3.2 Superadiabatic temperature rise in a system of multiple batch reactors in series

We now study another system capable of superadiabatic behavior: a system of batch reactors in series. This system creates a fuel reaction and temperature profile effect similar to that observed in propagation of a reaction wave through a single continuous fuel domain. As can be seen from Figure 2-1 b), heat provided to the first reactor initiates an exothermic reaction, releasing heat which propagates to the next reactor. An adiabatic boundary condition imposed at the last reactor has the potential to concentrate the resulting reaction wave to temperatures exceeding the adiabatic limit. The system of non-dimensional equations for reactor n at time point i is given by:

$$\left(\frac{du_{n,i}}{d\tau_i}\right) = \gamma_n\left(u_{n-1,i} - 2u_{n,i} + u_{n+1,i}\right) + \left(w_{n,i}e^{-\frac{1}{u_{n,i}}}\right) \tag{16}$$

$$\frac{dw_{n,i}}{d\tau_i} = -\beta w_{n,i}e^{-\frac{1}{u_{n,i}}} \tag{17}$$

where

$$\gamma_n = \frac{hA_nE_a}{k_0R(-\Delta H)C_{ref}} \tag{18}$$

In equation (16), the left hand side term corresponds to changes in the temperature of the n^{th} reactor with respect to time. The two terms on the right hand side correspond to heat exchange with the reactor that lies before and after the n^{th} reactor and the heat released because of reaction of the fuel in the n^{th} reactor. γ_n again stands for a non-dimensional heat transfer term that accounts for heat exchange between reactor n and the adjacent reactors n-1 and n+1. In equation (16), h is the heat transfer coefficient governing exchange of heat across reactors over the shared surface area A_n and containing C_{ref} amount of fuel.

This coupled system of equations was solved using ode solver ode15s in MATLAB. A system of 50 equal-sized reactors (n = 50) was solved for a common heat transfer rate corresponding to $\gamma_n=10^{-5}$. A non-zero input temperature $u_0=0.075$ was used to start the reaction in the first reactor.

The output temperatures of each of the reactors were analyzed with respect to time. We note that the temperature profile of the reactors in series is approximately described by the continuous wave solution derived previously.[14] As anticipated, this system also demonstrates superadiabatic temperature rise where ($u\beta$) > 1. Figure 2-5 b) shows the temperature profile in each of the entire system of reactors, just after the last reactor has reached complete conversion. As can be seen, all the reactors except the last one are at the adiabatic temperature rise i.e. ($u\beta$=1). However, the last reactor, which cannot lose heat in any way except via reflection to the penultimate reactor, shows superadiabatic temperature. In Figure 2-5 c), we plot the normalized temperature ($u\beta$) as a function of the similarity variable $\eta = \xi - c\tau$, which captures the effect of wave propagation with distance travelled with respect to time. We compare the temperature profile of any two reactors, say reactor 25 and 35, to that of the 1D self-propagating reaction wave as obtained by using the analytical expression in equation (7). As can be deduced from the figure, because of the nature of this numerical simulation, each of the reactors exhibits a superadiabatic temperature during the course of its reaction. Thus, any fuel system with adiabatic boundaries exhibits superadiabatic temperature when nearing the end of its reaction.

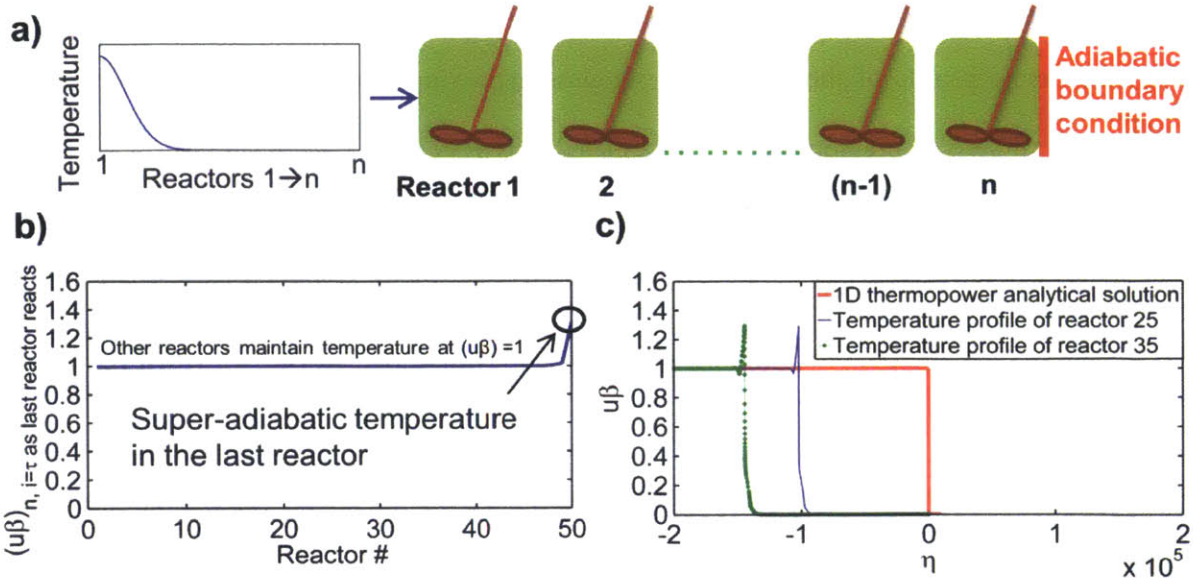

Figure 2-5 a) Schematic to study superadiabaticity in a system of multiple batch reactors in series, with the first reactor receiving input heat. b) Temperature (uβ) at the time point just after the last reactor reacts completely. As seen from the figure, the last reactor shows elevated superadiabatic temperature. c) Comparing temperature (uβ) for reactors 25 and 35 (of a total 50 reactors), with the analytical solution for a 1D self-propagating reaction wave as a function of similarity variable η(ξ,τ).

In this system, the temperature of the reactor spikes to superadiabatic temperature once the temperature wave-front reaches an adiabatic boundary. The concept of superadiabaticity arises because of unequal time scales for heat exchange. While heat is given out by the reaction with the representative time scale of $\frac{1}{k_0}$, the heat is lost by the system by representative conductive heat loss governed by the time scale $\left[(\frac{A}{\delta})^2/\frac{k}{\rho C_p}\right]$. An imbalance between these time scales leads to a sudden accumulation of heat in the system leading to superadiabatic temperatures. According to Fourier's law, we expect such a superadiabatic system to start losing heat backwards into the system.

2.3.3 Superadiabaticity from reaction waves over continuous reaction domains

Over a continuous reaction domain, superadiabaticity can be observed when the resulting reaction wave impinges upon an adiabatic boundary condition. Figure 2-6 a) shows a schematic of a 1D fuel layer along the dimension ξ. The coupled partial differential equations (5) and (6) were solved using COMSOL.

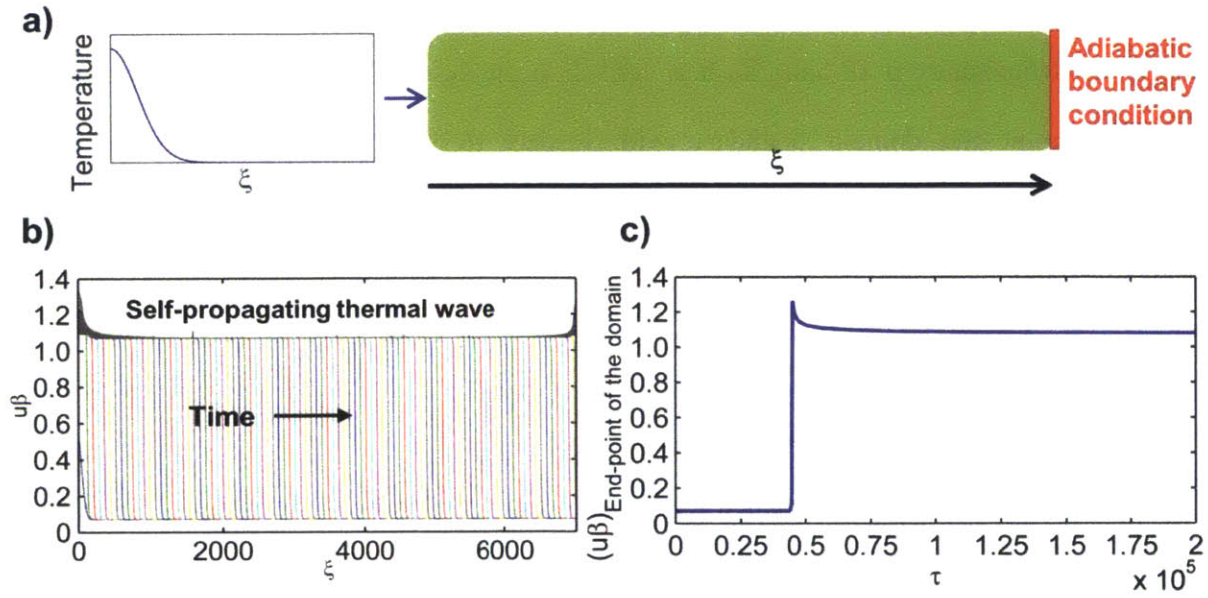

Figure 2-6 a) Schematic of a system of a 1D fuel layer with a Gaussian heat input. b) Plots for temperature along the length of the 1D domain. Each curve corresponds to the temperature profile at one time point. Output is obtained from COMSOL simulation for conditions β=4 for ξ=(0:2:7000) and τ=(0:500:200,000) c) Temperature at the last boundary point of the 1D domain plotted as a function of time. The peak in temperature corresponds to a superadiabatic temperature.

The simulation was carried out to study a non-dimensional domain 7000 units long and for $\beta = 4$. The total time of the simulation was chosen such that the fuel reaction would reach completion. Similar to the previous[14,15] analyses, we observe steady state wave propagation; however, in this case we examine the limit of the wave impingement upon the adiabatic boundary. Figure 2-6 b)

plots the temperature of the wave front as a function of distance, for each time point where calculations were performed. Each colored trace corresponds to the snapshot of temperature along the domain length at different reaction times. As the reaction proceeds, the temperature behind the wave front reaches a value of $(1/\beta)$ as expected. The simulation was conducted at $\beta=4$ and hence we observe a steady state (non-dimensional) temperature of about $u = 0.25$. As the wave front approaches the adiabatic boundary, the temperature becomes superadiabatic. Over time, this temperature peak loses its heat back into the system. In Figure 2-6 c), we plot the temperature at the domain boundary with respect to time τ. This plot clearly shows superadiabaticity with maximum temperature value almost up to $(u\beta) \sim 1.26$ as against the steady state propagation temperature of $(u\beta) \sim 1.07$.

2.3.4 Superadiabaticity in 2D reaction systems

We next study the concept of bounded self-propagating waves in two-dimensional (2D) systems. While the previously discussed work by Mercer,[39,40,41] Weber,[22] and others show the presence of 2D self-propagating waves, we also confirm it by using a different and simplified system of equations. For an isotropic system with uniform physical properties in all directions, a 2D Cartesian coordinate system is mathematically equivalent to a 1D radial system of equations, and is computationally less expensive than solving the 2D Cartesian equations. Here, we examined the radial 1D system shown in Figure 2-7 a), where an adiabatic boundary is established at the circumference at $r = r_{max}$. The governing set of non-dimensional 1D radial coordinate system equations for a solid fuel reaction are given by equations (19) and (20).

$$\frac{\partial u}{\partial \tau} = \frac{1}{r}\left[\frac{\partial}{\partial r}\left(r\frac{\partial u}{\partial r}\right)\right] + e^{-1/u}w \tag{19}$$

$$\frac{dw}{d\tau} = -\beta w e^{-1/u} \tag{20}$$

The non-dimensional radial coordinate is represented by r. A numerical solution for the above set of equations was obtained using COMSOL. Again, the simulation was carried out to study a non-dimensional domain of size (r_{max} = 7000 units) for β = 4, and the total time of the simulation was chosen such that the fuel reaction would reach completion. A Gaussian temperature peak was used for initiating the reaction:

$$u_0 = g e^{-\frac{r^2}{w_d}} + u_{ambient} \tag{21}$$

In equation (21), g corresponds to the maximum intensity of the Gaussian peak (i.e. the maximum input temperature) and w_d corresponds to the width of the peak. The numerical results were analyzed to study the steady state propagation of the wave by considering the adiabatic boundary condition. As can be seen in Figure 2-7, the results show the existence of a self-propagating reaction wave.

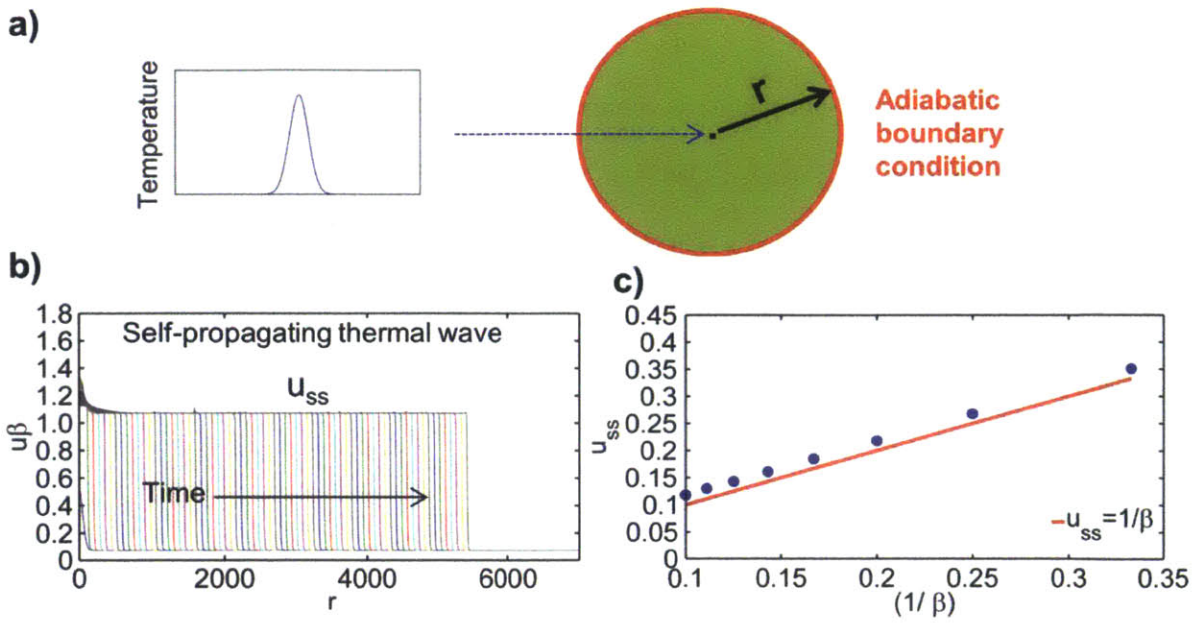

Figure 2-7 a) Schematic to study self-propagating reaction waves in a 1D radial system of a layer of fuel with a Gaussian heat input. b) Output from a 1D radial reaction wave simulation. Simulation parameters used were: β=4 for r=(0:2:7000) and τ=(0:500:200,000). u_0 was set using g=0.1 and w_d=5000. The figure plots u vs. r for multiple time points. c) Non-dimensional steady state propagation temperature u_{ss} plotted with respect to (1/β). As expected, we observe that $u_{ss} \sim (1/\beta)$ as the 2D wave becomes a 1D reaction front. The upshift in the points is because of the initiation condition.

Figure 2-7 b) is similar to Figure 2-6 b). Both these plots demonstrate self-propagating waves along a distance coordinate. As in the case of the 1D (Cartesian) thermal wave, the maximum temperature reached behind a steady-state 1D radial thermal wave was found to be proportional to $(1/\beta)$. This feature was confirmed for a range of β values from 3 to 10, as shown in Figure 2-7 c).

After confirming the existence of these waves, we moved onto computationally expensive 2D Cartesian simulations for a physically 2D system, where ξ_1 and ξ_2 are the two perpendicular non-dimensional distance coordinates.

$$\frac{\partial u}{\partial \tau} = \frac{\partial^2 u}{\partial {\xi_1}^2} + \frac{\partial^2 u}{\partial {\xi_2}^2} + we^{-\frac{1}{u}} \tag{22}$$

$$\frac{dw}{d\tau} = -\beta we^{-\frac{1}{u}} \tag{23}$$

To study the 2D Cartesian system, the initial Gaussian peak condition was also modified to a 2D Cartesian form:

$$u_0 = ge^{-\frac{{\xi_1}^2 + {\xi_2}^2}{w}} + u_{ambient} \tag{24}$$

Simulations were carried out with adiabatic boundary condition at all the boundaries.

$$\left.\frac{\partial u}{\partial \xi_1}\right|_{boundary} = \left.\frac{\partial u}{\partial \xi_2}\right|_{boundary} = 0 \tag{25}$$

Figure 2-1 d) shows schematic of a square fuel layer receiving temperature input in the form of a Gaussian curve. Simulations for such a square geometry re-confirmed existence of self-propagating two dimensional reaction waves. The temperature behind the wave-front was found to be proportional to $(1/\beta)$. This type of system also showed superadiabaticity where a sudden rise in temperature was observed once the wave reached the boundary, because there is no 'forward' path to lose heat generated by the exothermic reaction of the fuel. This leads to the heat being confined to the region near the boundary, and leads to increased temperature. Experimentally, while it is not possible to obtain perfectly adiabatic conditions, it is possible to reduce heat loss by tuning experimental conditions such as carrying out the reaction in vacuum to reduce convective losses or performing the reaction in an enclosed chamber with walls having low thermal conductivity.

For the purpose of confirming superadiabaticity in additional 2D systems, a fuel layer in the shape of an equilateral triangle was selected to explore the effect of geometry, as shown in

Figure 2-8. The reaction is initiated with heat along the bottom edge of the triangle, with the form given below:

$$u_0 = ge^{-\frac{\xi_2^2}{w}} + u_{ambient} \tag{26}$$

Figure 2-8 a-d show color maps of the temperature across the triangular fuel layer as the reaction wave propagates. Here, the system exhibits a superadiabatic temperature rise at $\tau = 360$. Figure 2-8 e) plots temperature ($u\beta$) at the two vertices of an equilateral triangle: vertex 1 is at one of the corners along the edge where the reaction is initiated, and vertex 2 is at the corner opposite the initiation edge. The temperature peak shown by vertex 2 demonstrates superadiabaticity.

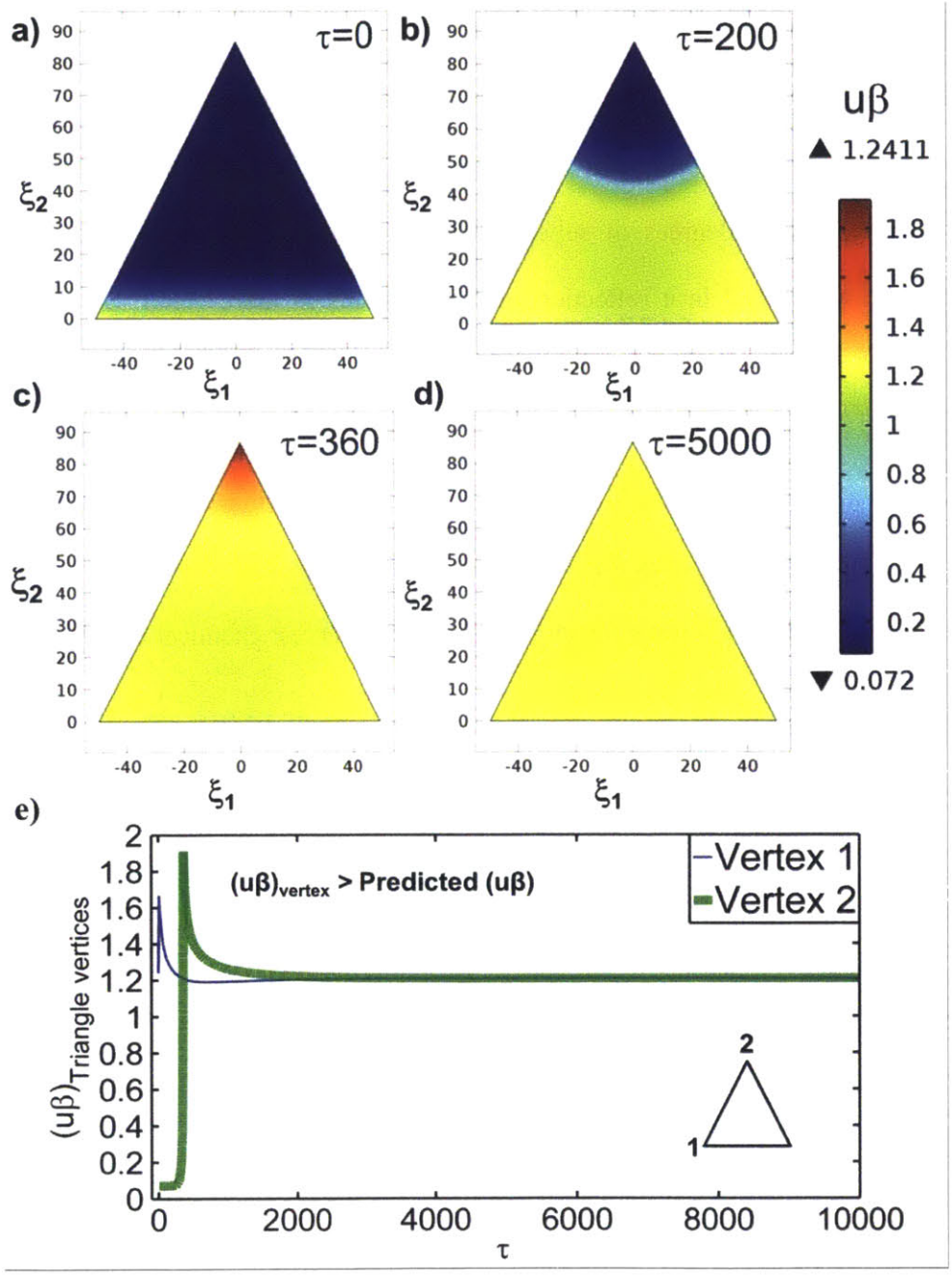

Figure 2-8 Output from 2D Cartesian reaction wave simulation for an equilateral triangle geometry with line initiation, at β=4. (a-d) These sections show a color-maps of temperature across the surface of the 2D fuel layer at various time points of τ=0, τ=200, τ=360 and τ=5000. Superadiabatic temperature can be seen at τ=360 when temperature at the top vertex of the triangle shows a maximum. e) The figure shows presence of superadiabaticity at the top vertex of the triangle away from the line of initiation with temperature as high as (uβ) ~ 1.9. Peak in temperature at vertex 1 corresponds to the initiation input heat.

This result opens up new avenues for research to study the bounds of superadiabaticity in 2D domains. Preliminary work on 2D numerical COMSOL simulations for different shapes for 2D fuel conduits show interesting temperature profiles, in that edges or regions of adiabatic boundary show varying degrees of superadiabaticity. Future work in this area can focus on studying these waves and heat reflection in such systems in more detail. Simulations can be carried out on adiabatic systems with the reaction waves being launched along the entire boundary. This would allow us to study wave reflections as these reaction waves meet at the center and can aid in studying the bounds on superadiabaticity when concentrating energy at the center of the domain rather than at the boundaries. Wave-guides can be designed to maximize the temperature reached thus allowing for improved ways to harvest chemical energy in the form of heat.

2.4 Applications of superadiabaticity

Superadiabaticity allows one to extract higher temperatures from the same quantity of fuel by manipulating reaction conditions. This has the potential to offer advantages for converting chemical energy to electrical energy. In systems that use a thermal conduit to aid the self-propagation of fuel reactions, we can choose thermoelectric materials as the thermal conduit. Therefore, higher temperatures will give rise to an increased temperature gradient and thus increased electrical output. It might also give an added advantage when using materials like annealed ZnO thin films, annealed Ga-doped ZnO thin films or Ga-doped ZnO alloy that exhibit Seebeck coefficients that increase with increasing temperature of operation.[28,32]

2.4.1 Modified thermophotovoltaics

A conventional thermophotovoltaic consists of a reaction chamber that heats an emitter, which in turn gives out radiation that is absorbed by an absorber or a photovoltaic (PV) and then converted to an electrical output.[34,35] Often there is an additional filter included to moderate the wavelength of the light incident on the photovoltaic and thus increase the efficiency of operation.[34,35] To exploit superadiabaticity, we envision a modified thermophotovoltaic wave system where our reaction chamber and the emitter is the reacting fuel layer.

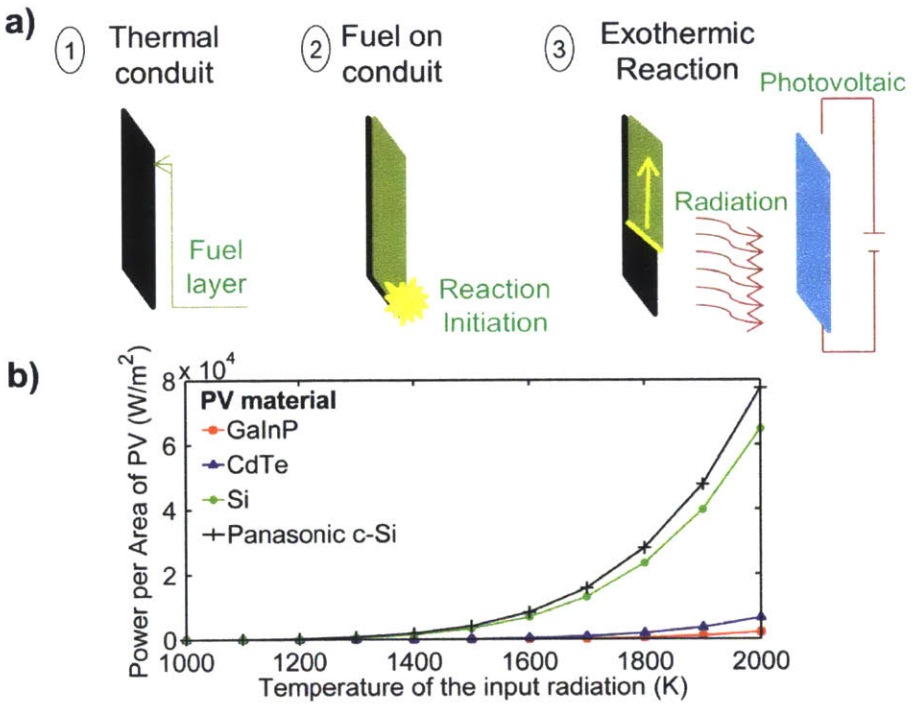

Figure 2-9 a) Schematic explaining the concept of modified thermophotovoltaic wave system. First step involves depositing a fuel layer, possibly atop a thermal conduit. Fuel reaction is then initiated by means of an external source of ignition. As the reaction wave propagates, radiation is emitted by the reaction wave-front. This radiation is harvested by a photovoltaic. b) Comparing the power output per unit area from modified thermophotovoltaic for different materials for PV, studied as a function of temperature of input radiation.

Figure 2-9 a) shows the schematic for a modified thermophotovoltaic. The device operation consists of three steps: (1) fuel loading, possibly onto a thermal conduit, (2) chemical reaction and (3) harvesting the radiation using a PV. Thus, overall efficiency of this modified thermophotovoltaic system depends on two factors: (1) the temperature of the reaction, which affects the radiation emitted by the reaction, which then acts as the input to the photovoltaic, and (2) the efficiency of the photovoltaic to convert the input radiation into electricity. The second factor is dependent on the rapidly developing field of photovoltaics.[43] Device efficiency as high as 37.9% has been reported for an InGaP/GaAs/InGaAs solar cell fabricated by Sharp.[43] We assume the radiation emitted by the fuel reaction is governed by Planck's law of blackbody radiation, so that the higher the temperature at which the radiation is emitted, the higher the intensity of light radiated at each wavelength. Also, as the temperature at which the radiation is emitted increases, the wavelength at the peak of the intensity spectrum shifts towards the visible region. Currently, the best photovoltaics being developed are designed to harvest the radiation of the visible solar spectrum. Higher reaction temperatures disproportionately shift the radiation to wavelengths that are more efficient for visible photovoltaics to harvest. Thus, by appropriate tuning of the system properties and proper fuel selection, we can obtain superadiabatic temperatures, which will improve the overall operation efficiency of the modified thermophotovoltaic system. We have performed calculations that show that the overall energy efficiency of this system increases as the temperature of the input radiation increases. The PV materials we studied were based on GaInP,[44] CdTe,[45] Si,[46] and a large area Si cell from Panasonic (i.e. Panasonic c-Si cell),[43] in increasing order of their efficiency.

The radiation output profile emitted by the fuel layer $B_\lambda(T)$ was calculated using Planck's law. It is a function of absolute temperature T and wavelength λ. Other parameters used are speed of light c, Boltzmann constant k_B and Planck constant h.

$$B_\lambda(T) = \frac{2hc^2}{\lambda^5} \frac{1}{e^{\frac{hc}{\lambda k_B T}} - 1} \tag{27}$$

At the same temperature, the heat losses in the form of conduction, convection and radiation were calculated. Conductive heat loss L_d is a function of the mass of the fuel or conduit layer (if any) m_f, specific heat capacity $C_{p,f}$, duration of the fuel reaction t_{rxn} and the area available for heat exchange A.

$$L_d(T) = \frac{m_f C_{p,f}(T - T_{amb})}{t_{rxn} A} \tag{28}$$

Convective heat loss L_v is a function of mass of the (gaseous) products m_p, specific heat $C_{p,p}$, duration of the fuel reaction t_{rxn} and the area available for heat exchange A.

$$L_v(T) = \frac{m_p C_{p,p}(T - T_{amb})}{t_{rxn} A} \tag{29}$$

Radiative heat loss L_r is given by the Stefan-Boltzmann law, where σ is the Stefan-Boltzmann constant:

$$L_r(T) = \sigma(T^4 - T_{amb}^4) \tag{30}$$

The sum of these three heat fluxes (unit of power per unit area) is the total input in the system consisting of the photovoltaic and the fuel layer, although only the radiative energy will be used by the PV to generate electrical energy. In order to calculate the output of electrical energy from the system, the input radiation curve $B_\lambda(T)$ was then super-imposed over the external quantum efficiency (EQE) curve for the photovoltaic cell being studied. The EQE curve of a PV cell

measures the efficiency with which the cell can convert the incident photons (i.e. absorbed radiation) into electricity. In order to obtain the total output from the cell, this value of product of EQE with the input radiation spectrum was integrated over the entire range of wavelength to obtain the net power output.

$$L_{out}(T) = \int B_{\lambda}(T) \times EQE(\lambda)\, d\lambda \tag{31}$$

The overall efficiency of the system E was calculated as a ratio of the net electrical power output upon the total input to the system.

$$E(T) = \frac{L_{out}(T)}{L_d(T) + L_v(T) + L_r(T)} \tag{32}$$

From our calculations, as seen in Figure 2-9 b), an increase in temperature gives an improved output in power obtained per unit area of the photovoltaic cell type. Also, photovoltaic devices of materials such as Si which have a higher overall efficiency can make better use of this improved input leading to a much higher output at higher temperatures, especially when compared to lower overall efficiency photovoltaic cells such as GaInP and CdTe. Improvement in temperature of the input radiation from 1000 K to 2000 K leads to an almost 4000-fold increase in output power per unit area.

For carrying out calculations for efficiency of thermophotovoltaics at different temperatures of input radiation, as shown in equation (32), the temperature dependent output from the thermophotovoltaic system is calculated using the Planck's law and the photovoltaic cell's EQE curve (Figure 2-9 b). Calculations pertaining to the input to the system were based off of a preliminary experiment carried out in our lab where about a 4 second long reaction wave of 60 mg of nitrocellulose was launched over the thermal conduit of 44 mg of aluminum over a surface

area of about 10 cm^2. Since we wanted to perform input calculations only as a function of temperature, we calculated the heat input not via the fuel energy content but by calculating the total power per unit area from all three modes of heat transfer; radiation (equation (30)), convection (equation (29)) and conduction (equation (28)). In evaluating the convective component of the heat transfer rate per unit area, we assumed ideal gas properties for the specific heat capacity of gaseous products formed and about 11 moles of gaseous products formed per mole of fuel reacted with the total fuel content of about 0.24 moles (where molar values are based on the case of nitrocellulose reaction).

At the input radiation temperature of 2000 K, the overall efficiency of operation of such modified thermophotovoltaics setup was calculated to be about 8.2% for the Panasonic c-Si cell, about 6.9% for the conventional Si cell, about 0.7% for the CdTe cell and just about 0.24% for the GaInP cell.

Thus, when superadiabaticity is used in combination with high efficiency photovoltaic cells such as the Si-based photovoltaic cells, it is possible to obtain electrical output with almost 8% overall efficiency. These values are comparable to the demonstrated efficiencies in the range of 0.6 % to 11% for prototypes of conventional thermophotovoltaic systems.[35] Traditional thermophotovoltaic reaction chambers use fossil fuels to reach high temperatures.[34,35] With this new thermophotovoltaic wave setup, we can use novel fuels such as nitrocellulose to reach comparably high temperatures by superadiabaticity. Moreover, this helps us obtain higher temperatures without the disadvantage of additional nitrous oxide production at higher temperature combustion reactions.[34,35] Also, as mentioned before, the preliminary calculations shown above do not account for using a filter for wavelength selection and re-using unused

photons to heat the thermal conduit.[35] Thus, there is the possibility for further improvement in operation of the modified thermophotovoltaic wave system.

2.5 Conclusion

After analytical and numerical analysis of heat transfer in various systems of self-propagating reaction waves such as a self-propagating 1D reaction wave, multiple batch reactors in series and a self-propagating 2D reaction wave, we showed the occurrence of superadiabatic temperatures in the presence of adiabatic boundaries. Numerical analysis of various systems of governing heat and mass balance equations was performed using MATLAB and COMSOL. Adiabatic bounds for superadiabaticity were obtained by simplifying the governing non-linear differential equations. For all these cases, when a reaction wave impacts on an adiabatic boundary, the interplay of the heat retaining capacity of the fuel and the heat transfer coefficient within the system leads to superadiabaticity. Our simulations for these cases predict temperatures up to 1.8 times higher than that expected by the adiabatic temperature rise. This result opens up avenues for applications in areas such as thermopower waves, high temperature self-propagating synthesis, thermoelectrics and modified thermophotovoltaics. Further research is needed to take advantage of superadiabaticity to more efficiently convert chemical energy to usable electrical energy.

Chapter 3 Higher Efficiency Thermopower Wave Devices and a Continuous Fuel Layer Reaction Model to Analyze Thermopower Wave Devices' Voltage Output

3.1 Introduction

Thermopower waves (TPWs) convert chemical energy into electrical energy by means of launching self-propagating reaction waves along thermal conduits.[2] TPW devices give voltage output higher than that predicted by just thermoelectricity. This is due to the contribution of excess thermopower because of the chemical potential gradient established across the ends of the system during the propagation of the reaction wave.[3] In this work, we exploit the theory of excess thermopower to increase the chemical-to-electrical conversion efficiency of the single-walled carbon nanotubes (SWNTs) TPW devices from about 10^{-4} % to about 10^{-2} %. This increase in efficiency was obtained by using novel reaction wave fuels such as sodium azide and sucrose with oxidizer potassium nitrate (KNO_3). Because of high temperature of many of these TPW reaction propagations, depending on the temperature reached by the system, a lot of heat released gets transmitted via radiation. Part of the radiative and convective heat losses from the reaction system was harvested using external thermoelectrics allowing us to obtain net device efficiency of operation of up to 1%. We also developed a reaction model to analyze the time dependent voltage output from TPW devices. The model allows us improved intuitive understanding of the different voltage output profiles (e.g. single polarity, double polarity, multiple peaks of single polarity etc.). Taking into account the theory of excess thermopower along with the thermoelectric effect, to predict the net voltage output from the thermopower wave device, we can analyze actual experimental data using this model by fitting for system parameters such as the Seebeck coefficient of the carbon nanotube-fuel conduit, chemical potential gradient induced by doping of carbon nanotubes with the fuel layer atop it, etc. We

used this model to study voltage output data from nitrocellulose-SWNT TPW devices. The parameter analysis combined with Raman analysis on fuel doping of carbon nanotubes points towards using n-doping fuels with these SWNT fibers to boost the TPW efficiency even more.

3.2 Higher Efficiency Thermopower Wave Devices

Phenomenon of reaction waves has been studied extensively before. Reaction waves have applications in a wide variety of fields such as high-temperature self-propagating synthesis,[27] thermopower waves[2] etc. Reaction waves are launched by starting the reaction at one end of the fuel region with the aid of an external ignition source. The heat that is released because of reaction of the fuel that lies around the region of ignition is carried ahead along the fuel, either because of the high thermal conductivity of the fuel or the thermal conduit beneath it. This heat conducted ahead now initiates reaction of the fuel that lies in its path. This gives rise to a self-propagating reaction wave.

Thermopower waves (TPWs) is one such application of self-propagating reactions used to convert chemical energy into electrical energy. In such systems, a layer of fuel is coated atop the thermal conduit. Reaction wave launched across this layer of fuel allows us to harvest this chemical energy as a voltage output across the ends of the reaction system or the ends of the thermal conduit. Previous work in the field of TPWs has been carried out using a wide variety of thermal conduits and fuels. TPW reactions have been launched with fuels such as 2, 4, 6-Trinitroaniline (TNA), picramide and nitrocellulose (with sodium azide),[4,5] nanothermites consisting of aluminum (Al) iron oxide (γ-Fe_2O_3)[10] etc. Different thermal conduits including multi-walled carbon nanotubes (MWNTs),[2] single-walled carbon nanotubes (SWNTs),[4] SWNT

yarns, ZnO,[8,11] Bi_2Te_3 coated on alumina and terracotta,[6,7] Sb_2Te_3 coated on alumina, terracotta and MWNT,[7,12] MnO_2 coated alumina[9] etc. have been used to launch reaction waves. Previous demonstrations of TPW devices using TNA coated MWNT have shown electrical specific power as high as 7 kW/kg.[2] Such TPW devices have been shown to exhibit high power density comparable to that of Li-ion batteries (80,000 $\mu W/mm^3$ versus about 10,000 $\mu W/mm^3$ demonstrated for Li microbattery).[20] Also, unlike other traditional power sources such as Li-ion batteries or fuel cells which show degraded performance with time, TPW devices have a longer shelf life since the energy is stored in the form of chemical bonds. These advantages combined with the small size of these devices could make them suited for Micro-Electro-Mechanical Systems (MEMS)[17] or smart dust applications[18] or wireless sensor networks[19]. However, to make this young and developing technology viable and competitive on a commercial scale, work needs to be done to improve factors such as its chemical-to-electrical energy conversion efficiency, safety and ease of operation. Accordingly, our recent research efforts have been focused on studying scaling up of these devices and improving the ease of operation and efficiency of operation of such devices. In this chapter, by demonstrating reaction waves up to 25mm long, we show the possibility of launching longer reaction waves with longer duration of expected voltage output. We improve the net efficiency of operation of SWNT TPW device setups from about 10^{-4}% to up to 1%, by changing the reaction wave fuel as well as using external thermoelectric harvesters to capture part of the heat losses.

Traditional TPW reactions are launched from one end of the sample by using an external heat source such as a joule heater or a laser. As this reaction wave propagates, we obtain a voltage output across the ends of the device. Theory of excess thermopower predicts that the superior performance of TPW devices, as compared to just thermoelectric output from operating under

similar (temperature) conditions, is because of the chemical potential gradient that arises because of the presence of reacted and unreacted regions of fuel coated atop the thermal conduit.[3] Both, the temperature gradient and the chemical potential gradient, established as the reaction wave propagates, give rise to the voltage output from the thermopower waves devices. We can quantify the voltage output from the TPW devices by equation (1).

$$\Delta V_{TPW} = S(T_{end} - T_{start}) - \frac{1}{e}(\mu_{end} - \mu_{start}) \tag{1}$$

In equation (1), S is the Seebeck coefficient of the device, T is the temperature and μ is the chemical potential of the electrons. The equation gives the electrochemical potential difference established across the ends of the device. The first term in equation (1) corresponds to the voltage contributed by the thermoelectric effect due to the temperature gradient established across the ends of the TPW device. The second term in equation (1) corresponds to the excess thermopower voltage contribution to the TPW voltage output because of the additional chemical potential gradient $\Delta\mu$ that exists across its ends as the reaction wave propagates along the length of the device. Thus, knowing the temperature gradient and the chemical potential gradient along with the Seebeck coefficient exhibited by the system should allow us to compute the expected voltage output from the TPW device. In using this equation to analyze our experimental data, apart from the magnitude of the Seebeck coefficient exhibited by the system, we are interested in studying or confirming if the excess thermopower effect indeed boosts the voltage output over that given by thermoelectric effect.

The chemical-to-electrical conversation efficiency of these devices is defined as the ratio of the output electrical energy that can be obtained from these devices to the input chemical energy in the system.

$$\eta(\%) = \frac{\text{Output Electrical Energy}}{\text{Input Chemical Energy}} \times 100 \tag{2}$$

$$\therefore \eta(\%) = \frac{\int_{t_{start}}^{t_{end}} \frac{\Delta V_{out}{}^2}{R_{ext}} dt}{m_{fuel}(-\Delta H_{rxn})} \times 100 = \frac{\int_{t_{start}}^{t_{end}} \frac{\Delta V_{OC}{}^2}{R_{\text{int}}} dt}{m_{fuel}(-\Delta H_{rxn})} \times 100$$

Analyzing a TPW device as a battery with an internal resistance R_{int}, we can calculate the expected voltage output across an external resistance R_{ext}. Figure 3-1 a shows a circuit diagram analyzing a TPW device as a battery or a voltage source producing open circuit voltage ΔV_{OC}.[47] ΔV_{out} is the output voltage from the TPW device when connected to an external resistance or load R_{ext}. Physically, the device internal resistance R_{int} is contributed to by the resistance of the thermal conduit and any contact resistance that arises as the device is connected to the load. The output power from a TPW device can be computed either from the open circuit voltage ΔV_{OC} (and R_{int}) or from the potential difference ΔV_{out} obtained across the external resistance R_{ext} attached across the ends of the TPW device to harvest the output energy. Figure 3-1 b shows a typical voltage output obtained from a nitrocellulose-SWNT yarn TPW device. The input energy for this device operation is the chemical energy released by the fuel undergoing the exothermic reaction. While the initiation energy is also theoretically an input to the system, we ignore it for the purpose of the calculation of the energy conversion efficiency. Not only is the magnitude of this energy small as compared to the input energy for the traditional size of TPWs launched, it is theoretically possible to launch infinitely long reaction waves with this input energy. In such a case, the chemical energy input from the reaction will definitely render the initiation heat insignificant when calculating the device efficiency. As described later, we have already launched reaction waves as long as 25 mm. Moreover, simple experiments involving a TPW device-like construction, using carbon nanotube thermal conduit with copper tape electrodes but

without fuel coating showed no voltage output when contacted with joule heater as when it is used to launch reaction waves. TPWs launched using thermal conduit of single and multi-walled carbon nanotubes (SWNTs and MWNTs) and high energy density fuels such as nitrocellulose, TNA and picramide have exhibited chemical- to-electrical conversion efficiency (η) in the range of about 10^{-4} %. Because of the high velocity of these reaction wave propagation (order of magnitude of meters per second)^2 and the usual millimeter scale lengths of these devices, the time during which the heat release happens and the voltage output from the TPW devices lasts is a short period of time, on the order of magnitude of a couple of hundreds of milliseconds for such devices.

The concept of excess thermopower can be effectively used to improve the efficiency of TPWs to make them competitive with other sources of energy conversion. Fuels play a very important role in the operation of TPW devices by affecting the chemical potential gradient created across the ends of the device while the reaction wave propagates. Thus, the fuel used to launch the reaction wave is an important tunable parameter to optimize the performance of the device. By changing the fuel used to launch a TPW, we change the maximum temperature gradient possible as it changes the amount of heat that is released during the chemical reaction. Similarly, different fuels will dope the thermal conduit to different extents thus also allowing us to manipulate the excess thermopower contribution. With this background, we wanted to test fuels that have lower energy content and that are safe to handle to improve the device efficiency and operation-ability. We studied improving the efficiency of operation of TPW devices by working on optimizing the input to the system, the fuel; and maximizing the output that can be extracted from the system. Experiments were carried out for different fuels and different experimental configurations to harvest higher amounts of heat that is given out by the chemical reaction.

TPWs were launched with novel fuels such as lower energy content fuel of sodium azide and easily accessible fuel such as a mixture of sucrose with oxidizer potassium nitrate or KNO_3. When analyzing their open circuit voltage outputs, we observed that these fuels led to improved efficiency of operation as compared to that obtained by using nitrocellulose fuel. As can be seen in Figure 3-1 c, up to 100 times improvement in efficiency was observed with sodium azide based open circuit device efficiencies being around 10^{-2} %.

Sodium azide (NaN_3) has been previously used in TPW devices fuel mixtures as an initiator because of its low activation energy as compared to nitrocellulose. Its heat of reaction is less than one-tenth that of nitrocellulose (calculated to be 320 J gm^{-1} for NaN_3 compared to 4200 J gm^{-1} for nitrocellulose[48]). Our experiments using just sodium azide as fuel atop SWNT showed output comparable to that obtained by launching nitrocellulose thermopower wave reaction waves. The magnitude of the voltage output was found to be unaffected (order of magnitude of tens of millivolts) by the change of fuel from nitrocellulose to sodium azide. Moreover for TPW devices made atop the traditional glass slide support, sodium azide reaction waves propagated for shorter distances as compared to nitrocellulose reaction waves. Accounting for these shorter reaction waves (leading to lower input fuel chemical energy) with a lower heat of reaction combined with the impact on the chemical potential gradient leads to improvement in efficiency of operation of sodium azide TPW devices. Moreover, we confirmed that if needed, it is possible to launch longer sodium azide reaction waves by suspending SWNT fiber devices (instead of being supported on a glass slide). Such devices consistently showed complete wave propagation over longer distances (longer than 10 millimeters compared to a few millimeters). Thus we conclude that the lower heat of reaction of sodium azide combined with the glass slide support acting as heat sink hinders long or complete propagation of such reaction waves. Future work in this

direction can study how exactly sodium azide impacts the operation with its effect on the temperature gradient and the doping of carbon nanotubes. One means of studying the doping effect of these different fuels is by analyzing their Raman spectra. Shift in the positions of the G- or G+ peaks can be used to infer about p or n doping of carbon nanotubes.[49] Magnitudes of these shifts can be further correlated to get an estimation of the excess thermopower voltage contributions from these fuels. A short Raman analysis carried out in this regards is discussed in the later part of this chapter. To summarize, traditional TPWs launched with sodium azide showed efficiency of conversion of up to 10^{-2} % as compared to values of 10^{-4} % showed by the commonly used nitrocellulose based TPW devices.

Another fuel mixture tried was sucrose with oxidizer potassium nitrate (KNO_3). Commonly used as a fuel mixture for rocketry, sucrose and KNO_3 were dissolved in water to form a fuel mixture (mass ratio 35:65). As with sodium azide, partial reaction wave propagations were observed when launched using SWNT thermal conduit. However unlike sodium azide, this fuel mixture showed shorter reaction waves even for reactions launched on suspended SWNT devices. This fuel mixture is slightly less energy dense (mass basis) as compared to nitrocellulose. The heat of reaction for this reaction was calculated to be about 4173.3 J/gm of KNO_3 or about 2712.6 J/gm of the fuel mixture compared to 4200 J gm^{-1} for nitrocellulose. Launching these waves opens avenues to use other commonly available and safe to store energy rich materials. In terms of efficiency, sucrose-KNO_3 devices showed slight improvement in efficiency as compared to nitrocellulose with values around 10^{-3} %.

Thus as seen in Figure 3-1 c, we observe an increasing trend in efficiency as we change TPW fuel from nitrocellulose (with sodium azide) to sucrose with KNO_3 to only sodium azide. Sodium azide devices showed highest efficiency, reaching about 10^{-2} % compared to 10^{-3} % shown by

sucrose-KNO_3 devices and 10^{-4} % shown by traditional nitrocellulose (with sodium azide) devices, all made with SWNTs. Thus fuels play a very important role in optimizing the energy conversion efficiency of the device. The future work in this field can focus on developing an extensive library of fuels that can be used to launch high efficiency TPWs. Also, when studying TPW reaction and voltage outputs corresponding to different fuels, factors such as the electrical energy output per unit of fuel, wave velocity, maximum voltage output etc. can be studied. This will allow us more insight in tuning the device depending on the intended application of the electrical output.

Experiments were also carried out to improve the conversion of energy released from the chemical reaction to electricity by harvesting the radiative and convective heat losses. Thermopower wave reactions launched using sodium azide have been observed to reach temperatures of up to 900°C and reaction waves launched using nitrocellulose have reached temperatures up to 1100°C. Our calculations confirm that at such high temperatures, a high percentage (> 95%) of the energy is outputted via radiation as compared to other modes such as conduction and convection. To be able to harvest the heat losses, we improved the TPW design such that the device was now no longer supported on the glass slide but was instead 'suspended' with its end connected to the copper tape electrodes. We then used thermoelectric (TE) harvesters to harvest the radiative (and convective) energy given out by such a TPW reaction. Figure 3-1 d shows a schematic of a suspended TPW device with external heat harvesters. By keeping the TE energy harvesters in the proximity of the propagating reaction wave, we capture part of the convective heat loss and thermalize the radiation energy emitted by the propagating reaction front and the (reacted) hot region of the thermal conduit. Thus, we increase the net amount of energy given out by the chemical reaction that is effectively converted into electrical

energy. The final experimental setup tested had a Bi_2Te_3 TE harvester on top and bottom of the TPW device. Since only the energy given out by the fuel reaction is the focus of the TE converter, when carrying out these experiments, care was taken to ensure that the TE harvesters were not exposed to the heat radiated by the joule heater used to initiate the TPW reaction. For this method of utilizing the heat that is given out by the system, a long enough reaction wave has to be launched and sustained across the length of the TPW device for optimum utilization of the available TE area beyond the length of the device that is used for the purpose of reaction initiation. For samples where sufficiently long reaction waves were launched, we were successfully able to obtain an electrical output from both the TPW device and the TEs surrounding it. As seen in Figure 3-1 e, having the TPW device suspended allowed us to harvest the radiative energy given out by the propagating reaction wave-front from even the bottom of the device which was previously inaccessible. Success of this experiment brought forth more opportunities that can be explored to improve efficiency. This experimental design was then combined with higher efficiency fuels such as sucrose-KNO_3 and sodium azide to boost the overall efficiency of operation even further. Other point to note, these experiments were carried out using an external resistance in all the three electrical circuits, i.e. in the setup with the TPW device and the two TEs, to obtain a more realistic and conservative estimate of efficiency than the efficiency values for TPWs launched without external electrical load i.e. when measuring open circuit voltage output. As can be seen in Figure 3-1 f, the net efficiency of operation of these suspended devices when combined with both the top and bottom TE harvesting gave us maximum efficiency of higher than 1%. One interesting point to note is that the efficiency of just the suspended sodium azide TPW reaction on its own is in some cases lower than the efficiencies seen when the sodium azide devices are supported using a glass slide. One of the reasons for this

outcome could be the complete propagation of sodium azide waves when suspended rather than being supported on glass slide. Removal of the heat sink of the glass slide on which the previous versions of the devices were placed can affect the wave propagation characteristics such as wave velocity, maximum temperature reached, the lengths of propagation of the reaction wave etc. and should be explored further to how it affects the efficiency of just the TPW voltage output on its own. In cases such as nitrocellulose fuel where the reactions could propagate longer distances even when supported on the glass slide, the glass slide supported device construction could be more advantageous due to possible slower reaction waves as compared to suspended devices. This slowing of reaction wave could possibly lead to a longer duration of voltage output, thus leading to higher output energy. However this heat sink also possibly reduces the magnitude of the temperature gradient established across the ends of the device and the thermoelectric component of the voltage output could thus be compromised. Hence more analysis is warranted to study the impact of removal of the bottom glass slide or heat sink support. Another aspect causing this variation in performance between the glass slide-supported TPW devices and the suspended TPW devices could be because our comparison is based on analyzing open circuit voltage for glass slide-supported TPW devices and closed circuit voltage for suspended TPW devices. Hence future work in this field could involve gathering data for and comparing the more accurate glass slide-supported TPW device based efficiency calculations involving a closed circuit analysis. Thus, in regards to our updated setup, even incorporating the more accurate external load electrical measurements, we demonstrated efficiencies as high as 1% when combining high efficiency TPWs with external heat harvesting using TEs.

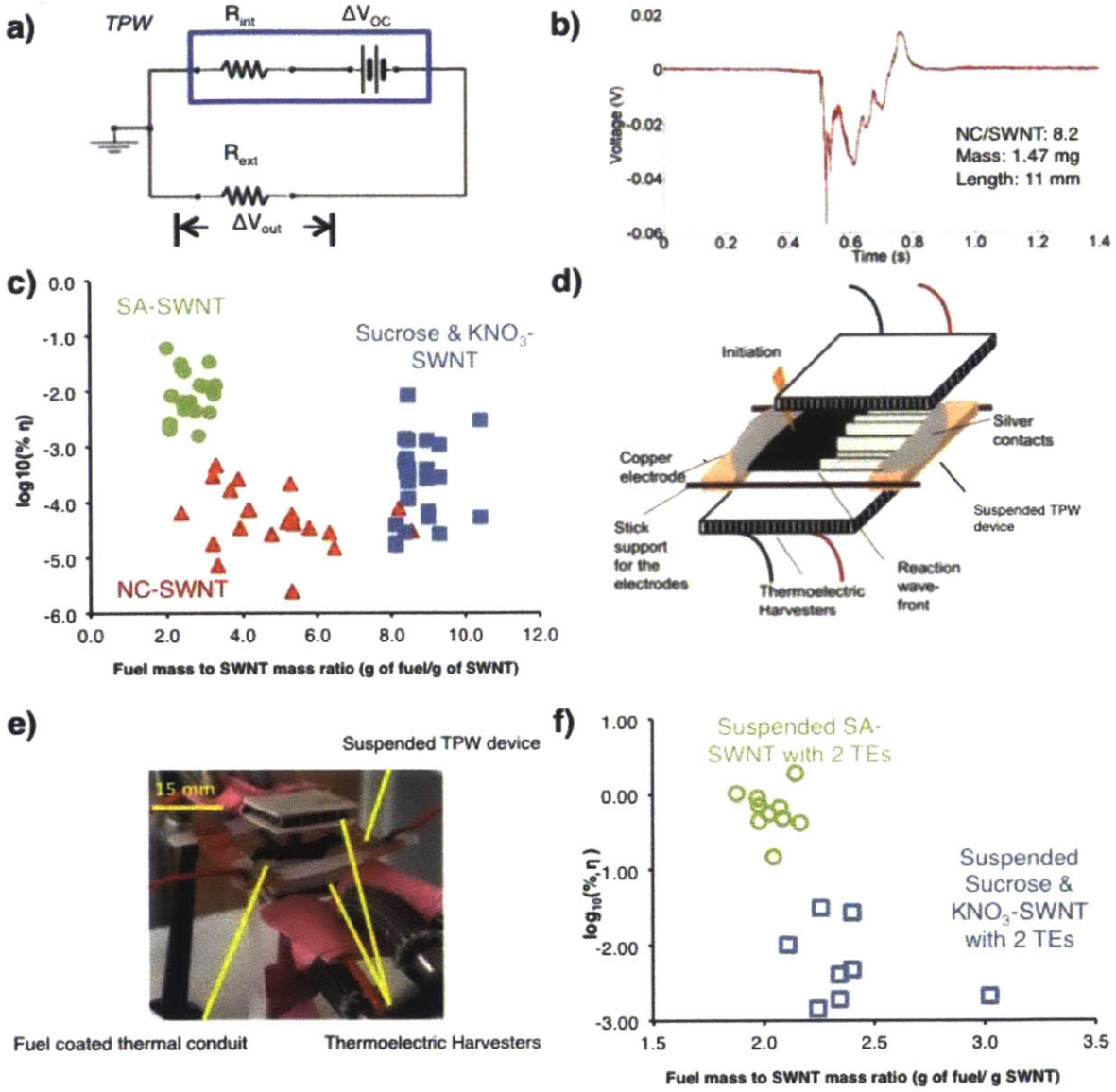

Figure 3-1 a) Circuit diagram for electrical analysis of thermopower wave (TPW) devices where we connect an external load R_{ext} to measure the voltage drop ΔV_{out} across it. b) Sample of an actual thermopower wave voltage output. The voltage output for this 11 mm long reaction wave lasts for about 600 ms. c) Chemical-to-electrical conversion efficiency of TPW devices using different fuels (Nitrocellulose (with sodium azide) or NC, Sodium azide or SA and Sucrose with KNO_3). d) Schematic of the updated TPW setup using suspended TPW devices such that TE harvesters can be suspended from the top and bottom of the device. e) A photo of an experimental setup involving TE harvesters (seen as white squares) suspended above and below a TPW device. f) Chemical-to-electrical conversion efficiencies of the updated TPW setups (i.e. including the electrical output from the reaction wave as well the TE harvesters).

3.3 Launching Longer Nitrocellulose Thermopower Waves & Comparison with TPW Device Efficiency Over Years

We studied the effect of length of propagation of reaction wave to understand more its relation to energy generation and power density. Traditional SWNT TPW devices were made with nitrocellulose (and sodium azide) fuel. To make these TPW devices, we start with clusters of SWNT fibers that will be individual devices. The fuel, nitrocellulose and the initiator, sodium azide are dissolved in solvents acetonitrile and water respectively. Usual concentrations for both the solutions range around 20 g/L. The final aim is to get a layer of fuel atop the carbon nanotube conduit, first a layer of the fuel i.e. nitrocellulose, followed by a layer of the initiator i.e. sodium azide. For this, the conduit is weighed and suitable amounts of the nitrocellulose-acetonitrile solution followed by sodium azide-water solution are added. Sodium azide is deposited only once the conduit has gained enough nitrocellulose mass. Once the solvent evaporates, in about 1 hour for acetonitrile and 4 hours in case of water based fuel solution, the conduit coated with the fuel is weighed. According to the previously followed experimental protocol, the final aim is to coat the thermal conduit in the mass ratio of about (1:3) with the fuel in the ratio of 2:1 of nitrocellulose to sodium azide. These ratios have been tried and tested to have enough fuel to coat the conduit uniformly to launch a successful reaction wave. Sodium azide has been traditionally added during the device preparation as the reaction initiator. It has a lower activation energy (and lower heat of reaction) as compared to nitrocellulose and is theoretically used to reduce the input heat needed to set off the reaction wave. However this current work shows that it is possible to launch reaction waves using just sodium azide as the fuel. The reaction wave from one end of these nitrocellulose samples was launched by using an external heat source of a joule heater heated to a high temperature by passing current through it. Previous work has shown that nitrocellulose starts losing weight because of reaction starting at about

175°C.[50] Thus in practical scenarios, such TPW devices could be initiated via any high enough spikes in the surrounding temperatures that would heat up at least one end of the TPW device beyond the reaction initiation temperature for the fuel, for example, in the vicinity of the car exhaust. As this reaction wave propagates, we obtain a voltage output across the ends of the device. The fuel coated cluster of SWNT fibers prepared as explained above is connected to the copper electrodes via silver paste for intimate electrical contact. The copper electrodes are supported on a glass slide. Figure 3-2 a shows a schematic of a typical TPW device with reaction wave propagation in progress. With the reaction initiated at one end of the fueled conduit, the reaction wave front proceeds to the other end of the device. Because various factors such as non-uniform coating of the fuel on carbon nanotubes or non-uniformity or defects in the thermal conduit, sometimes the reaction wave doesn't propagate all the way or slows down mid-way during propagation. Experimentally obtained voltage outputs from TPW devices have shown different profiles. Longer devices with tens of millimeter reaction wave propagation show broader voltage peaks. Figure 3-2 b plots sample voltage outputs from sodium azide-SWNT and sucrose-KNO_3-SWNT TPW devices. Apart from these single polarity peaks, we also obtain voltage outputs that show double polarity output, multiple peaks of single polarity etc. As has been discussed in the later parts of the chapter, in our proposed model for analyzing the voltage output from TPW devices, we explain how the interplay between the thermoelectric effect and the additive or negative effect of the chemical potential gradient induced voltage, coupled with complete or partial propagation of the reaction wave, can lead to different voltage output profiles. Figure 3-2 c shows snapshots of a reaction wave as it propagates. The reaction wave front can be clearly seen advancing with time. In Figure 3-2 d, we study the impact of length of propagation of TPW reaction on the duration of the voltage output. The TPW voltage output

profile not only accounts for the duration of the reaction but also the cooling of the system till the voltage output drops to zero. As seen in Figure 3-2 d, we can scale-up the system to launch longer reaction waves to obtain longer voltage output from the system. Comparison between fuels shows us that sucrose waves are much slower than nitrocellulose reaction waves. This combined with similar order of magnitude of voltage output and lower input chemical energy makes sucrose-KNO_3 TPW devices more efficient than nitrocellulose TPW devices. In another set of data collected with nitrocellulose-SWNT devices, reaction waves as long as 25 mm were successfully launched. In order to better understand these reaction wave propagations and exploit them for improved performance of TPW devices, more work needs to be done to study the reaction wave velocities for different fuel-thermal conduit pairs. Even for a chosen pair of fuel-thermal conduit, there is often non-uniformity in the reaction wave velocities observed experimentally. This could arise because of sample-to-sample variation in the thermal conduits being used. This factor is especially important for devices made out of SWNT clusters where each device is made by hand-plucking sections of SWNT forest or mat. This introduces visible non-uniformities in the devices e.g. different 'width' of the sample which in turn changes the cross sectional area of the sample which could impact not only the reaction wave propagation but also the electrical performance because of varying internal electrical resistance of the device. Another factor which can cause delays in the reaction wave propagation is the increased thickness of fuel layer over only a certain region of the thermal conduit. Non-uniformities in the fuel layer thickness can lead to stalling of the reaction in a particular region until either all the 'extra thickness' fuel reacts or can lead to extinction of the reaction wave if there is too much fuel to be able to sustain the reaction wave.

In order to evaluate the state of the art in the field of thermopower wave devices, on the basis of the literature published so far, making estimations where needed, we estimated the efficiency of operation for a wide variety of thermopower wave devices. As seen in Figure 3-2 e, starting with the efficiency of about 10^{-6} % for SWNT based devices in 2010, this current work (highlighted with external red circles in the year 2015) demonstrates the highest TPW device efficiency till date, for both just the TPW devices launched with sodium azide fuel (about 10^{-2} %) and newer TPW wave setups with higher efficiency fuel and external TE harvesting (about 1%).

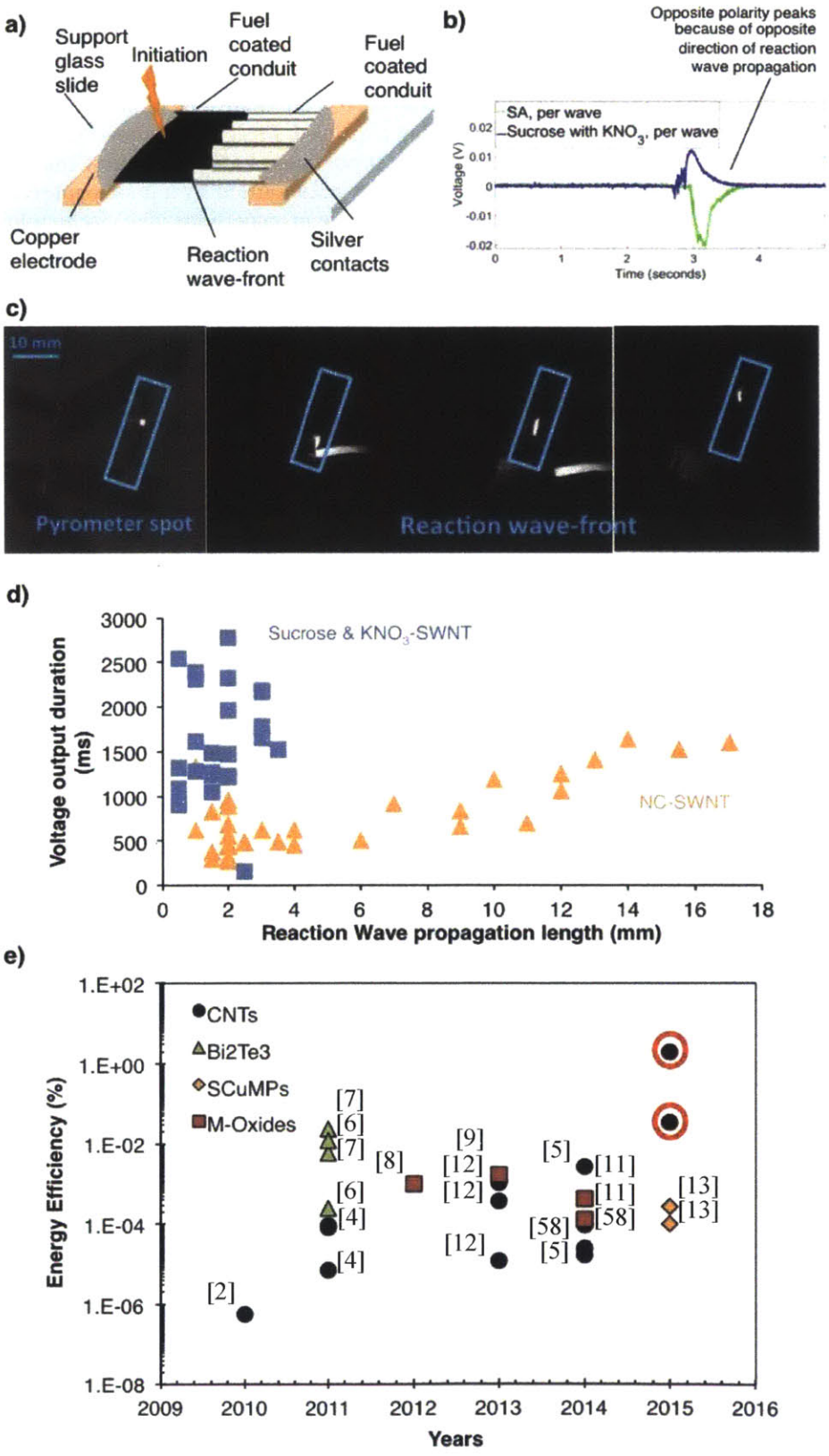
a)
Support glass slide
Initiation
Fuel coated conduit
Fuel coated conduit
Copper electrode
Reaction wave-front
Silver contacts
b)
Opposite polarity peaks because of opposite direction of reaction wave propagation
SA, per wave
Sucrose with KNO3, per wave
Voltage (V)
Time (seconds)
c)
10 mm
Pyrometer spot
Reaction wave-front
d)
Sucrose & KNO3-SWNT
NC-SWNT
Voltage output duration (ms)
Reaction Wave propagation length (mm)
e)
CNTs
Bi2Te3
SCuMPs
M-Oxides
Energy Efficiency (%)
Years

Figure 3-2 a) Schematic for a traditional thermopower wave device consisting of thermal conduit coated with a layer of fuel and connected to the copper tape electrodes via silver paste. The entire setup is supported on a glass slide. b) Sample voltage output from SWNT thermopower reaction waves launched using sodium azide and sucrose-KNO_3. c) Snapshots of an actual thermopower wave device with the reaction propagation being captured. First image shows the pyrometer spot focused at the center of length of the sample. The three images after that show the propagation of reaction front from the bottom to the top once it has been ignited by a joule heater. d) While not perfectly correlated, longer thermopower reaction wave propagations give rise to a longer voltage output. e) Master plot for chemical to electrical conversion efficiencies of all thermopower wave device setups published so far. The highest efficiency highlighted points in 2015 correspond to this work.

3.4 A Simplified Heat and Mass Balance Based Reaction Model to Analyze the Voltage Output from Thermopower Wave Devices

TPW devices convert chemical energy into electrical energy via self-propagating reaction waves.[2] A layer of fuel coated atop a thermal conduit is used to launch this self-propagating reaction wave that is initiated from one end of the device. For any chemical reaction carried out in an adiabatic system which disallows transfer of heat and mass of its contents with the surroundings, the difference between the temperature reached by the products of the reaction once the reaction is complete and the temperature of the system at the start of the reaction is known as the adiabatic reaction temperature (rise) of that chemical reaction. Theoretical and numerical analysis shows that for such steady state TPW type of a self-propagating reaction wave launched in an adiabatic system, the temperature behind the reaction wave front should be the adiabatic reaction temperature of the chemical reaction (plus the ambient or the starting temperature).[14] At the same time, the unreacted region of the fuel-thermal conduit will be at the ambient temperature or the temperature of the device before the reaction is initiated. Thus, while the reaction is propagating, there exists a temperature gradient equivalent to the adiabatic reaction temperature rise across the ends of the TPW system. Moreover, the region of thermal conduit that is coated with the fuel gets doped because of the fuel molecules sitting atop it.[3] As the reaction proceeds and the fuel molecules desorb, a chemical potential gradient is established

across the ends of the device. This gradient arises because of the difference in the chemical potential of the fuel coated (unreacted) and fuel un-coated (reacted) regions of the thermal conduit. Thus as the self-propagating reaction wave proceeds along the length of the thermopower wave device or the thermal conduit, there is a temperature gradient and a chemical potential gradient created across the ends of the device. Both these gradients lead to generation of a voltage output that can be harvested across the ends of the TPW device as electrical output.

As explained before, TPW devices can be studied as constant voltage sources giving rise to an open circuit voltage difference (ΔV_{OC}) across its ends. When connected to an external electrical load or electrical resistance (R_{ext}), we can obtain useable output voltage (ΔV_{out}) and current flow through the load. In an ideal adiabatic system, during the entire duration of the reaction wave propagation, the magnitude of the temperature gradient and the chemical potential gradient should remain constant for a chosen pair of uniformly coated layer of a fuel over a chosen thermal conduit. Thus, if we can estimate the magnitude of the thermal gradient and the chemical potential gradient, for a system with a known Seebeck coefficient S, we can calculate the expected open circuit voltage (ΔV_{OC}) for a given pair of fuel-thermal conduit TPW device. Using the values of the internal resistance of the TPW device (R_{int}) and the resistance of the load attached (R_{ext}), we can compute the expected output voltage (ΔV_{out}).

However in practice, for a TPW device, factors such as heating up of the thermal conduit (which is the dominant thermal mass in the system), conductive heat losses to the copper electrodes, radiative and convective heat losses from the device to the surrounding etc. lead to the actual temperature gradient being not only lower than that expected under adiabatic conditions but also time variant. Similarly, depending on the properties of the thermal conduit and the fuel coated

thermal conduit, the internal resistance of the device (R_{int}) changes as the reaction proceeds. As the reaction wave proceeds, the ratio of the length or the region of the thermal conduit that is heated due to the reaction of the fuel that was laid atop of it and the region of the thermal conduit that is at the ambient temperature changes. This can affect the net internal resistance of the device, especially in the case of thermal conduits such as carbon nanotubes which exhibit temperature dependent resistivity.[51] Ideally, the chemical potential gradient should also be just dependent on the fuel-thermal conduit pair and should remain constant as long as there is uniform reaction wave propagation. However factors such as non-uniform coating of fuel layer atop the thermal conduit, lack of enough fuel to coat the entire surface area leading to a lower than maximum possible level of doping etc. can lead to variable chemical potential gradient across samples and even while the reaction wave is propagating along a single sample. Also, this chemical potential gradient stops existing as soon as the reaction has completely propagated or has stopped propagating after partial propagation along the device length. In cases where the reaction propagation ceases as the reaction wave front reaches the opposite end of the thermal conduit, the temperature gradient doesn't necessarily drop to zero as the 'other' side of the thermal conduit where the reaction wave was launched cools during the time of reaction propagation. Thus, depending on the internal heat transfer properties of the system and the rate at which it loses heat to the surroundings, there is a possibility of reversal of the temperature gradient leading to opposite polarity voltage output contribution because of the thermoelectric effect. Interplay of factors such as time dependence of the temperature gradient and the chemical potential gradient and practical conditions for device operation e.g. non-adiabatic system and device-to-device differences in the experiments can possibly explain different varieties of

voltage outputs e.g. double polarity voltage output, single polarity voltage output etc. obtained from the TPW devices.

In an attempt to gain more understanding about voltage output from TPW devices, a theoretical model for analyzing self-propagating reaction waves was setup. This model, based on the heat and mass transfer balance for the reaction wave, and the theory of excess thermopower, computes TPW voltage output for different scenarios for reaction and heat propagation. With this model, via known or calculated thermal and electrical properties of the system, we can calculate the expected electrical output for a chosen fuel-thermal conduit TPW system. Using this model, one can reverse calculate the fuel and the system properties needed in order to obtain a specific voltage output profile as needed for any specific application. We demonstrate using this model for fitting the experimental data from nitrocellulose (and sodium azide)-SWNT TPW devices. We analyze the experimentally obtained voltage output profiles by fitting for various parameters in the model and learn more about the heat transfer and electrical properties of our system.

3.4.1 Method of Lines applied to 1D Continuous Domain Heat and Mass Balance Equations

To predict the voltage output from a TPW device, we need to calculate the voltage contribution due to the thermoelectric effect i.e. the temperature gradient, and the voltage contribution due to the excess thermopower i.e. the chemical potential gradient. To calculate the temperature gradient across the reaction system ends' as a function of time, we solve a system of heat and mass balance equations that simulates TPW propagation. This allows us to obtain the

temperature gradients established along the ends of the system as a function of time. Using the magnitude of the temperature gradient with the value of the Seebeck coefficient of the system S, we calculate the thermoelectric contribution of the voltage output. For a known or fitted value of the chemical potential gradient (which we assume stays constant and active during the reaction wave propagation), we then estimate the value of the voltage contribution because of excess thermopower. Thus, using the information about the temperature gradient and the chemical potential gradient along with other physical properties of the system, the final expected voltage output of the system can be calculated. When fitting the experimental data for system property parameters, this model output voltage profile (generated using some initial guess values for the parameter values) is compared with the experimentally obtained output voltage profile. With the aim of minimizing this difference, we try to fit values to the parameters involved (example, Seebeck coefficient of the system S, magnitude of the chemical potential gradient $\Delta\mu$, conductive losses via copper electrodes etc.) till a good fit is obtained. Thus, using this model, we can extract parameter values representative of our experimental system. These can then be used with the model to predict other future voltage output profiles that can be obtained experimentally. Analyzing these parameter values for multiple of the voltage output data can help in studying device-to-device variation in operation and guide us towards characteristics of higher efficiency devices.

As shown previously,[15] a 1D self-propagating reaction wave can be analyzed by studying the corresponding heat and mass transfer equations for a system of continuous fuel layer undergoing reaction in a one dimensional system. This continuous layer of a fuel is provided with input heat to launch or start the reaction wave. Internal heat transfer properties of the system control the heat propagation that leads to the sustenance of the reaction wave. The external heat transfer

properties of the system allow for us to model the heat lost by the reaction system to the surrounding. In this model, we account for conductive heat loss via the ends of the fuel layer and convective and radiative losses from the TPW device.

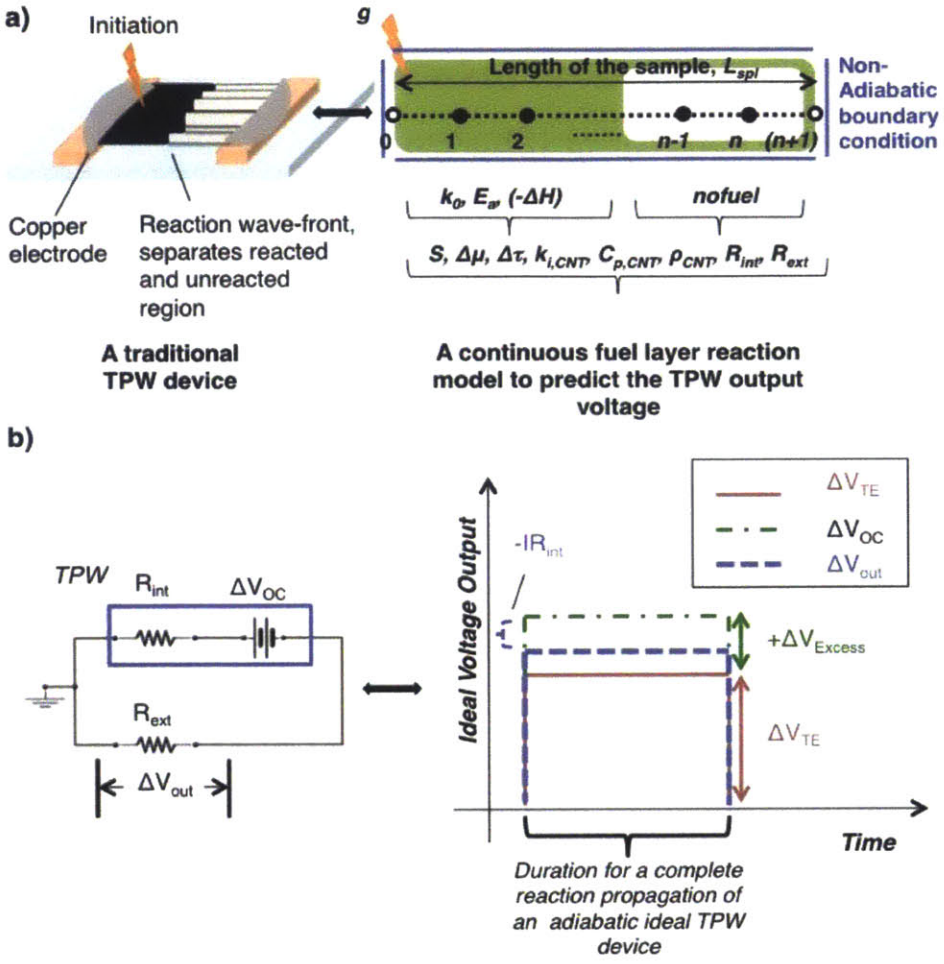

Figure 3-3 a) The left side shows a schematic of a traditional thermopower wave device with a reaction wave propagation along a fuel coated thermal conduit connected to copper tape electrodes and supported on a glass slide. The right hand side section is a visualization of a model of a continuous layer of a fuel undergoing reaction to predict or fit the voltage output from a thermopower wave device. All the properties (except the device's external heat loss properties) needed to completely define a thermopower wave device using such a scheme have been noted. b) The left side shows a schematic of the electrical circuit diagram for analyzing the output voltage ΔV_{out} across an external resistor or load R_{ext} powered by a thermopower wave device with internal resistance R_{int}. The right hand side shows a schematic of how an ideal voltage output profile for a thermopower wave device undergoing complete reaction propagation from one end of the device to other, under adiabatic heat transfer condition, would look like. The open circuit voltage ΔV_{OC} from a thermopower wave device is contributed to by both the temperature gradient and the chemical potential gradient. When being modeled as a battery giving voltage output ΔV_{out} across an external resistor R_{ext}, potential drop across the internal resistance R_{int} is also accounted for.

The corresponding set of heat and mass balance equations being studied is as below. In equations (3) and (4), T denotes the temperature, Y denotes the concentration, t denotes the time and x denotes the space coordinate. The subscripts are used to denote the type of the property and/or the material it is attributed to. We assume that the reaction system starts off at the ambient temperature T_{amb}. The system's temperature profile changes as heat is released because of the fuel reaction. Heat is generated in the system because of propagating reaction wave, which releases heat via ($-\Delta H$), the heat of reaction. Fuel reaction is modeled by assuming first order reaction kinetics. E_a denotes the activation energy of the reaction and k_0 denotes the Arrhenius pre-exponential factor. Since the thermal mass of carbon nanotubes dominates that of the fuel (which often gets converted to mainly gaseous products post-reaction), the energy balance equation considers the thermal mass of the carbon nanotubes to be representative of the system. We make this assumption since we know that the thermal transport is dominated by transport though the carbon nanotubes rather than the layer of the fuel surrounding the cluster of carbon nanotubes. Previous work analyzing a more detailed model consisting of separate energy balances for the fuel and thermal conduit showed that for practical systems consisting of carbon nanotubes based thermal conduits, there is a fast thermal equilibrium between the thermal conduit and the fuel layer leading to almost equal temperature profiles.[15] Thus the thermal mass of the system i.e. the mass of the carbon nanotubes present can be calculated using ρ_{CNT}, density of carbon nanotubes, and $C_{p,CNT}$, specific heat capacity of carbon nanotubes. The energy balance for the continuous fuel system is as shown in equation (3). During practical experimental conditions, while the reaction wave is propagating across the length of the device, it loses heat through multiple modes such as conductive heat losses through the copper electrodes, convective heat losses because of heating up of the surrounding air, convective heat losses through the

heating of the gaseous products lost to the atmosphere, radiative losses due to heating up of the carbon nanotube thermal conduit etc. On the right hand side of equation (3), the two right-most terms account for the radiative and convective losses from the fuel system to the surroundings. Here, $(A_{surface}/V)$ denotes the device's surface area per volume that is active when losing heat to the surroundings and h_{conv} is the convective heat transfer coefficient.

$$\rho_{CNT}C_{p,CNT}\frac{\partial T}{\partial t} = k_{CNT}\frac{\partial^2 T}{\partial x^2} + (-\Delta H)k_o Y e^{-\frac{E_a}{RT}} - \varepsilon\sigma_B\left(\frac{A_{Surface}}{V}\right)\left(T^4 - T_{amb}^4\right) - h_{conv}\left(\frac{A_{Surface}}{V}\right)\left(T - T_{amb}\right) \quad (3)$$

The mass balance equation which assumes the 1st order Arrhenius form of reaction for the fuel is as shown in equation (4).

$$\frac{\partial Y}{\partial t} = -(k_o Y)e^{-\frac{E_a}{RT}} \quad (4)$$

For the ease of solving these coupled heat and mass balance equations, we non-dimensionalize the variables of temperature, concentration, time and space coordinate to define non-dimensional variables u, y, τ and ξ respectively.

$$u = T\left(\frac{R}{E_a}\right) \quad (5)$$

$$y = Y\left(\frac{1}{\rho_{CNT}}\right) \quad (6)$$

$$\tau = t\left(\frac{(-H)k_0 R}{C_{p,CNT}E_a}\right) \quad (7)$$

$$\xi = x\sqrt{\left(\frac{\rho_{CNT}C_{p,CNT}}{k_{CNT}}\right)\left(\frac{(-\Delta H)k_0 R}{C_{p,CNT}E_a}\right)} \tag{8}$$

Non-dimensional form of the heat and mass balance equations is shown in equations (9) and (10).

$$\frac{\partial u}{\partial \tau} = \frac{\partial^2 u}{\partial \xi^2} + ye^{-\frac{1}{u}} - w_{rad}(u^4 - u_{amb}^4) - w_{conv}(u - u_{amb}) \tag{9}$$

$$\frac{dy}{d\tau} = -\beta y e^{-\frac{1}{u}} \tag{10}$$

Here, w_{rad} corresponds to the non-dimensional net radiative heat transfer coefficient exhibited by the system. For a known ($A_{surface}/V$), we can estimate w_{rad} for a chosen system. Similarly, w_{conv} corresponds to the non-dimensional net convective heat transfer coefficient exhibited by the system. Non-dimensionalization of variables also gives rise to the important non-dimensional factor of β. β is the inverse non-dimensional adiabatic temperature rise of the fuel.

$$\beta = \frac{C_{p,CNT}E_a}{(-\Delta H)R} \tag{11}$$

Thus [$(1/\beta)$ + u_{amb}] gives the maximum non-dimensional temperature that can be reached by the system when all the heat released by the fuel reaction stays within the system.

To obtain the required time dependent temperature gradient along the ends of the device, we need to solve the above set of partial differential equations combined with equations for their heat loss to the surrounding. To simplify solving this set of partial differential equations, we use the technique of Method of Lines. This method involves discretization along one of the two

independent variables (τ and ξ) to convert the set of partial differential equations to ordinary differential equations that are more easily solvable. In this case, as shown in equation (12), we discretize along the distance coordinate by using the central difference form for simplifying the second order derivative term in equation (9). As can be seen in Figure 3-3 a, when applying the method of lines, the entire domain along the direction ξ is divided into grid points at a distance of $\Delta\xi$ from the starting point or starting interface with the surrounding. Assuming we divide the domain in $(n+1)$ equal regions, $\Delta\xi$ can be calculated by dividing the non-dimensional sample length ξ_{spl} into $(n+1)$ parts. The 1st and the last point on this new grid, denoted by subscript *0* and $(n+1)$, act as interfaces between the surroundings at ambient temperature u_{amb} and the actual internal reaction wave region which is probed or studied by analyzing the concentration and temperature at internal points with subscripts *1* to *n*.

For a general point *i* within the reaction domain, the second order derivative with respect to the space coordinate can be simplified using equation (12).

$$\left.\frac{d^2u}{d\xi^2}\right|_i = \frac{u_{i+1} - 2u_i + u_{i-1}}{\Delta\xi^2} \tag{12}$$

Substituting for discretization along the space coordinate, the partial differential heat transfer equation (9) now is converted to a system of ordinary differential equation as shown in equation (13). This equation applies to each grid point $i = (1 \text{ to } n)$ along the reaction domain.

$$\frac{du_i}{d\tau} = \frac{u_{i+1} - 2u_i + u_{i-1}}{\Delta\xi^2} + y_i e^{-\frac{1}{u_i}} - w_{rad}(u_i^4 - u_{amb}^4) - w_{conv}(u_i - u_{amb}) \tag{13}$$

$$\frac{dy_i}{d\tau} = -\beta y_i e^{-\frac{1}{u_i}} \tag{14}$$

In this model, we account for the external heat transfer losses through the ends of the device to the copper tape electrodes the carbon nanotubes based waves devices are attached to. At the boundary or the interface, the system is assumed to exchange heat with the surrounding (which is assumed to be always at non-dimensional temperature u_{amb}) via (external) conductive heat transfer coefficient k_e=k_{Cu} acting over external heat transfer length scale L_e, and with the internal reaction wave system via conductive heat transfer through carbon nanotubes which can be quantified using thermal conductivity of carbon nanotubes k_{CNT} and internal heat transfer length scale $\Delta\xi$. Since for the purpose of this model we assume that the reaction thermopower wave sample to be uniformly thick, we can ignore the variation in the cross-sectional area across which the heat transfer occurs i.e. A_i=A_e=A_{CNT}. In defining the conductive heat loss through the system, we define two more heat transfer coefficients acting in the system: the internal heat transfer coefficient $g_i = \frac{k_{CNT}}{\Delta\xi}$ and the external heat transfer coefficient $g_e = \frac{k_e}{L_e}$.

$$\frac{k_e}{L_e}(u_{amb} - u_0) = \frac{k_{CNT}}{\Delta\xi}(u_0 - u_1) \tag{15}$$

$$\therefore u_0 = \frac{\left(\frac{k_e}{L_e}u_{amb} + \frac{k_{CNT}}{\Delta\xi}u_1\right)}{\left(\frac{k_e}{L_e} + \frac{k_{CNT}}{\Delta\xi}\right)}$$

Similarly, we can write the equation for the boundary condition at the other end of the sample, denoted by subscript (n+1).

$$\frac{k_{CNT}}{\Delta\xi}(u_n - u_{n+1}) = \frac{k_e}{L_e}(u_{n+1} - u_{amb}) \tag{16}$$

$$\therefore u_{n+1} = \frac{\left(\frac{k_e}{L_e}u_{amb} + \frac{k_{CNT}}{\Delta\xi}u_n\right)}{\left(\frac{k_e}{L_e} + \frac{k_{CNT}}{\Delta\xi}\right)}$$

These boundary conditions can be used to simplify the heat transfer equation at the grid points 1 and *n*. Thus, after employing the technique of method of lines and modeling the heat loss through the ends of system as conductive losses, the updated set of equations governing the reaction domain between interfaces is given below in equations (17-20).

$$\frac{du_1}{d\tau} = \frac{u_2}{\Delta\xi^2} + \frac{\left(-2\frac{k_e}{L_e} - \frac{k_{CNT}}{\Delta\xi}\right)}{\left(\frac{k_e}{L_e} + \frac{k_{CNT}}{\Delta\xi}\right)}\frac{u_1}{\Delta\xi^2} + \frac{\left(\frac{k_e}{L_e}\right)}{\left(\frac{k_e}{L_e} + \frac{k_{CNT}}{\Delta\xi}\right)}\frac{u_{amb}}{\Delta\xi^2} + y_1 e^{-\frac{1}{u_1}} \tag{17}$$

$$\frac{du_i}{d\tau} = \frac{u_{i+1} - 2u_i + u_{i-1}}{\Delta\xi^2} + y_i e^{-\frac{1}{u_i}} - w_{rad}(u_i^4 - u_{amb}^4) - w_{conv}(u_i - u_{amb}) \tag{18}$$

for i =2 to (n-1)

$$\frac{du_n}{d\tau} = \frac{\left(-2\frac{k_e}{L_e} - \frac{k_{CNT}}{\Delta\xi}\right)}{\left(\frac{k_e}{L_e} + \frac{k_{CNT}}{\Delta\xi}\right)}\frac{u_n}{\Delta\xi^2} + \frac{\left(\frac{k_e}{L_e}\right)}{\left(\frac{k_e}{L_e} + \frac{k_{CNT}}{\Delta\xi}\right)}\frac{u_{amb}}{\Delta\xi^2} + \frac{u_{n-1}}{\Delta\xi^2} + y_n e^{-\frac{1}{u_n}} \tag{19}$$

$$\frac{dy_i}{d\tau} = -\beta y_i e^{-\frac{1}{u_i}} \quad \text{for } i = 1 \text{ to } n \tag{20}$$

This coupled set of equations (17-20) when solved with appropriate initiation condition allows us to fully characterize the temperature and the fuel concentration profile of the thermopower wave device. The input heat needed to start the reaction can be simulated by setting the temperature of the grid point 1 at zero time or start of the reaction to be high enough for the fuel reaction to be activated. From the previous work in analyzing self-propagating reaction waves in one dimension, the minimum non-dimensional temperature needed to initiate the fuel reaction was found to be $g=g_0e^{0.37\beta}=0.16e^{0.37\beta}$.[15]

In fitting our SWNT-nitrocellulose TPW device data, we try to use this input equation or some other value of g_0 when fitting for the data. Since experimental work has shown that nitrocellulose starts showing reduction in weight due to reaction starting at about 175°C,[50] care was taken to ensure that dimensionalized g value was always practical. Partial propagation of the reaction wave along the length of the device was modeled by setting the input fuel concentration of *nofuel* number of grid points (beginning from the end of the system) to zero. When fitting experimental data, value of *nofuel* is chosen such that the ratio of the difference between the total number of reactors n and the empty reactors *nofuel* i.e. $(n\text{-}nofuel)/n$ can be correlated to the % of the thermopower wave device length that has successfully reacted due to propagation of the reaction wave. Thus, knowing the experimental value of the % conversion or % propagation along the length of the sample, *nofuel* can be calculated for the chosen value of n.

Using this temperature profile obtained by solving equations (17-20) and with equations (15) and (16), for each time point the system is being analyzed for, we can calculate the temperature gradient established across the ends of the system by calculating $(u_{n+1}-u_0)$. Using the value of the energy of activation E_a, we can convert this non-dimensional temperature gradient into dimensional temperature gradient $(T_{n+1}-T_0)$. For known S, the Seebeck coefficient of the carbon

nanotube – fuel system, we can calculate $\Delta V_{TE}(t)$, the expected thermoelectric voltage output from the system. In practice, the Seebeck coefficient of the system is a temperature dependent property[52] and thus for a realistic thermopower wave system, should vary with time. However, for the ease of modeling, we assume it to be a fixed quantity that doesn't vary with time, but varies from device to device to account for differences in the thermal conduit (% of metallic and semi-conducting nanotubes), the differences in the temperatures reached by each reaction system and the extent of contact between the fuel layer and the thermal conduit.

$$\Delta V_{TE}(t) = S(T_{n+1}(t) - T_0(t)) \tag{21}$$

The theory of excess thermopower predicts that the voltage output from the thermopower wave devices also gets contribution from $\Delta\mu$, the chemical potential gradient that is established across the ends of the system. This chemical potential gradient depends on the doping of the thermal conduit by the fuel and exists during reaction wave propagation as long as there is presence of both reacted and unreacted region of the fuel layer atop the thermal conduit. This gradient drops to zero once the reaction wave has fully propagated and all the fuel coated atop the thermal conduit has reacted. In case of partial reaction wave propagation, when the reaction wave propagation halts mid-way, there still exist two regions, fuel coated and fuel uncoated or bare thermal conduit. However, in such a situation, we hypothesize that the charge carriers internally diffuse towards equilibration within the thermal conduit layer (rather than flowing through the external electrical circuit) thus not contributing to a measurable voltage output across the ends of the device. Hence, even in case of partial reaction propagation, the excess thermopower wave voltage contribution has been assumed to stop as soon as the reaction wave propagation stops. Knowing $\Delta\mu$, we can calculate ΔV_{Excess}, the excess thermopower contribution to the net voltage output across the thermopower wave device.

$$\Delta V_{Excess}(t) = -\frac{1}{e}(\Delta\mu(t)) \tag{22}$$

We assume the ideal thermopower wave device preparation where the fuel dopes the thermal conduit uniformly and so the chemical potential gradient is just a function of the presence of a moving reaction wave front and is not device length dependent. Thus for a given sample, we assume the value of $\Delta\mu$ to be time invariant for as long as the reaction wave is propagating. Changes in values of $\Delta\mu$ as obtained while fitting different experimental voltage output profiles from different samples using the same fuel-thermal conduit combination could be insightful in trying to understand all different types of voltage outputs we observe and point to inconsistencies in sample preparation leading to device-to-device performance variation.

ΔV_{TPW} or ΔV_{OC}, the net (open circuit) voltage output from the thermopower wave device is given by the presence or addition of both the thermoelectric voltage output and the excess thermopower output.

$$\Delta V_{TPW} = \Delta V_{OC} = \Delta V_{TE} + \Delta V_{Excess} \tag{23}$$

When calculating this net voltage output by simulating a system of a continuous domain of fuel undergoing reaction, the time variance in the presence of the chemical potential gradient is accounted for by making its contribution dependent on the presence of the reaction wave. This is done by keeping the $\Delta V_{\mathrm{Excess}}$ contribution 'on' only as long as the reaction wave propagates. Complete conversion or expected reaction conversion is ensured by making sure that the concentration in the last filled grid point falls below non-dimensional concentration 10^{-2}.

$$\Delta V_{TPW} = \Delta V_{TE} + \Delta V_{Excess} \tag{24}$$
$$\therefore \Delta V_{TPW} = S(T_{n+1} - T_0) - \frac{1}{e}(\Delta\mu)(y_{lastfilledgridpoint} - y_1)$$

Equation (24) gives the voltage output equivalent of an open circuit voltage output for a voltage source. For more accurate power and energy output calculations, the experimental data is collected for the voltage output across an external resistance R_{ext}. Hence when predicting the experimental voltage output, we need to calculate the (closed circuit) output voltage corresponding to the open circuit voltage in equation (24). R_{int} denotes the internal resistance of the thermopower wave device. Since the resistance mainly depends on the carbon nanotube thermal conduit, it is a function of temperature and should change as the reaction propagates along the length of the device.[51] Also, presence of the fuel layer atop carbon nanotubes leads to changes in the resistance and thus the device internal resistance is expected to change as the fuel layer atop it reacts. However to simplify this model, we assume R_{int} to be a time (and temperature) invariant property of the device. Experimentally, R_{int} is the average of the TPW device resistance, measured before and after the reaction propagation.

$$\Delta V_{out} = \Delta V_{OC} - IR_{\text{int}}$$
$$\therefore \Delta V_{out} = S(T_{n+1} - T_0) - \frac{1}{e}(\Delta\mu)(y_{lastfilledgridpoint} - y_1) - IR_{\text{int}}$$
$$\therefore \Delta V_{out} = S(T_{n+1} - T_0) - \frac{1}{e}(\Delta\mu)(y_{lastfilledgridpoint} - y_1) - \left(\frac{\Delta V_{out}}{R_{ext}}\right)R_{\text{int}}$$
$$\therefore \Delta V_{out} = \frac{S(T_{n+1} - T_0) - \frac{1}{e}(\Delta\mu)(y_{lastfilledgridpoint} - y_1)}{1 + \frac{R_{\text{int}}}{R_{ext}}} \tag{25}$$

Equation (25) predicts the output voltage expected from a TPW device having an internal resistance R_{int}, Seebeck coefficient S, fuel dependent chemical potential gradient $\Delta\mu$ and external load resistance R_{ext}.

Thus, summarizing the steps involved in using this model in order to evaluate the output voltage profile, we need values for the following parameters to fully quantify the reaction system: ρ_{CNT}, $C_{p,CNT}$, k_{CNT}, k_e/L_e, β, k_0, E_a, S, $\Delta\mu$, R_{int}, R_{ext}, sample length L_{spl}, $\Delta\xi$ or n, *nofuel*, $(A_{surface}/V)$ and h_{conv}.

Table 3-1: Properties of Nitrocellulose

Parameter	Value	NC Specifications	Source
E_a	32.6 (kcal mol^{-1})=136.4 (kJ mol^{-1})	13.4%N NC	Chen & Brill[50]
$(-\Delta H)$	4200 (J gm^{-1})		Kim et al.[48]
k_0	$\log_{10}(k_0) = 16.4$ [s^{-1}] Or $k_0=2.512x10^{16}$ s^{-1}	13.4%N NC	Chen & Brill[50]

Table 3-2: Properties of Carbon Nanotubes

Parameter	Value	CNT Specifications	Source
$C_{p,CNT}$	0.65 (J gm^{-1} K^{-1})	300K for SWNT ropes samples	Hone et al.[53]
$k_{i,CNT}$	36 (J s^{-1} m^{-1} K^{-1})	Dense-packed SWNT mat	Hone et al.[54]
δ_{CNT}(Resistivity)	10^{-6} (Ω m)	Crystalline metallic SWNT ropes	Thess et al.[55]
ρ_{CNT}	$1.4x10^6$ (g m^{-3})	Metallic SWNT ropes	Collins & Avouris[56]

Since our experimental data corresponds to TPW launched using glass slide supported nitrocellulose-SWNT TPW devices, we note literature values for various properties for nitrocellulose (NC) and carbon nanotubes as shown in *Table 3-1* and *Table 3-2*.

3.4.2 Procedure for Predicting and Analyzing Experimental Data Using 1D Continuous Fuel Layer Model for Thermopower Wave Devices

With known values for the TPW device system properties discussed above, we can use the model to predict the form of the output voltage profile. Alternatively, we can use the thermopower wave device output voltage model with the experimental voltage output to fit for various parameters for our experimental system. For simplifying the fitting process for the experimental voltage profiles for SWNT-nitrocellulose based TPW devices, we calculate β using the literature values for specific heat of carbon nanotubes and heat of reaction for nitrocellulose. The value was found to be 2.54. However since nitrocellulose is a polymer with not a very well defined reaction mechanism, we fit for the reaction parameters: k_0 and E_a. Also, both k_0 and E_a need to be fitted for, rather than using the literature values, in order to get model predicted voltage in the right order of magnitude for both the magnitude of voltage output and the time scales for the output. Fixing β but varying E_a means that $(-\Delta H)$ is indirectly varied too. For non-dimensionalizing length, we use literature values for thermal conductivity of carbon nanotubes ($k_{i,CNT}$) and density of carbon nanotubes (ρ_{CNT}). This allows us to calculate ξ_{spl} from L_{spl}. The value of R_{ext} was 47Ω on the basis of the experimental data. The starting temperature condition for all the reactors was assumed to be the non-dimensional equivalent of room temperature of 298K. Similarly, the fueled grid points had starting input of non-dimensional 1 fuel unit whereas

the *nofuel* grid points had no input fuel. For these parameter fittings, the value of *n* was chosen to be 100 on the basis of previous practice runs where *n* was also one of the system parameters that was optimized for to obtain the best possible prediction of the system voltage output. List of all the parameters that are given as input to the model is shown in *Table 3-3*.

Table 3-3: TPW Output Voltage Model Parameters: Inputs

Parameter	***Parameter Description***	***Input Form***
$\beta = \frac{C_{p,CNT} E_a}{(-\Delta H) R}$	Inverse of the non-dimensional adiabatic temperature rise for the chosen fuel	Fixed and calculated input
$C_{p,CNT}$=0.65 (J gm^{-1} K^{-1})	Specific heat capacity of carbon nanotubes	Literature input used to calculate β
$k_{i,CNT}$ = 36 (J s^{-1} m^{-1} K^{-1})	Thermal conductivity of carbon nanotubes	Literature input to non-dimensionalize x
ρ_{CNT} = 1.4x10^6 (g m^{-3})	Density of carbon nanotubes	Literature input to non-dimensionalize x
R_{int}	Average internal resistance of the thermopower wave device (Ω)	Experimental input
R_{ext} = 47 Ω	External resistance used to measure the TPW output voltage	Experimental input
$g=g_0 e^{(0.37\beta)}$	Initiation heat pulse (non-dimensional temperature) provided to the 1st grid point	
$fuel_{each\ reactor}$	Fuel quantity in each reactor (either 1 or 0)	User Input to decide fuel content in filled and *nofuel* reactors
u_{amb}	Non-dimensional ambient temperature	Input assuming 298 K
n=100	Number of grid points in the system	Fixed
nofuel	Number of un-fueled grid points in the system	Experimental input from % propagation or % conversion

Using the inputs from *Table 3-3*, we fit for the remaining parameters to obtain numerical values for them. In *Table 3-4* is the list of the parameters being optimized for and the interpretation from each parameter fitted.

Table 3-4: TPW Output Voltage Model Parameters: Outputs

Parameter	***Parameter Description***
$g_e=k_e/L_e$	External heat transfer coefficient for the transfer between the reaction system and the copper electrodes (conductive transfer)
S	Seebeck Coefficient of the TPW system (μV/K)
$\Delta\mu$	Chemical Potential Gradient (Coulombs-Volts)
k_0	Arrhenius pre-exponential factor (s^{-1}) such that $\tau_{fac}=\left(\frac{C_{p,CNT}E_a}{(-H)R}\frac{1}{k_0}\right)=\frac{\beta}{k_0}$ Used to calculate non-dimensional time step equivalent of experimental voltage data time steps of $\Delta t_{exp}=0.0005$ s
E_a	Activation Energy for the fuel reaction (J mol^{-1})
$(A_{surface}/V)$	Exposed area per unit volume, which contributes to convective and radiative heat loss along the length of the device, calculated using the fitted w_{rad}.
h_{conv}	Calculated using w_{conv}, it represents the convective heat transfer coefficient for the device.

We start the fitting procedure by using the input parameters and guess values for all the parameters involved in the model (from *Table 3-3* and *Table 3-4*). We then solve the coupled ODEs corresponding to the non-dimensional system of heat and mass balance equations to obtain a complete temperature and concentration profile for our reaction system. In order to obtain maximum accuracy, MATLAB's in-built ode15s solver is used with the modified (and

more stringent) *RelTol* criteria of 10^{-6}. The (non-dimensional) time span over which the ode solver operates is evaluated using the corresponding dimensional times at which the experimental data is available and using the values of k_0 and β.

$$\tau_{end} = \Delta\tau_{ode} \times (\#\text{ of experimental points} - 1)$$

$$\tau_{span} = 0 : \Delta\tau_{ode} : \tau_{end} \tag{26}$$

Calculations are then performed using equation (25) and the Seebeck coefficient (S) exhibited by the system and the chemical potential gradient ($\Delta\mu$) to obtain an output voltage profile with respect to time. This predicted output voltage is then compared with an actual experimental output voltage. The parameter values that are to be fitted are then varied with the aim of replicating the experimental voltage output. The final aim of this analysis is to obtain numerical values for the 7 parameters from *Table 3-4* which are representative of the properties of the system.

One point to note is that when fitting or predicting the experimental voltage output using this model, the ramping up voltage as observed in some samples is excluded for the ease of fitting. Ramping up voltage is the slight voltage output before the actual peak, as seen in some experimental output profiles. One hypothesis for these ramp ups is it being the thermoelectric output from the system while the reaction initiation point heats up one end of the system to the minimum temperature needed for the reaction to initiate. By excluding this portion of the voltage output, we can focus on fitting the main voltage output peak that carries more important data about the reaction wave propagation and device efficiency and operation.

We test the accuracy of our model by performing a rough order of magnitude analysis for the various parameters involved. Single-walled carbon nanotubes have been shown to exhibit Seebeck coefficient of about 40 μV/K.[20] From our experiments, we know that the experimental output for nitrocellulose-SWNT devices supported on glass slide gives voltage output ranging up to tens of millivolts. Using this as the metric of the rough order of magnitude analysis and knowing that the voltage contribution from the chemical potential gradient is of the form of $\frac{1}{e}\Delta\mu$ where e is the elementary charge or 1.6×10^{-19} *Coulombs*, rough calculation shows that Δμ will roughly be of the order of magnitude of 10^{-21} Coulomb-Volt. According to the literature about nitrocellulose reaction, the activation energy of the reaction is of the order of magnitude of 10^5 J/mol. Preliminary fits for our experimental data using the above orders of magnitude for S, $\Delta\mu$ and E_a show that k_0 of order of magnitude between 10^2 to 10^5 (1/sec) is needed to be able to fit the experimental data.

For systems not leaking out heat very fast to the surroundings i.e. if the reaction wave is actually sustained, we expect a double polarity thermoelectric voltage output for a full reaction wave propagation. The temperature gradient during the reaction propagation should be much larger than the temperature gradient when the reaction wave reaches the end of the thermopower wave device. Accordingly, we expect to see a shorter or smaller in magnitude opposite polarity voltage output peak after the reaction has completely propagated. With the additional effect of excess thermopower acting on the sample, first of the double polarity peak will be either boosted or opposed, depending on the direction of the thermoelectric voltage output (governed by whether the Seebeck coefficient of the SWNT cluster is positive or negative, which in turn is governed by whether the carrier transport is dominated via metallic or semiconducting carbon nanotubes).[3] When the two voltages oppose each other, the first peak which is ideally higher in magnitude (as

compared to the reverse polarity second peak) is repressed because of the opposing effect of excess thermopower. In case of partial reaction wave propagation, since there is no chance of the temperature gradient reversal, we expect a single polarity thermoelectric voltage output. Again, depending on whether the effect of excess thermopower boosts or opposes the thermoelectric voltage output, you expect to see 'kinks' or multiple peaks in the single polarity peak voltage output.

Having gained this understanding about how this model can allow us to predict different trends in commonly observed voltage output profiles, we performed this fitting analysis for a set of nitrocellulose-SWNT samples showing a wide variety of voltage output profiles such as one single polarity peak, multiple single polarity peaks, double polarity peaks etc. *Table 3-5* below contains a list of the 7 parameters that are fitted and how their numerical values can be analyzed to obtain more information about the system. Each of the fitted parameters gives us information about factors such as the heat transfer properties exhibited by the TPW system, properties of the fuel reaction or the level of coupling between the fuel layer and the thermal conduit. Values fitted for S and $\Delta\mu$ have direct impact on the magnitude of voltage output and are one of the main indicators of how well the fuel layer has coated the thermal conduit. The properties of k_0 and E_a give us insight into the ease and rate of the reaction and play a role in not only how long the reaction propagates for but also the amount of heat needed to start the reaction. That has impact in terms of deciding which fuels can lead to self-propagating reaction waves and thus can be a suitable candidate for the technology of thermopower waves. Also, these fits will provide a rough check for the heat of the reaction of the fuel. It can be calculated from the known parameter β and the fitted value for E_a. This heat of reaction is an important quantity as it plays a

role in calculating the efficiency of operation of the device and can sometimes need very elaborate experimental setup to measure it.

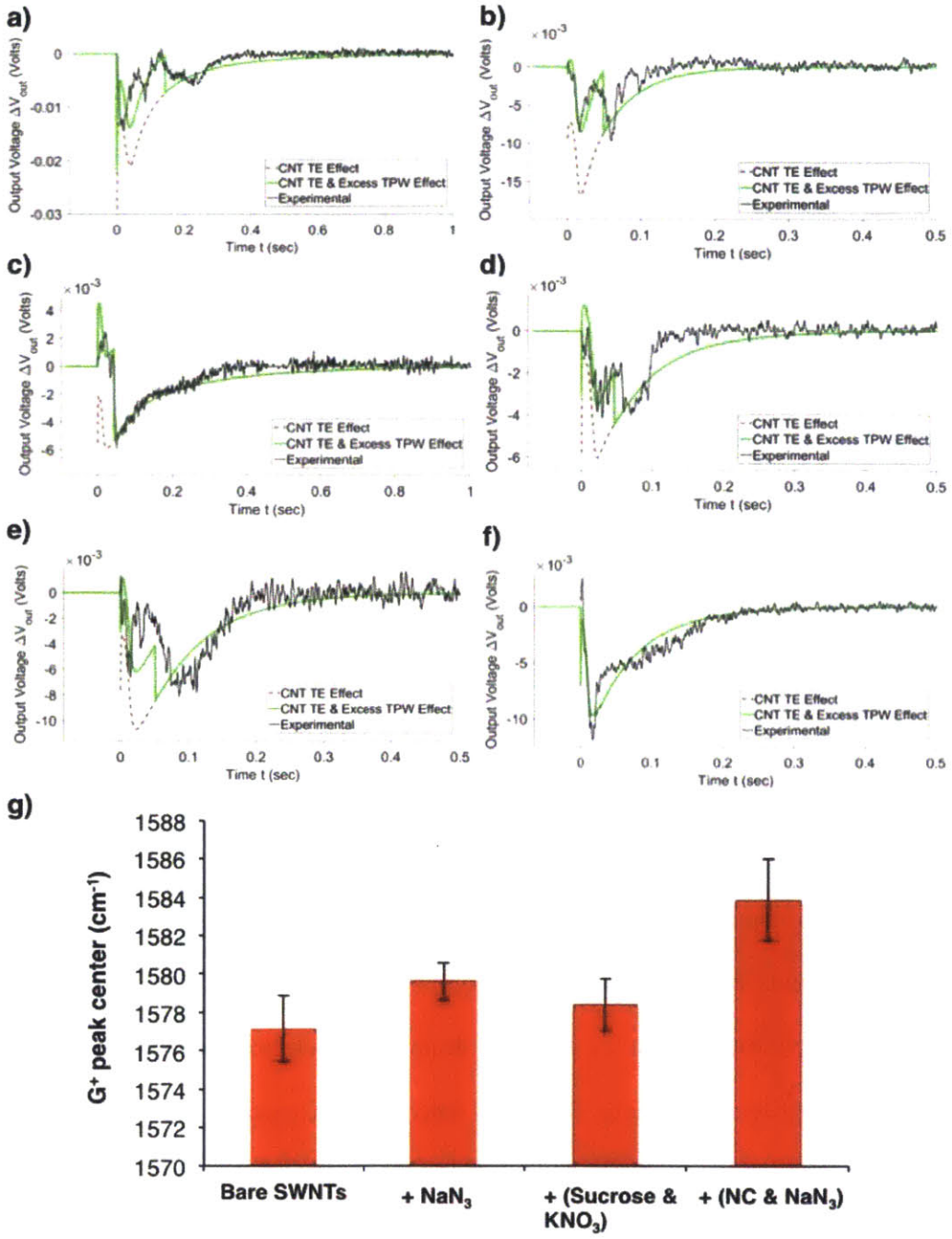

Figure 3-4 a-f) Thermopower wave voltage output prediction for a few experimental samples. The experimental output in shown in black, the model predicted thermoelectric output is shown in blue and the final model predicted output voltage accounting for excess thermopower and external resistor is shown in green e) Doping analysis using Raman spectroscopy for different fueled and unfueled SWNT samples. Upshift in the position of G^+ peak corresponds to p-doping for semiconducting carbon nanotubes.

Table 3-5 Interpreting from the numerical values for the fitted parameters of the TPW output voltage model

Parameter	*Interpretation*
g_e, $(A_{surface}/V)$ or w_{rad}, h_{conv} or w_{conv}	Sample to sample variation in heat losses. This could be representative of the sample contacts or the changes in the surrounding conditions when launching these reaction waves.
S and $\Delta\mu$	Seebeck Coefficient of the TPW system depends not only on the conduit but is also impacted by the presence of the fuel layer atop the thermal conduit and thus indicative of the level of contact between the fuel layer and the thermal conduit and hence can vary from device to device. Similar to the Seebeck coefficient, the Chemical Potential Gradient (Coulombs-Volts) strongly depends on how intimate of a contact exists between the thermal conduit and the fuel layer.
k_0, E_a	Arrhenius pre-exponential factor (s^{-1}) is indicative of the nitrocellulose chemical reaction and as such should remain invariant across samples.

From some of the sample fits, as shown in Figure 3-4 (a-f), we are able to well predict the experimental data. Subplots (a-e) correspond to cases where the excess thermopower opposes to the thermoelectric output leading to double or multiple peaks of single polarity. Subplot (f) corresponds to outputs where the excess thermopower impact on the voltage output is minimal leading to single polarity output as expected from thermoelectric voltage contribution from partially propagating reaction waves. The most interesting takeaway from these fits is noticing that for 20 samples that were fitted for, 17 samples show the effect of excess thermopower opposing the voltage output because of thermoelectric effect. This can have immense impact in choice of fuel (and the kind of doping) that best suits these kinds of SWNT fiber thermal conduits. To analyze this more, we carried out Raman analysis of the SWNT fiber in different states: bare SWNT fiber, SWNT fiber fueled with sodium azide, SWNT fiber fueled with sucrose

& KNO_3 and finally SWNT fiber fueled with nitrocellulose (and sodium azide). We observed that all of these fuels cause upshift in the G^+ peak position thus confirming that they all dope SWNT fibers.[49] Secondly, sodium azide causes the least doping whereas nitrocellulose causes the most doping. As was shown in Figure 3-1 c, this trend supports the trend observed in their corresponding TPW device efficiencies with sodium azide devices being the best and nitrocellulose devices showing the least efficiency amongst the three fuels. Thus, on the basis of opposing excess thermopower effect as inferred from the model fitting for nitrocellulose voltage plots and the correlation between Raman analysis and experimentally observed thermopower wave device efficiencies for different fuels, we conclude that for the chosen SWNT fiber thermal conduits, using fuels that p-dope the thermal conduit penalizes the thermoelectric voltage contribution. Thus, to even further improve the efficiency of TPW devices made using these SWNT fiber, we need to use fuels that n-dope the carbon nanotubes such that the excess thermopower voltage output will boost or support the thermoelectric voltage output leading to even superior performance of such devices.

To summarize this work, the proposed set of equations for reaction of a 1D fuel layer along with the concepts of thermoelectricity and excess thermopower provide a simple model that allows us to predict the voltage output from TPW devices. The model consists of a system of heat and mass balance ordinary differential equations and can help us predict the voltage output from thermopower wave devices. Various parameters used in the model are easily correlated to physical properties in the experimental setup thus giving us more insight into the TPW device's operation. This model can be used to fit any thermopower wave output voltage peak and study system properties such as Seebeck coefficient, chemical potential gradient established by fuel coating atop the thermal conduit, reaction propagation characteristics such as the reaction rate

constant etc. Using this model for fitting nitrocellulose-SWNT device voltage outputs with Raman spectroscopy and efficiency analysis for different fuels used with these SWNT fibers, we hypothesize that the TPW efficiency can be even further improved by launching reaction waves using fuels that n-dope the SWNT fibers.

3.5 Conclusion

On the basis of theory of excess thermopower, the chemical to electrical conversion efficiency of thermopower wave devices was improved from about 10^{-4} % to up to 10^{-2} % by using novel fuels such as sodium azide and (sucrose &KNO_3). Combining this improved performance of thermopower waves with external thermoelectric harvesting, we demonstrate the net setup efficiency of thermopower waves device setup to up to 1 %. We propose a simple continuous 1D fuel heat and mass transfer model to be used in combination with the theory of excess thermopower to be able to fit or predict experimental voltage output from thermopower wave devices. Fitting analysis for SWNT fiber-nitrocellulose samples combined with Raman and TPW device efficiency analysis shows that choosing n-doping fuels might further boost the efficiency of these SWNT fiber based thermopower wave devices.

Chapter 4 Experimental Demonstration of 2D Reaction Waves and Energy Harvesting using Thermoelectric Harvesters

4.1 Introduction

Thermopower waves is a novel technology for converting chemical energy into electrical energy by launching self-propagating reaction waves across thermally and electrically conducting conduits. Such reaction waves have been launched with a wide variety of fuels and thermal conduits. Thermopower wave devices with specific power of electrical output as high as 7 kW/kg have been demonstrated experimentally.[2] Thermopower wave devices have the advantage of storing the energy in the form of chemical bonds and so have a high or long shelf-life. High power density and specific power make them ideal candidate for research with the aim of developing high efficiency nano and micro-scale energy sources.[20] Concept of thermopower waves has been predominantly demonstrated in 1D systems using thermal conduits such as carbon nanotubes, alumina, terracotta, ZnO etc. However, there might be merit in extending this concept to a 2D reaction system if it allows us to better harvest the heat released during the chemical reaction to generate electrical energy. Scaling up the system could allow us to possibly exploit the higher surface area of the thermal conduit by using thermoelectric or photovoltaic harvesting techniques which can show improved output with higher input exposure areas.

Experiments were started by launching and studying 2D reaction waves. With the successful launching of these 2D reaction waves, and temperature profiling these systems, we can get a better idea of what thermal conduits best serve our purpose. Launching these 2D reaction waves have multiple advantages over the conventional 1D thermopower wave experimental systems. Because of the macro-scale of operation as compared to micro-scale of operation of conventional 1D thermopower wave devices, these experiments are easy to perform. Moreover, experimental

verification of such reaction waves will also allow us to test the theory of superadiabatic temperature rise described Chapter 2. With these motivations in mind, we set about to analyze self-propagating reaction waves in 2D.

4.2 Experiments to launch 2D reaction waves and test for superadiabatic temperatures

Nitrocellulose was used as the fuel for studying 2D reaction waves. Aluminum foil (Al foil) was used as the conduit for heat conduction. Simple experiments using joule heater initiation experimentally demonstrated self-propagating reaction waves of nitrocellulose. Experimental procedure involved attaching a piece of nitrocellulose to the Al foil using common use glue. The reaction was then initiated from the desired spot by contacting with the joule heater. After confirming the ability of being able to launch 2D reaction waves using nitrocellulose, we wanted to study the effect of heat transfer properties on factors such as the wave front shape and the temperatures reached. For measuring the temperature in the system, we use a non-contact pyrometer. This pyrometer temperature measurement spot is focused along the surface of the fuel area whose temperature is to be measured. From the preliminary 2D experiments and experiments involving using nitrocellulose as a fuel for 1D thermopower devices, we know that the temperatures at the reaction wave front with nitrocellulose can reach temperatures in excess of 800°C. Previous preliminary experiments in our lab showed that nitrocellulose does need oxygen to undergo the reaction and so the reaction cannot be carried out in vacuum when trying to reduce the convective heat loss. As a means of tuning the heat loss from the reaction system, we adjusted the size of the thermal conduit beneath the fuel layer. Extending the thermal conduit beyond the exact shape and size of the fuel layer allows that 'extra' region of thermal conduit to act as heat loss fins for the system. Hence, we studied the temperature and wave front properties

for nitrocellulose reaction atop Al foil in two situations: 'adiabatic boundary' condition where we match the shape and size of the fuel layer and thermal conduit layer, and non-adiabatic boundary where there is extra thermal conduit surface area that is not covered with a fuel layer atop it and acts as an additional heat sink.

With this sample setup, multiple reaction waves were launched for nitrocellulose brought in intimate contact with the Al foil using glue and the reaction initiated with a joule heater. Pyrometer was used to measure temperatures at the center point and the corner points for multiple samples, with both, the experimental 'adiabatic' and 'non-adiabatic' setups. As can be seen in Figure 4-1 a, we obtained differences in shapes of the wave front in those two cases. We observed a flat wave front versus curved wave front profile for the 'adiabatic' and 'non-adiabatic' heat loss conditions. These differences in wave front profiles can be explained by analyzing the effect of heat loss on wave propagation. One theory is that in cases where more heat is lost near the edges, as in the situation of non-adiabatic boundary versus adiabatic boundary, the wave speed gets compromised. This can happen if the area near the boundary now gets the heat needed for reaction initiation at a rate slower than the interior region which does not see or feel as much of the effects of the boundary condition.

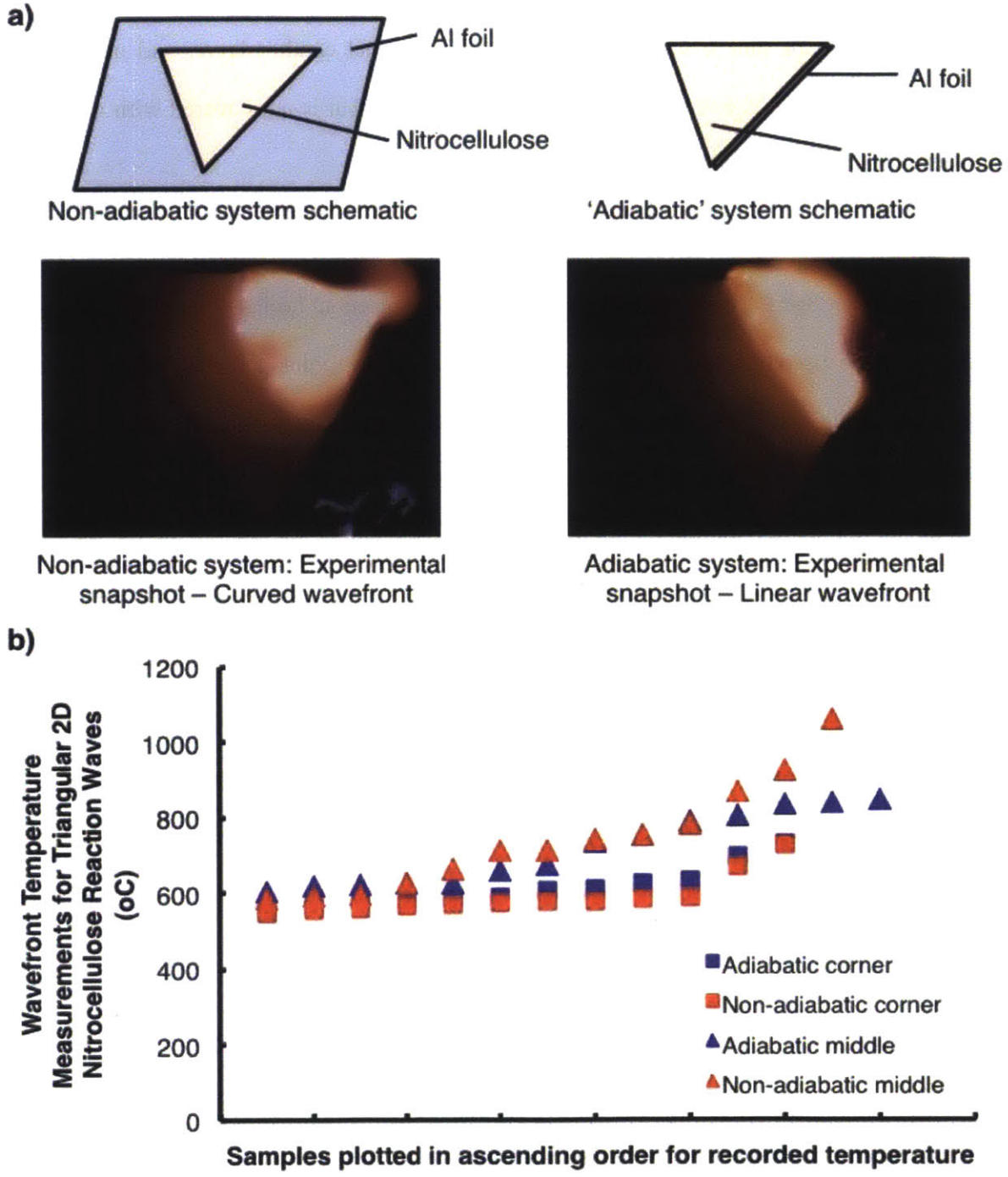

Figure 4-1 a) Schematic and experimental snap-shot of simplified 'adiabatic' and 'non-adiabatic' reaction conditions using nitrocellulose fuel with aluminum foil thermal conduit. b) Temperature of the nitrocellulose on Al-foil system wave front for differing boundary conditions and temperature read-out locations

In studying these reaction waves, we were unable to carry out temperature measurements at multiple the positions simultaneously because of availability of just a single pyrometer and hence no two data points on the temperature plots discussed correspond to a single sample. As described in Chapter 2, from our previous simulation results for self-propagating reaction waves, we expected that ideally, the temperature of points near the edge to be superadiabatic and greater than that at the center. However, as can be seen in Figure 4-1 b, while we did obtain some superadiabatic temperatures of greater than 1000°C (adiabatic temperature rise of nitrocellulose from our calculations is about 827°C), there have been experimental measurements of nitrocellulose reaction temperature reaching up to 300°C. We did not see any difference in temperatures with regards to boundary condition and the measurement spot. Reinvestigating the COMSOL results and dimensionalizing the space variable for which the COMSOL simulations were carried out showed that the simulation scale corresponds to a physical scale of about 5 mm. Simulations at the scale at which the experiments were carried out (~ 30 mm) were impractical because of the computational resources required.

To summarize, we were able to successfully launch reaction waves using nitrocellulose as a fuel atop Al foil as thermal conduit. By tuning the heat loss properties for the system by modifying the shape of the thermal conduit, we saw differences in the reaction wave front profile. However, we were not able to experimentally demonstrate superadiabaticity. This could have happened because of multiple reasons. First and foremost, practical reaction conditions were non-adiabatic whereas superadiabaticity analysis was carried out for adiabatic systems. For practical applications, that analysis now needs to be built upon by accounting for heat losses such as convection and radiation. Secondly, a very well characterized solid fuel should be used for these experiments. Nitrocellulose is a polymer with well-studied but complicated reaction pathways

with changing kinetics as the decomposition reaction proceeds.[50] Ideal solid fuel should have a well-characterized reaction and has a known and verified adiabatic temperature rise. Even without known theoretical adiabatic temperature rise, superadiabaticity demonstration experiments can still be carried by just demonstrating presence of higher temperature at regions where we expect superadiabaticity when compared to the experimental temperature in the regions where we expect adiabatic temperature rise to be the maximum temperature. However armed with theoretical values for adiabatic temperature rise and the expected superadiabaticity accounting for heat losses will definitely allow us to learn more from these 2D reaction wave experiments.

4.3 Electrical Energy Generation Using Thermoelectric Materials (TE)

The final aim of studying these 2D reaction waves was to study 2D thermopower waves as power source to convert chemical to electrical energy.

Since aluminum has a really low Seebeck coefficient (~ 1 $\mu V/K$[57] as compared to ~ 287 $\mu V/K$ for commonly used thermoelectric material bismuth telluride, Bi_2Te_3), it is not possible to obtain electrical output from the current electrical setup consisting of nitrocellulose fuel reacted atop Al foil thermal conduit. So as in case of harvesting heat losses from 1D thermopower wave devices, we decided to use commercially available thermoelectric (TE) devices for this purpose. As can be seen from Figure 4-1 b, while the temperature at the top of the Al foil can go above 1000°C, experiments using thermal imaging camera on the back side of the Al foil as the reaction was carried out on the front side showed temperatures in the range of 250 – 300 °C. Commercially available Bi_2Te_3 thermoelectric / cooling units, (15 mm by 15 mm) and (30 mm by 30 mm) in

size were ordered from TE Tech. Using thermal paste, the hot side of the TE harvester was brought in intimate contact with the back side of the Al foil contacted with nitrocellulose fuel layer on the top or the other side. Test experiments showed that the TE harvester acted as a heat sink and prevented reaction of nitrocellulose directly above the Al foil region that lay atop the TE harvester contact surface area. So, an appropriately large fuel layer size of a (30 mm by 30 mm) was chosen for the purpose of our experiments, such that there exists a layer of fuel over Al that isn't above the TE harvester. A 1.5Ω resistor was used in the circuit to accurately measure the current in the circuit by measuring the voltage output from the TE harvester by using an oscilloscope. This system gave an output of up to 250 mV with an efficiency of about 0.02 %, where efficiency is defined as:

$$\text{Efficiency } \% = \frac{\text{Total Output Electrical Energy}}{\text{Heat Input via the Exothermic Chemical Energy}} \times 100 \qquad (1)$$

At the scale of operation of these 2D reaction waves, it was observed that the nitrocellulose gives out a lot of energy as visible light during the course of its reaction. With this in mind, a Silicon (Si) photovoltaic cell (PV) was suspended above the reaction setup. This setup was successful too and gave about 200 mV voltage output from the PV. Another experimental setup akin to that used for harvesting energy losses from 1D thermopower wave devices' setup was to suspend a large surface area TE above the reacting nitrocellulose layer. This new set-up of suspended TE on top of the propagating reaction wave led to almost 5 times improvement in the overall efficiency reaching up to values as high as 0.1 %.

As a demonstration of harvesting the exothermic heat of reaction from 2D reaction waves using TE harvesters, experiment was designed to have a piece of nitrocellulose react below two TE harvesters that were then electrically connected in series. An output > 1.5V was obtained

allowing us to light up a light-emitting diode (LED). This simple experiment demonstrates the potential of using self-propagating reaction waves combined with other technologies such TE harvesters or photovoltaics to best convert the heat energy released during the chemical reaction into useful electrical energy.

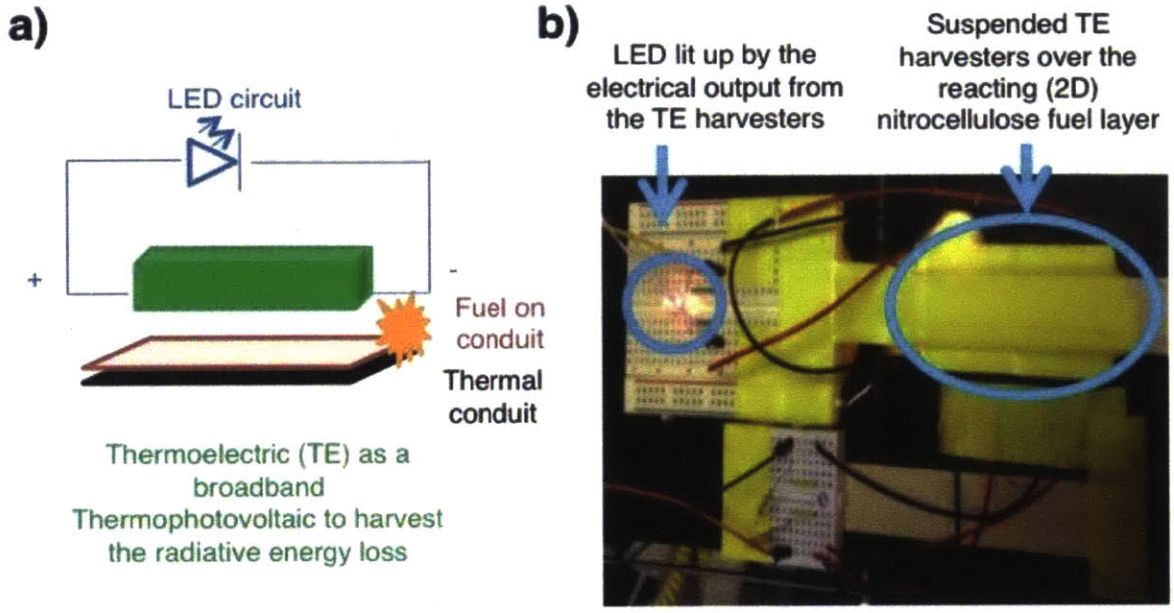

Figure 4-2 a) Schematic of the experimental setup for harvesting radiative heat given out by 2D reaction wave propagation by using TE harvesters b) Snap-shot showing lighting up of an LED by using electrical output from TE harvesters connected in series and placed above a piece of reacting nitrocellulose

Further experimental efforts in this area can be dedicated to improve the output of electrical energy from this kind of a 2D reaction wave setup. Work can be focused towards experimental realization of the concept of superadiabaticity which will further enhance the electrical energy generation in such systems. Additionally, the electrical output that can be obtained from this system can be enhanced by trying to realize the equivalent of excess thermopower in these 2D

systems. This would involve looking for a suitable thermal conduit that is macroscopically 2D and can support a thick layer of fuel atop it and can get doped by this fuel layer. Technique for depositing macro-scale thick layers of fuel atop thermal conduits could be explored to minimize the amount of input energy in the system and study its effect on the output electrical energy.

4.4 Conclusion

In summary, this chapter describes our efforts in experimentally studying 2D reaction waves. Nitrocellulose fuel layer atop a piece of aluminum foil were our chosen experimental components. We were able to successfully launch these 2D reaction waves and noticed changes in the reaction wave front propagation profile, as a function of the amount of 2D domain boundary heat loss experienced by the system. On the basis of rough calculations for the adiabatic temperature rise of the fuel i.e. nitrocellulose, we wanted to demonstrate superadiabaticity. However, unclear results were obtained when analyzing the temperature of the reaction wave front across different areas of the region. Preliminary experiments to convert the chemical energy stored in the bonds of the fuel into electrical energy were carried out using photovoltaics (PV) and Bi_2Te_3 TEs as external harvesters. The latter showed promise when used with a 2D nitrocellulose fuel layer, showing the final efficiency of operation of this device reaching almost 0.1%. With this experimental setup, we were able to obtain experiments voltage output >1.5 V. This allowed us to demonstrate lighting up of an LED. Future work in this field should involve aims of improving this efficiency of energy conversion by not only improving the energy harvesting but also incorporating the elements of thermopower wave propagation by choosing / discovering an appropriate pairs for fuel – 2D thermal conduit system.

Chapter 5 Conclusions and Outlook

The main aim of this thesis was to study different methods of conversion of energy, specifically chemical energy being converted to heat energy via chemical reaction which is then converted to electrical energy using various technologies such as excess thermopower, thermoelectricity and photovoltaics. In this thesis, we cover research studying various experimental, numerical and analytical aspects of one-dimensional (1D) and two-dimensional (2D) self-propagating reaction waves. Our numerical analysis of reaction waves shows possibility of the system reaching temperatures much higher than the adiabatic reaction temperatures when carrying out the reaction under specific conditions. Our experimental work with 1D thermopower waves has improved the chemical-to-electrical thermopower wave efficiency from about 10^{-4} % to up to 10^{-2} % and improved the net device efficiency to up to 1%. Finally we propose a model that delves into the details of the operation of a thermopower wave device and can be used to predict different forms of voltage profile outputs that can be obtained from thermopower wave devices. We also experimentally demonstrated 2D reaction waves using nitrocellulose fuel with an aluminum thermal conduit and showed their application in generating electricity using external thermoelectric (TE) harvesters.

In Chapter 1, we cover the basics of reaction waves, specifically thermopower waves technology of converting chemical energy into electrical energy via launching reaction waves by coating a layer of fuel over a thermal conduit. Previous experimental thermopower waves' work using various fuels and thermal conduits was covered. Following that, we cover the theory of excess thermopower which explains the superior performance of these thermopower wave devices over electrical outputs that would be obtained by just conventional thermoelectric effect. Analytical

expression governing the steady-state temperature profile of such reaction waves when propagating in an adiabatic environment was also discussed.

In Chapter 2, we extend the numerical analysis of reaction wave systems by studying multiple numerical systems all of which physically correspond to self-propagating reaction waves. This analysis showed that for self-propagating reaction waves with certain specific fuel and system properties, once the reaction wave reaches the adiabatic boundaries, temperatures can go up to twice that of the expected adiabatic temperature rise. This ability to reach high temperatures has applications in developing higher efficiency systems to convert this heat energy into usable electrical energy. Analysis was carried out to show the concept of a modified thermophotovoltaic wave setup, which would immensely benefit by using superadiabatic reaction wave as a source of radiation for its photovoltaic.

In Chapter 3, we first cover the experimental progress made in the field of 1D thermopower wave devices. We improved the chemical-to-electrical conversion efficiency of these thermopower waves almost 100-fold from about 10^{-4} % to 10^{-2} %. This improvement was obtained by changing the fuels used to launch these thermopower wave reactions. Energy input to the system was lowered by using sodium azide as the fuel (almost $1/10^{th}$ heat of reaction as compared to previous fuels such as nitrocellulose). Beginning our foray into relatively benign, safe to use and easily available fuels, reactions were launched using mixture of sucrose and an oxidizer (potassium nitrate or KNO_3). These devices are also about 10 times more efficient than the ones using nitrocellulose as fuel, and give rise to a much longer voltage output due to visibly slower reaction waves. Ability to capture the convective heat loss and thermalize the radiation emitted by these high temperature reaction waves further led to improvement in the efficiency. Experiments were carried out using external thermoelectric (TE) harvesters around the modified

suspended thermopower reaction wave devices to further increase the net electrical output from the system to as high as 1%. We then propose a model to analyze voltage output profiles of thermopower wave devices. To better understand the variety of voltage output profiles exhibited by these 1D thermopower wave devices (e.g. single polarity, double polarity etc.), a theoretical model studying a 1D thermopower reaction wave as a 1D layer of fuel was setup. Fitting for 7 reaction wave system parameters allowed us to simulate a variety of the experimental voltage output profiles. This method of analysis has given us deep insight into understanding how different kinds of reaction wave propagations and the thermal conduit properties along with the fuel-thermal conduit coupling give rise to the differences in the thermopower wave device voltage output profiles. In the future, this model can be used to select specific thermal conduits and fuels pairs on the basis of the needed voltage output profile for specific applications. Using this model in studying voltage output data from SWNT-nitrocellulose devices, combined with Raman analysis on fuel doping of carbon nanotubes, points towards using n-doping fuels with these SWNT fibers to boost the thermopower reaction wave efficiency even more.

In Chapter 4, we cover the experimental progress made towards extending the concept of thermopower waves to 2D systems. 2D reaction waves were experimentally demonstrated by using nitrocellulose as the fuel atop aluminum foil thermal conduit. Preliminary experiments to harvest the heat given out by nitrocellulose reactions (theoretically at both the adiabatic and superadiabatic temperatures) were carried out again using external TE harvesters. 2D nitrocellulose waves with Bi_2Te_3 TE harvesters were used to demonstrate lighting up of an LED with the voltage output as high as 1.5V.

This thesis has been successful in making contribution to the novel area of energy generation using 1D thermopower waves and 2D reaction waves, which could finally someday be used to

build portable energy sources with high power density. However a lot needs to be explored before that becomes a commercial possibility. Research in a variety of directions can benefit the final aim of actualizing a high efficiency chemical-to-electrical energy conversion device that has a long shelf-life, high power density, and is safe to use.

Future experimental work on 1D thermopower waves should focus on launching reaction waves using liquid fuels with catalyst coated thermal conduits. There is work already underway in the lab with the final aim of using liquid fuels to launch these thermopower waves. This will not only make the device operation safer because of lower temperatures reached because of combustion of liquid fuels, but will also take us on the path of continuous power generation using thermopower waves. Along those lines, efficiency of operation of these devices should be continued to be explored by testing out different fuels with possibly lower heat of reaction but still enough heat released to sustain a self-propagating reaction wave. There is scope to optimize the experimental protocol by finding the lowest fuel to thermal conduit ratio that will give rise to a reaction wave while minimizing the amount of fuel used. For SWNT fiber based devices, n-doping fuels show high promise to improve the efficiency of thermopower reaction waves. Thermal conduits also play a very important role in affecting the propagation of a thermopower wave and its electrical output. Recent work by Hwang et al. studies the influence of alignment of the carbon nanotubes based thermal conduit.[58] As expected, their work shows that alignment of carbon nanotubes prevents cancellation of charge carrier movements and produced improved energy generation performance for when obtaining single polarity output voltage signal. Research work along the side of thermal conduits can be focused on finding thermal conduits, either newer materials or modified forms of carbon nanotubes that show properties that aid thermopower wave operation: improved internal alignment of the conduit to aid in fast carrier

transport and reaction wave propagation, high Seebeck coefficient, a balance for the thermal conductivity such that it is high enough to sustain a reaction wave but low enough to reduce the reaction wave velocity. This reduced wave velocity when fine-tuned with reduced heat losses can essentially increase the duration and magnitude of voltage output thus improving the total electrical energy extracted from the system. Fuels that do not need oxygen to react can be used under vacuum to get rid of convective losses. Convective losses can be reduced by carrying out reaction wave experiments in quiescent surroundings.

On demonstrating direct applications for thermopower wave devices, research efforts can be focused on looking for niche applications for these nanoscale high power density devices. Working on optimum circuit setup to capture and store the electrical energy output in a capacitor that can then be extracted at higher voltages or current as-needed will also be instrumental in commercializing and large-scale implementation of this technology.

Similar ideology can also be applied towards experiments relating to developing 2D reaction waves based energy sources. Preliminary experiments to demonstrate superadiabaticity with nitrocellulose gave mixed results. To conclusively demonstrate superadiabaticity, experiments need to be carried out with solid fuels whose reactions have been well characterized and adiabatic temperature rise well known. As in the case for 1D thermopower waves, reactions should preferably be carried out in environments that minimize heat losses, for example in an insulated chamber under vacuum or quiescent air. Efforts to look for a 2D conduit that has high Seebeck coefficient and can sustain the weight of a thin solid fuel layer which also dopes it will allow us to extend the concept of thermopower waves to two dimensions. Because of the unique nature of this new reaction wave-front (line versus a point), it could be possible to operate multiple circuits off of a single 2D reaction wave. Higher surface area of the reaction region i.e.

the fuel layer surface area also provides opportunity for better energy harvesting for external TEs and external thermophotovoltaics which will benefit from the increased area of hot temperature thermal conduit. However care should be taken when choosing the optimum technology in this case as the increased surface area can cause an impact in whether radiation or convection turns out to be the dominant mode of heat transfer.

Along with carrying out experiments, it would be in our best interest to continue with our thrust on the numerical and computational aspect of these reaction waves. The current models for both superadiabatic temperature rise and the 1D thermopower reaction wave voltage output are simplified models not accounting for heat losses or accounting for only part of the heat loss mechanisms. Accounting for these heat losses and incorporating more complex but realistic reaction kinetics terms when analyzing the temperature of these systems will give us a computationally more expensive but physically more accurate description of our system. Delving more into the modeling aspect of the heat losses will also guide us in our experimental efforts to convert most of the chemical energy released as heat into electrical energy.

Thus by focusing our efforts on various aspects of these 1D and 2D reaction waves, we can be closer to our aim of developing a high efficiency chemical to electrical energy generation nano and micro-scale portable energy device technology.

Chapter 6 References

1. Schaber, C.; Mazza, P.; Hammerschlag, R., Utility-Scale Storage of Renewable Energy. *The Electricity Journal* **2004,** *17* (6), 21-29.
2. Choi, W.; Hong, S.; Abrahamson, J. T.; Han, J.-H.; Song, C.; Nair, N.; Baik, S.; Strano, M. S., Chemically driven carbon-nanotube-guided thermopower waves. *Nat Mater* **2010,** *9* (5), 423-429.
3. Abrahamson, J. T.; Sempere, B.; Walsh, M. P.; Forman, J. M.; Şen, F.; Şen, S.; Mahajan, S. G.; Paulus, G. L. C.; Wang, Q. H.; Choi, W.; Strano, M. S., Excess Thermopower and the Theory of Thermopower Waves. *ACS Nano* **2013,** *7* (8), 6533-6544.
4. Abrahamson, J. T.; Song, C.; Hu, J. H.; Forman, J. M.; Mahajan, S. G.; Nair, N.; Choi, W.; Lee, E.-J.; Strano, M. S., Synthesis and Energy Release of Nitrobenzene-Functionalized Single-Walled Carbon Nanotubes. *Chemistry of Materials* **2011,** *23* (20), 4557-4562.
5. Yeo, T.; Hwang, H.; Jeong, D.-C.; Lee, K. Y.; Hong, J.; Song, C.; Choi, W., Effects of chemical fuel composition on energy generation from thermopower waves. *Nanotechnology* **2014,** *25* (44), 445403.
6. Walia, S.; Weber, R.; Latham, K.; Petersen, P.; Abrahamson, J. T.; Strano, M. S.; Kalantar-zadeh, K., Oscillatory Thermopower Waves Based on Bi2Te3 Films. *Advanced Functional Materials* **2011,** *21* (11), 2072-2079.
7. Walia, S.; Weber, R.; Sriram, S.; Bhaskaran, M.; Latham, K.; Zhuiykov, S.; Kalantar-zadeh, K., Sb2Te3 and Bi2Te3 based thermopower wave sources. *Energy & Environmental Science* **2011,** *4* (9), 3558-3564.
8. Walia, S.; Weber, R.; Balendhran, S.; Yao, D.; Abrahamson, J. T.; Zhuiykov, S.; Bhaskaran, M.; Sriram, S.; Strano, M. S.; Kalantar-zadeh, K., ZnO based thermopower wave sources. *Chemical Communications* **2012,** *48* (60), 7462-7464.
9. Walia, S.; Balendhran, S.; Yi, P.; Yao, D.; Zhuiykov, S.; Pannirselvam, M.; Weber, R.; Strano, M. S.; Bhaskaran, M.; Sriram, S.; Kalantar-zadeh, K., MnO2-Based Thermopower Wave Sources with Exceptionally Large Output Voltages. *The Journal of Physical Chemistry C* **2013,** *117* (18), 9137-9142.
10. Hong, S.; Hong, S.; Lee, T.-R.; Kim, Y.-J.; Ryu, C.; Baik, S., Surface thermochemical reaction control utilizing planar anisotropic thermal conduit. *Energy & Environmental Science* **2011,** *4* (6), 2045-2049.
11. Lee, K. Y.; Hwang, H.; Choi, W., Advanced Thermopower Wave in Novel ZnO Nanostructures/Fuel Composite. *ACS Applied Materials & Interfaces* **2014,** *6* (17), 15575-15582.
12. Hong, S.; Kim, W.; Jeon, S.-J.; Lim, S. C.; Lee, H.-J.; Hyun, S.; Lee, Y. H.; Baik, S., Enhanced Electrical Potential of Thermoelectric Power Waves by Sb2Te3-Coated Multiwalled Carbon Nanotube Arrays. *The Journal of Physical Chemistry C* **2013,** *117* (2), 913-917.
13. Lee, K. Y.; Hwang, H.; Shin, D.; Choi, W., Enhanced thermopower wave via nanowire bonding and grain boundary fusion in combustion of fuel/CuO-Cu2O-Cu hybrid composites. *Journal of Materials Chemistry A* **2015,** *3* (10), 5457-5466.
14. Abrahamson, J. T.; Strano, M. S., Analytical Solution to Coupled Chemical Reaction and Thermally Diffusing Systems: Applicability to Self-Propagating Thermopower Waves. *The Journal of Physical Chemistry Letters* **2010,** *1* (24), 3514-3519.

15. Abrahamson, J. T.; Choi, W.; Schonenbach, N. S.; Park, J.; Han, J.-H.; Walsh, M. P.; Kalantar-zadeh, K.; Strano, M. S., Wavefront Velocity Oscillations of Carbon-Nanotube-Guided Thermopower Waves: Nanoscale Alternating Current Sources. *ACS Nano* **2010,** *5* (1), 367-375.
16. He, J.-H., Asymptotic Methods for Solitary Solutions and Compactons. *Abstract and Applied Analysis* **2012,** *2012*, 130.
17. Walther, D. C.; Ahn, J., Advances and challenges in the development of power-generation systems at small scales. *Progress in Energy and Combustion Science* **2011,** *37* (5), 583-610.
18. Sailor, M. J.; Link, J. R., "Smart dust": nanostructured devices in a grain of sand. *Chemical Communications* **2005,** (11), 1375-1383.
19. Roundy, S.; Steingart, D.; Frechette, L.; Wright, P.; Rabaey, J., Power Sources for Wireless Sensor Networks. In *Wireless Sensor Networks*, Karl, H.; Wolisz, A.; Willig, A., Eds. Springer Berlin Heidelberg: 2004; Vol. 2920, pp 1-17.
20. Choi, W.; Abrahamson, J. T.; Strano, J. M.; Strano, M. S., Carbon nanotube-guided thermopower waves. *Materials Today* **2010,** *13* (10), 22-33.
21. Chakraborty, A. K.; Coleman, K. S.; Dhanak, V. R., The electronic fine structure of 4-nitrophenyl functionalized single-walled carbon nanotubes. *Nanotechnology* **2009,** *20* (15-155704), 6pp.
22. Weber, R. O.; Mercer, G. N.; Sidhu, H. S.; Gray, B. F., Combustion Waves for Gases (Le = 1) and Solids (Le $\rightarrow \infty$). *Proceedings: Mathematical, Physical and Engineering Sciences* **1997,** *453* (1960), 1105-1118.
23. Zeldovich, Y. B.; Frank-Kamenetskii, D., A theory of thermal propagation of flame. *Zh. Fiz. Khim* **1938,** *12* (1), 100-105.
24. Schmidt, L. D., Engineering of Chemical Reactions (2nd Edition). Oxford University Press.
25. Hada, S.; Harrison, B. K., Prediction of energy release hazards using a simplified adiabatic temperature rise. *Journal of Loss Prevention in the Process Industries* **2007,** *20* (2), 151-157.
26. McAllister, S.; Chen, J.-Y.; Fernandez-Pello, A. C., *Fundamentals of combustion processes [electronic resource] / Sara McAllister, Jyh-Yuan Chen, A. Carlos Fernandez-Pello.* New York : Springer, 2011: 2011.
27. Merzhanov, A. G., The chemistry of self-propagating high-temperature synthesis. *Journal of Materials Chemistry* **2004,** *14* (12), 1779-1786.
28. Smith, J. M.; Van Ness, H. C.; Abbott, M. M., Introduction To Chemical Engineering Thermodynamics. 6th ed.; McGraw Hill Higher Education: 2003.
29. DiSalvo, F. J., Thermoelectric Cooling and Power Generation. *Science* **1999,** *285* (5428), 703-706.
30. Snyder, G. J.; Toberer, E. S., Complex thermoelectric materials. *Nature Materials* **2008,** *7* (2), 105-114.
31. Bejan, A.; Kraus, A. D., Heat Transfer Handbook. John Wiley & Sons.
32. Lienhard , J. H. V.; Lienhard , J. H. I. V., A Heat Transfer Textbook. 4th edition ed.; Dover Publications: 2011.
33. Baehr, H. D.; Stephan, K., Heat and Mass Transfer. 3rd Revised ed.; Springer Berlin Heidelberg: 2011.
34. Coutts, T. J.; Fitzgerald, M. C., Thermophotovoltaics. *Scientific American* **1998,** *279* (3), 68-73.

35. Bosi, M.; Ferrari, C.; Melino, F.; Pinelli, M.; Spina, P. R.; Venturini, M. In *Thermophotovoltaic Generation: A state of the art review*, Proceedings of the 25th int conf on efficiency, cost, optimization, simulation and environmental impact of energy systems, Perugia (Italy), 26–29 June 2012; Perugia (Italy), 2012; pp 1-6.
36. Rinnerbauer, V.; Ndao, S.; Yeng, Y. X.; Chan, W. R.; Senkevich, J. J.; Joannopoulos, J. D.; Soljacic, M.; Celanovic, I., Recent developments in high-temperature photonic crystals for energy conversion. *Energy & Environmental Science* **2012,** *5* (10), 8815-8823.
37. Aruna, S. T.; Mukasyan, A. S., Combustion synthesis and nanomaterials. *Current Opinion in Solid State and Materials Science* **2008,** *12* (3–4), 44-50.
38. Gray, P.; Kordylewski, W., Standing Waves in Exothermic Systems. *Proceedings of the Royal Society of London. Series A, Mathematical and Physical Sciences* **1985,** *398* (1815), 281-288.
39. Mercer, G. N.; Weber, R. O., Combustion waves in two dimensions and their one-dimensional approximation. *Combustion Theory and Modelling* **1997,** *1* (2), 157-165.
40. Mercer, G. N.; Weber, R. O., Combustion Wave Speed. *Proceedings: Mathematical and Physical Sciences* **1995,** *450* (1938), 193-198.
41. Mercer, G. N.; Weber, R. O.; Sidhu, H. S., An oscillatory route to extinction for solid fuel combustion waves due to heat losses. *Proceedings of the Royal Society of London Series a-Mathematical Physical and Engineering Sciences* **1998,** *454* (1975), 2015-2022.
42. Mahajan, S. G.; Wang, Q. H.; Strano, M. S.; Abrahamson, J. T., Energy generation using thermopower waves: Experimental and analytical progress. *AIChE Journal* **2013,** *59* (9), 3333-3341.
43. Green, M. A.; Emery, K.; Hishikawa, Y.; Warta, W.; Dunlop, E. D., Solar cell efficiency tables (version 42). *Progress in Photovoltaics: Research and Applications* **2013,** *21* (5), 827-837.
44. Lu, S.; Ji, L.; He, W.; Dai, P.; Yang, H.; Arimochi, M.; Yoshida, H.; Uchida, S.; Ikeda, M., High-efficiency GaAs and GaInP solar cells grown by all solid-state molecular-beam-epitaxy. *Nanoscale Research Letters* **2011,** *6* (1), 576-576.
45. Hädrich, M.; Metzner, H.; Reislöhner, U.; Kraft, C., Modelling the quantum efficiency of cadmium telluride solar cells. *Solar Energy Materials and Solar Cells* **2011,** *95* (3), 887-893.
46. Xia, Y.; Liu, B.; Liu, J.; Shen, Z.; Li, C., A novel method to produce black silicon for solar cells. *Solar Energy* **2011,** *85* (7), 1574-1578.
47. Johnson, D. H., Fundamentals of Electrical Engineering I.
48. Kim, C.; Thomas, S. W.; Whitesides, G. M., Long-Duration Transmission of Information with Infofuses. *Angewandte Chemie International Edition* **2010,** *49* (27), 4571-4575.
49. Das, A.; Sood, A.; Govindaraj, A.; Saitta, A. M.; Lazzeri, M.; Mauri, F.; Rao, C. R., Doping in carbon nanotubes probed by Raman and transport measurements. *Physical Review Letters* **2007,** *99* (13), 136803.
50. Chen, J. K.; Brill, T. B., Thermal decomposition of energetic materials 50. Kinetics and mechanism of nitrate ester polymers at high heating rates by SMATCH/FTIR spectroscopy. *Combustion and Flame* **1991,** *85* (3–4), 479-488.
51. Kane, C.; Mele, E.; Lee, R.; Fischer, J.; Petit, P.; Dai, H.; Thess, A.; Smalley, R.; Verschueren, A.; Tans, S., Temperature-dependent resistivity of single-wall carbon nanotubes. *EPL (Europhysics Letters)* **1998,** *41* (6), 683.
52. Yu, C.; Shi, L.; Yao, Z.; Li, D.; Majumdar, A., Thermal Conductance and Thermopower of an Individual Single-Wall Carbon Nanotube. *Nano Letters* **2005,** *5* (9), 1842-1846.

53. Hone, J.; Batlogg, B.; Benes, Z.; Johnson, A. T.; Fischer, J. E., Quantized Phonon Spectrum of Single-Wall Carbon Nanotubes. *Science* **2000,** *289* (5485), 1730-1733.
54. Hone, J.; Whitney, M.; Zettl, A., Thermal conductivity of single-walled carbon nanotubes. *Synthetic Metals* **1999,** *103* (1–3), 2498-2499.
55. Thess, A.; Lee, R.; Nikolaev, P.; Dai, H.; Petit, P.; Robert, J.; Xu, C.; Lee, Y. H.; Kim, S. G.; Rinzler, A. G.; Colbert, D. T.; Scuseria, G. E.; Tománek, D.; Fischer, J. E.; Smalley, R. E., Crystalline Ropes of Metallic Carbon Nanotubes. *Science* **1996,** *273* (5274), 483-487.
56. Collins, P. G.; Avouris, P., Nanotubes for electronics. *Scientific American* **2000,** *283* (6), 62-69.
57. Kasap, S., Thermoelectric effects in metals: thermocouples.
58. Hwang, H.; Yeo, T.; Um, J.-E.; Lee, K. Y.; Kim, H.-S.; Han, J.-H.; Kim, W.-J.; Choi, W., Investigation of the effect of the structure of large-area carbon nanotube/fuel composites on energy generation from thermopower waves. *Nanoscale research letters* **2014,** *9* (1), 1-9.